THERMAL DECOMPOSITION OF MIXED METAL OXALATES

Submitted in fulfilment of the requirements

for the degree of

Master of Science

of Rhodes University

by

ANITA COETZEE

January 1993

ABSTRACT

The mixed metal oxalates, $FeCu(ox)_2.3H_2O$, $CoCu(ox)_2.3H_2O$, and $NiCu(ox)_2.3.5H_2O$, [ox = C_2O_4] have been prepared by coprecipitation from solution. The thermal behaviour of these compounds in nitrogen and in oxygen has been examined using thermogravimetry (TG), thermomagnetometry (TM), differential scanning calorimetry (DSC) and evolved gas analysis (EGA), and results are compared with results obtained for Cuox and $Mox.yH_2O$.

The thermal behaviour of the mixed oxalates, $MCu(ox)_2.xH_2O$, differed from that of the individual metal oxalates, Cuox, $Coox.2H_2O$, $Niox.2H_2O$ and $Feox.2H_2O$. All three mixed oxalates on heating in N_2, first dehydrate and then decompose in at least two overlapping endothermic stages. Both CO and CO_2 were evolved in proportions which varied with the surrounding atmosphere, and from compound to compound, and with extent of reaction of a given compound.

The mixed oxalates, $MCu(ox)_2.xH_2O$, do not show the exothermic behaviour characteristic of Cuox, and reasons for this are discussed. Thermochemical calculations were done and the enthalpies of formation of the hydrates and dehydrated oxalates were determined. It was found that the enthalpy of mixing was very small or within experimental error.

X-ray powder diffraction patterns for the individual and mixed oxalates were compared. The pattern for Cuox differs from the patterns obtained for the other oxalates, confirming suggestions that Cuox has a structure different to most other transition metal oxalates.

The kinetics of dehydration and decomposition of the mixed oxalates were investigated, using isothermal and programmed temperature TG and DSC experiments. The yield and composition of evolved gases during isothermal decomposition were measured and compared with the enthalpy changes.

X-ray photoelectron spectroscopy studies provided some information on the electron environment of the metal atoms in the various oxalates.

ACKNOWLEDGEMENTS

I would like to express my sincere gratitude and appreciation to my two supervisors Professors M.E. Brown and D.J. Eve for their guidance and encouragement throughout this project.

I would also like to thank:

Dr R.B. English, for his suggestions and encouragement;

Dr R.C. Cosser, for his helpful assistance with the vacuum system;

Dr C. Strydom of the University of Pretoria, for her help with the XPS studies;

the staff of the Department of Chemistry at Rhodes University, for their interest and support;

my fellow students and friends for their moral support, particularly Mr M.J. Tribelhorn and Mr S.J. Taylor for all their help and encouragement;

the Foundation of Research and Development for its financial assistance.

Finally I would like to extend a special word of thanks to my parents and my fiance, Charles, for their loving support during the course of my studies.

TABLE OF CONTENTS

Table of contents

LIST OF FIGURES

Chapter 1

Chapter 4

List of Figures

List of figures

LIST OF TABLES

List of Tables

Chapter 6

Chapter 7

Chapter 8

LIST OF SYMBOLS

A	pre-exponential factor in Arrhenius equation
E_a	activation energy (kJ mol^{-1})
ΔH	enthalpy change
K	equilibrium constant
R	gas constant
T	temperature (°C)
t	time (s)
ox	oxalate ion ($C_2O_4^{2-}$)
k	rate constant
α	fractional extent of reaction
φ	dT/dt heating rate (°C min^{-1})

CHAPTER 1 INTRODUCTION

Much research has been done on the structure, properties and thermal behaviour of metal oxalates [1]. Available evidence suggests that the oxalates of divalent transition metals are polymeric, with the oxalate ion acting as a bridging ligand. The oxalate ion [ox $=C_2O_4$], which is divalent, can act as either a bidentate or quadridentate ligand [2].

1.1 THE STRUCTURE OF TRANSITION METAL OXALATES

The structure of humboldtine ($FeC_2O_4.2H_2O$) was determined by Caric [3] and found to be monoclinic. The C_2O_4 groups were found to be linked to the Fe atoms in such a fashion as to form chains following the y-axis, arranged as shown in Figure 1.1 [4].

Figure 1.1.
The structure of humboldtine ($FeC_2O_4).2H_2O$) [4].

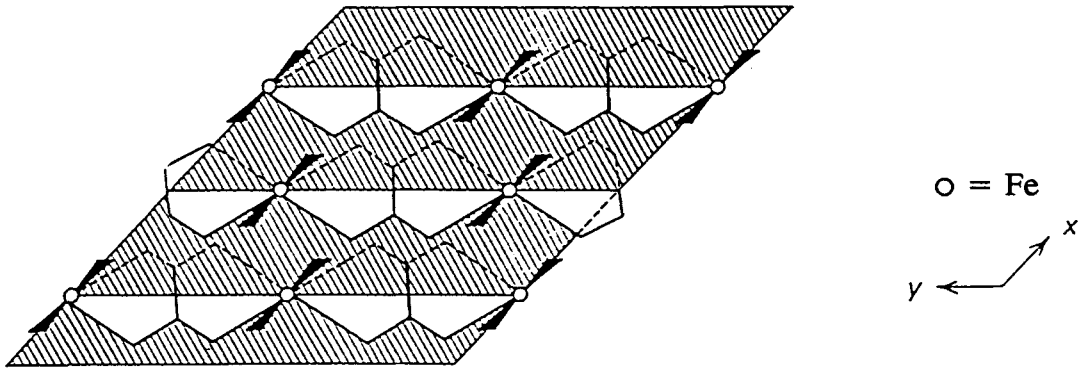

Dubernat and Pezerat [5] have concluded, from X-ray powder diffraction data, that the dihydrated oxalates of Fe, Co, Ni and Zn may exist either as a three-dimensional ordered phase, isostructural with humboldtine (see Figure 1.1), or as a disordered phase with stacking faults parallel to (001) planes. These compounds consist of ribbon chains stacked in the following manner [6], where A,B,C,D represent the position of the metal atoms:

A C
B D
C A
D B

The well-ordered structure can be represented as a layer succession, ABCDABCD... The disordered phase consists of stacking faults corresponding to permutations between A and C on the one hand, and between B and D on the other.

Schmittler [6] stressed the difficulties in obtaining crystal data from powder photographs of substances with defective ordering. He claimed that the X-ray crystallographic data for Mox [M= Fe, Co, Ni and Zn] were not necessarily consistent with space group C2/c quoted by Mazzi and Garavelli [7]. The origin of the inconsistency was a 1-dimensional error in position ordering with order-disorder (OD) character.

Much controversy surrounds the bridging in copper oxalate. Copper oxalate exhibits high antiferromagnetic behaviour. This has been explained [8-12] in terms of the bridging of the oxalate ion. There is substantial evidence that copper oxalate has a linear chain structure of strongly antiferromagnetically coupled spin doublets. Girerd [10] and Bloomquist [11] claimed that (independent) EXAFS studies revealed that the oxalate ion acted as a double bidentate ligand, coordinating to two copper ions, as shown in Figure 1.2. This is the same structure as that put forward for other transition metal oxalates, e.g. Ni, Co and Fe, except that water plays no part in the structure of Cuox.

Figure 1.2.

Proposed structure of Cuox [10, 11]

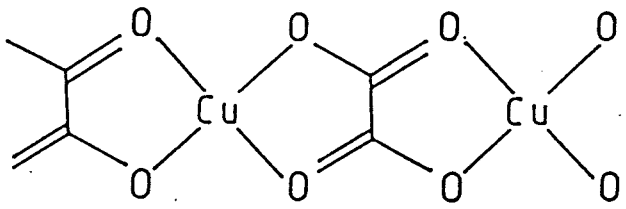

According to Dubicki [11], the considerable thermal stability and marked lack of chemical reactivity of copper oxalate are consistent with this infinite chain-like structure. He claims that this structure might also involve interchain interaction to complete a distorted octahedron of oxygen atoms about each central metal atom. He also suggests that the exchange mechanisms for spin coupling involve the delocalised π-cloud of the bridging

oxalate ion. This theory is supported by Martin and Waterman [12]. This argument is further supported by Gleizes [13] who suggests closely-packed chains, arranged as in Figure 1.3, to explain the antiferromagnetic behaviour. He deduced the structure of Cuox from that of $Na_2Cu(C_2O_4)_2.2H_2O$, which has been determined using X-ray crystallography. It was assumed that Cuox consisted of ribbon-like chains. The chains pile up in such a way that the coordination geometry of the Cu(II) ions is close to that observed in $Na_2Cu(C_2O_4)_2.2H_2O$. Progressive removal of the water molecules results in the limit, the structure of anhydrous Cuox, in which layers are linked by van der Waal's forces between oxygen atoms.

Figure 1.3.

Proposed structure of Cuox [13].

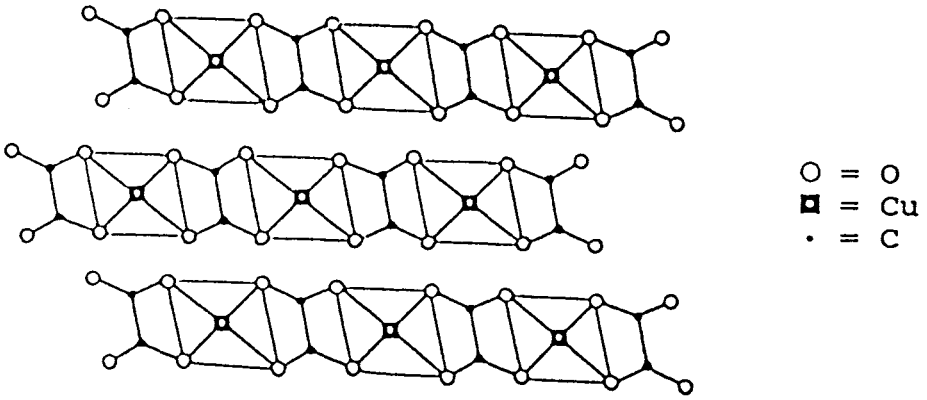

It is significant that Cuox incorporates little or no water of crystallisation in the crystal lattice. Schmittler [6] showed that Cuox has a water content ranging between 0 and 0.5 moles of H_2O per mole of Cuox, and concluded that chains of (ox)Cu(ox)Cu... exist.

X-ray crystallographic studies by Edwards *et al* [14] further support the ribbon-like structure with polymeric chains stacking in a progressively staggered fashion. They suggested that the symmetry group is ($P2_1/c$). This is different from that of Ni(II) oxalate dihydrate, which crystallises in the monoclinic system C_2/c (C_{2h}^6), with four formula units in the cell, in which the planar metal oxalate layers are held together by hydrogen bonds from water molecules.

Figgis and Martin [15] considered the ribbon-type structure as well as a structure in

which the adjacent ions are bridged by two different oxalate groups, shown in Figure 1.4. This structure is similar to the type of bridging found in copper acetate monohydrate, except that the chain formed is linear. McGregor and Soos [16] found that this structure was consistent with the relatively large exchange interaction observed, but that the ribbon-type structure was more consistent with their EPR data.

Figure 1.4.

Proposed structure of Cuox [15].

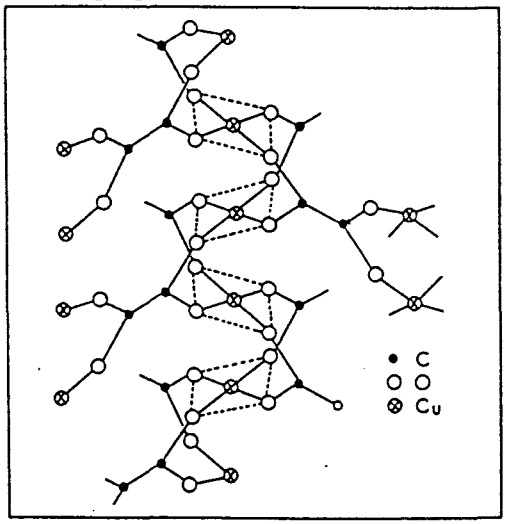

Earlier Kuroda and Kubo [17] suggested that Cuox consisted of an extending 2-dimensional network in which pairs of copper atoms are bridged by a single carboxylate group as in Cu(II) acetate monohydrate. However, magnetic susceptibility measurements show a weaker anti-ferromagnetic coupling than in Cu(II) acetate. Infrared absorption bands between 1300 and 1400 cm^{-1}, which are assigned to C-O stretching vibrations, and regarded as diagnostic of oxalate bridging, are similar to those observed for Ni(II), Co(II) and Fe(II) oxalate. There has been no support for this structure in the recent literature.

1.2 THERMAL BEHAVIOUR

Most of the transition metal oxalates show one or more endothermic decomposition steps on heating in N_2. The decomposition routes are affected by the prevailing atmosphere. Decomposition may be preceded by endothermic dehydration step(s). In O_2, overall reaction is strongly exothermic, owing to the reaction of evolved CO with oxygen to form CO_2, or to the oxidation of the metal decomposition product to a metal oxide [18].

The thermal decomposition of Cuox differs substantially from that of most of the other bivalent transition metal oxalates [18]. Cuox exhibits a strongly exothermic decomposition reaction when heated in N_2 [1]. The decompositions of silver(I) oxalate [19-26] and mercury(I) oxalate [27] in N_2, are also exothermic. The decomposition of Ag_2ox is a complex process, which is dependent on the reaction conditions [21]. The reaction is governed by the formation and growth, in the crystal, of nuclei of silver metal [22]. The reaction is autocatalytic [23]. Prout and Tompkins [27] suggested that the mode of decomposition of mercury(I) oxalate might be similar to that of silver oxalate.

$2Hg_2ox \rightarrow 3Hg + HgO + 3CO_2 + CO$

1.3 DECOMPOSITION ROUTES

The oxalates can decompose according to one of three (endothermic) decomposition routes in N_2 [28].

$Mox \rightarrow M + CO_2$ ....(1)

$Mox \rightarrow MO + CO + CO_2$ ....(2)

$Mox \rightarrow MCO_3 + CO$ ....(3)

In addition, there is the possibility of some disproportionation of CO:

$2CO \rightleftharpoons CO_2 + C$

which may be catalysed by the solid product of decomposition.

The alkali- and alkaline-earth metal oxalates decompose according to route (3). The transition-metal oxalates either decompose according to route (1) e.g. Znox or (2) e.g. Niox.

The environment can influence the thermal decomposition of an oxysalt [18]:

a) by causing changes in the mechanism of chemical decomposition, or

b) by altering the physical nature of the solid product or solid intermediates.

For example, both Niox and Znox show endothermic decomposition steps in inert atmospheres, but decomposition is exothermic in air or oxygen. The reasons for the

exothermic nature of the reactions in oxygen are different. When the oxalate, e.g. Niox, follows route (1), the exothermic peak observed in O_2 is due to the following reaction:

$M + \frac{1}{2}O_2 \rightarrow MO$.

If decomposition occurs according to route (2), e.g. Znox, the carbon monoxide will be oxidised in an O_2 atmosphere, according to the exothermic reaction:

$CO + \frac{1}{2}O_2 \rightarrow CO_2$

which is also catalysed by the ZnO product surface [29].

1.4 DECOMPOSITION MECHANISMS

Dollimore [1] has discussed these different decomposition mechanisms in more detail. In oxalates of bivalent metals, the extent to which the metal-O_1 bond is covalent depends on the electronegativity of the metal. Decomposition takes place at a temperature at which rupture of the metal-O_1 bond (Figure 1.5) or rupture of the C-O_1 bond takes place [30]. As the metal-O_1 bond becomes stronger, the C-O_1 bond is lengthened. The C-O_1 bond thus breaks first, followed by rupture of the other metal-O bond, to yield the metal oxide and equimolar quantities of CO and CO_2. If simultaneous rupture of the two metal-O_1 bonds takes place, the products are the metal and two moles of CO_2. This reaction depends on the size and the charge of the metal cation. When the products are CO and CO_2, the reaction is less critically dependent on the nature of the cation.

Figure 1.5.

Bonding in the metal oxalato species [1].

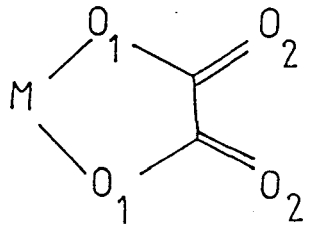

Fujita *et al* [31] studied the infrared spectra of the oxalato complexes, $K_2M(ox)_2.nH_2O$, with M= Cu, Fe, Co, Ni. They found that as the M-O bond becomes stronger, lowering of the symmetry becomes more distinct, and the shifts of the oxalate, relative to that of the free ion, increase. As the M-O bond becomes stronger, the C-O_1 bond becomes

lengthened and the C-O_2 bond becomes shortened, as shown by the shifts of ν(C-O_1) and ν(C-O_2) to lower and higher frequencies, respectively. The M-O bond was found to become stronger in the order of the metals Ni, Co, Cu, Fe.

Boldyrev [28] has emphasised the ionic nature of the three decomposition routes discussed above and has suggested three different mechanisms of rearrangement of the oxalate ion:

$C_2O_4^{2-} \rightarrow 2CO_2^{-} \rightarrow 2CO_2 + 2e^-$ (1)

$\downarrow$

$[OCOCO_2]^{2-} \rightarrow O^{2-} + CO + CO_2$ (2)

$\downarrow$

$CO_3^{2-} + CO$ (3)

The overall mechanism for route (1) involves electron transfer from the oxalate ion to the metal ion [32]:

$C_2O_4^{2-} \rightarrow 2CO_2 + 2e^-$

$M^{2+} + 2e^- \rightarrow M.$

The ease with which the process occurs will depend partly on the electron affinity of the oxalate ion and on the second ionisation potential of the metal atom. A qualitative correlation was expected between the second ionisation potential, the activation energy of the decomposition and the temperature of decomposition. Broadbent *et al* [32] found the following correlation: (silver oxalate does not conform, since it is monovalent with two metal atoms for each oxalate ion)

Table 1.1.
DECOMPOSITION OF METAL OXALATES IN N_2 [32]

oxalate	2nd ionisation potential / eV	E_a / kJ mol^{-1}	decomposition temp. / °C
Co^{2+}	17.3	165	375
Ni^{2+}	18.2	138	355
Cu^{2+}	20.3	128	280
Ag^{+}	7.57 (1st)	75	140

Nagase *et al* [33] attempted to relate the ionic radii of the metals to the decomposition

temperatures of the oxalates. They found that the oxalates of Cu, Ni and Co decomposed at higher temperatures as the metal ion radius increased along the period, whereas the oxalates of Mg, Mn, Fe and Zn decomposed at lower temperatures, as the radii of the metal ions increased.

Table 1.2.
DECOMPOSITION OF METAL OXALATES IN N_2 [33]

compound	product	decomposition temp. / °C	radius of metal ion / Å
Feox	FeO	310	0.83
Coox	Co	338	0.82
Niox	Ni	310	0.78
Cuox	Cu	235	0.72
Znox	ZnO	329	0.83

Robin [34] attempted to relate the decomposition temperatures of transition metal oxalates to the atomic numbers of the metals. The decomposition temperature of copper oxalate does not fit into the general pattern.

Dollimore [1] warns that results from different thermal analysis techniques should not be expected to match exactly. Each technique imposes special conditions on the sample which may not be present in another technique. The effect of the environment imposed by the technique can cause alterations in the course of the chemical reaction, as discussed above, and in the texture of the solid residue.

1.5 THERMODYNAMICS [18]

For the two possible reactions:

$Mox \rightleftarrows MO + CO + CO_2$ ....(1)

$Mox \rightleftarrows M + 2CO_2$ ....(2)

the equilibrium condition for the first reaction is:

$K_1 = ([MO][CO][CO_2]) / [Mox]$

and for the second reaction:

$K_2 = ([M][CO_2]^2) / [Mox]$

The ratio K_1/K_2 is then given by:

$(K_1/K_2) = ([MO][CO]) / ([M][CO_2])$

A similar ratio can be obtained from the reactions in oxygen:

$2CO + O_2 \rightleftarrows 2CO_2$ ....(3)

$2M + O_2 \rightleftarrows 2MO$ ....(4)

with $[K_4/K_3]^{1/2} = ([MO][CO]) / ([M][CO_2])$

then $(K_1/K_2) = [K_4/K_3]^{1/2}$

If the standard free energy of the reaction $CO \rightarrow CO_2$ is ΔG_a, and for the formation of the metal oxide is ΔG_b, then for $\Delta G_a > \Delta G_b$, $K_3 < K_4$ and it follows that $K_1 > K_2$. This implies that decomposition of oxalates to the oxide predominates over the decomposition to the metal. Under the usual experimental conditions, where the product gases are removed by the inert carrier gas as they are formed, the reaction proceeds to the oxide. If $\Delta G_b > \Delta G_a$, then the reaction will proceed to the metal [30].

1.6 KINETICS

As mentioned earlier, the environment has a marked effect on the route followed by decomposition [1]. The kinetics of decomposition are affected by factors which include the shape, size and material of the container crucible, the sample size and the heating rate, all of which determine the atmosphere in the neighbourhood of the sample, the crystal shape, size, presence of defects and various prehistory treatments.

Problems are encountered in studying the kinetics of a reaction when there are considerable structural differences between the solid products and solid reactant [35]. This may lead to a distortion of the geometry upon which many of the kinetic mechanisms are based, leading to shifts from one mechanism to another. If the study covers a wide temperature range there is the possibility of different kinetic mechanisms being found, owing to abrupt changes in the mode of diffusion. The occurrence of sintering also affects the kinetics, because it causes a decrease in surface area. Other factors which would influence the kinetic measurements are the degree of compaction and adhesion between particles and the rate of removal of product gases.

1.7 MIXED OXALATES

Since the structure and the thermal behaviour of copper oxalate differ so much from that of most of the other transition metal oxalates the thermal behaviour of the mixed metal oxalates, $MCu(ox)_2.xH_2O$, are of interest.

Dollimore [35] points out that the production of metals and alloys by decomposition of oxysalts is interesting because the metal is produced well below its melting point in a highly active particulate form. If mixtures of oxalates are used, the end product is an intimate mixture of the metals or metal oxides. It is a useful method of producing alloys below the melting points of the metals concerned.

Recently there has been a lot of interest [36-40] in the use of mixed metal oxides as catalysts in various reactions. Mixed copper-cobalt oxides, especially those with the

spinel structure, are active catalysts for the oxidation of CO with O_2. Cu-Co oxides (containing Al or Cr, Zn and an alkali metal) are also used for conversion of synthesis gas ($CO-CO_2-H_2O$) to higher alcohols [36,38]. Mixed Cu-Co-Zn-Cr oxides have also been tested as catalysts for the synthesis of hydrocarbons.

A copper-zinc oxide/alumina catalyst [41] has been successfully used for low-pressure (50-100 bar) methanol synthesis. The principal active site for methanol synthesis seems to be the copper centre. The activity of the copper-zinc oxide was found to be dependent on the catalyst precursor. In their study Waller *et al* [41] used hydroxy-carbonate precursors.

The chemical and physical properties of mixed oxide materials depend on the mode of preparation and on their thermal history, since these affect the component interdispersion and morphology [42]. Considerable effort has been put into finding preparative methods that are capable of giving precursors where two or more metals are in the same parent crystalline structure and which, after calcination, may provide well-interdispersed mixed oxides of the required chemical and physical properties. One of the most promising methods of preparation of such multi-component materials is the coprecipitation technique by which oxysalt precursors, such as hydroxycarbonates, oxalates, acetates, etc. are produced and where all the metals are possibly in the same crystalline structure. Mixed oxalates of Ni, Fe and Zn are useful precursors to the formation of ferrites with a spinel structure [43].

Dalvi and Chaval [44] studied the thermal decomposition of a coprecipitated zinc-copper oxalate. The solid products were ZnO, Cu and CuO:

$$Cu_xZn_{1-x}ox \rightarrow mCu + (x-m)CuO + (1-x)ZnO + (1+m)CO_2 + (1-m)CO$$

The onset temperature of decomposition of the mixed oxalate was substantially higher than that of Cuox and the temperature of completion of decomposition was lower than for the completion of decomposition of Znox. This suggests that zinc and copper oxalates form an interpenetrating matrix during coprecipitation.

Mixed metal oxalates, are thus useful precursors of mixed metal oxides, and detailed

studies of their thermal decomposition are important in determining the factors which control the properties of the solid products.

1.8 OVERVIEW OF WORK DONE ON THE INDIVIDUAL OXALATES

Thermal Analysis

The thermal analysis results, reported in the literature on Feox.$2H_2O$, Coox.$2H_2O$, Niox.$2H_2O$, Cuox and Znox.$2H_2O$ are summarised in Table 1.3.

Table 1.3.

THERMAL ANALYSIS DATA FOR THE INDIVIDUAL OXALATES

(a) Thermal analysis data for $Feox.2H_2O$

atmosphere	Temp. range / °C	TG % mass loss	product	DSC/ DTA/ kJ mol^{-1}	ref
dehydration					
self generated	187-267			95±5	45
air	177-217				45
O_2	161-178			endo	46
N_2 and air	140	20		endo	47
N_2	161-196			endo	46
N_2	120-185				60
decomp.					
self generated	357-427		Fe_2O_3		45
air	357-457				45
air	200		Fe_2O_3	exo	47
air	<195	44.7	$\alpha+\gamma Fe_2O_3$	exo	49
air	220			exo	50
air	235	44.4	Fe_2O_3		51
O_2	178-221		oxide	exo	46
N_2	235	43	Fe_2O_3		51
N_2	315-364		Fe+FeO	endo	46
N_2	190-320		Fe		60
N_2	330	40.8	FeO	endo	49
N_2	316-428	49.3	FeO	endo	52
N_2	384		FeO	endo	50
N_2	320	40.8	Fe_3O_4	endo	47

(b) Thermal analysis data for Coox.$2H_2O$

atmosphere	Temp range /°C	TG %mass loss	product	DSC/ DTA/ kJ mol^{-1}	ref
dehydration					
self generated	187-267			90 ± 5	45
air	120-250			endo	53
air	200	17.2			54
air	240	21.0			51
air	130-200				60
O_2	147-187			endo	46
N_2	125-270			endo	53
N_2		19.7			51
N_2	130-200				60
decomp.					
self generated	337-407		Co_2O_3	30 ± 2	45
air	357-417				45
air	280		Co_3O_4	exo	53
air	283			exo	50
air	253	44.0	Co_3O_4	exo	49
air	250	48.5	CoO		54
air	305	46.0	Co_3O_4		51
air	225-275		Co_3O_4		60
O_2	219-269		CoO	exo	46
N_2	297-392	42.5	Co+CoO	endo	52
N_2	359		Co	endo	50
N_2	355-371		Co	endo	46
N_2	350-370		CoO	endo	53
N_2		32.3	Co		51
N_2	149-197			endo	46
N_2	280-350		Co		60
N_2	355	33.6	Co+CoO	endo	49

(c) Thermal analysis data for $Co[Co(ox)_2].4H_2O$

atmosphere	Temp range /°C	TG %mass loss	product	DSC/ DTA/ kJ mol^{-1}	ref
dehydration					
air	150-235			endo	55
N_2	60-206	18.84		endo	55
decomp.					
air	251-300	56.31	Co_2O_3 $+Co_3O_4$	exo	55
O_2	300-420	63.15	Co+CoO	endo	55

(d) Thermal analysis data for Niox.$2H_2O$

atmosphere	Temp. range / °C	TG % mass loss	product	DSC/ DTA/kJ mol^{-1}	ref
dehydration					
self generated	217-287			91 ± 5	45
air	177-237				45
air	100-275			endo	53
air	250	21.2			54
air	260	22.0			51
air	135-260				60
O_2	173-260			endo	47
N_2		19.7			51
N_2	185-231			endo	46
N_2	135-260				60
N_2	255			endo	53
decomp.					
self generated	327-397		Ni+NiO	32 ± 2	45
air	367-407				45
air	310	41.0	NiO	exo	49
air	338			exo	50
air	255-350		NiO		60
air	340		NiO	exo	53
air	350	42.0	NiO		54
air	362	38.5	NiO		53
O_2	312-350		NiO	exo	46
N_2		32.2	Ni		53
N_2	318-349		Ni	endo	46
N_2	320	34.0	Ni+NiO	endo	49
N_2	292-378	40.8	Ni+NiO	endo	52
N_2	346		Ni	endo	50

(e) Thermal analysis data for $Ni[Ni(ox)_2].5H_2O$

atmosphere	Temp. range / °C	TG % mass loss	product	DSC/ DTA/kJ mol^{-1}	ref
dehydration					
N_2	270			endo	56
decomp.					
air	340			exo	56
N_2	340			endo	56

(f) Thermal analysis data for Cuox

compound atmosphere	Temp range / °C	TG %mass loss	product	DSC/ DTA/ kJ mol^{-1}	ref
Cuox dehydration					
air	200	3.5			51
N_2		3.5			51
decomp.					
self generated	287-357		$Cu+Cu_2O$	-29 ± 2	45
air	327-357				45
air	185-280		CuO		60
air	310	49.7	CuO		51
O_2	255-302		CuO	exo	46
N_2		58.6	Cu		51
N_2	255-280		Cu	exo	47
N_2	175-245		Cu		60
N_2	260		Cu	-65	57
N_2	232-265	57.6	$Cu+Cu_2O$	exo	52

(g) Thermal analysis data for $Cu[Cu(ox)_2].2H_2O$

compound atmosphere	Temp. range / °C	TG %mass loss	product	DSC/ DTA	ref
dehydration					
air	>298				58
N_2	292				58
decomp.					
air	260-297 297-324			exo exo	58
N_2	292		$Cu+CuO$		58

(h) Thermal analysis data for Znox.$2H_2O$

compound atmosphere	Temp. range / °C	TG %mass loss	product	DSC/ DTA	ref
dehydration					
air	170	18.5			51
O_2	109-156			endo	46
N_2		18.3			51
N_2	105-135				60
N_2	<220				59
decomp.					
air	390	55.3	ZnO		51
O_2	342-389		ZnO	exo	47
N_2	300-417	46.9	ZnO	endo	52
N_2		55.3	ZnO		51
N_2	342-383		ZnO	endo	47
N_2	320-380		ZnO		60
N_2	>300		ZnO		59

(i) Thermal analysis data for $Zn[Zn(ox)_2].5H_2O$

atmosphere dehydration	Temp range /°C	TG %mass loss	product	DSC/ DTA/	ref
air	91-180			endo	58
N_2	92-180			endo	58
decomp.					
air	347-412			endo	58
N_2	331		ZnO	endo	58

Deb and Dass [55,56,58] claim to have synthesised complexes of the type $M[M(C_2O_4)_2].xH_2O$, where M = Ni(II), Co(II), Cu(II) or Zn(II). They reported thermal analysis and spectroscopic data for these compounds. From Table 1.3 it seems as if their thermal analysis data correspond to that generally published for the simple oxalates, $Mox.xH_2O$. There also does not seem to be a marked difference between the infrared peaks quoted by Deb and Dass, and those obtained for $Mox.xH_2O$.

KINETICS

The solid-state rate expressions commonly used in isothermal kinetic analyses are summarised in Table 1.4 [81].

Table 1.4.
BROAD CLASSIFICATION OF SOLID-STATE RATE EXPRESSIONS [81]

	$f(\alpha) = kt$	$g(\alpha) = 1/k\ (d\alpha/dt)$
Acceleratory		
P1 power law	$\alpha^{1/n}$	$n(\alpha)^{(n-1)/n}$
E1 exponential law	$\ln \alpha$	α
Sigmoid		
A2 Avrami-Erofe'ev	$[-\ln (1 - \alpha)]^{1/2}$	$2(1-\alpha)(-\ln(1-\alpha))^{1/2}$
A3 Avrami-Erofe'ev	$[-\ln (1 - \alpha)]^{1/3}$	$3(1-\alpha)(-\ln(1-\alpha))^{2/3}$
A4 Avrami-Erofe'ev	$[-\ln (1 - \alpha)]^{1/4}$	$4(1-\alpha)(-\ln(1-\alpha))^{3/4}$
B1 Prout-Tompkins	$\ln [\alpha / (1 - \alpha)]$	$\alpha(1 - \alpha)$
Deceleratory		
geometrical models		
R2 contracting-area	$1 - (1 - \alpha)^{1/2}$	$2(1 - \alpha)^{1/2}$
R3 contracting-volume	$1 - (1 - \alpha)^{1/3}$	$3(1 - \alpha)^{2/3}$
diffusion		
D1 one-dimensional	α^2	$\frac{1}{2}\ \alpha$
D2 two-dimensional	$(1-\alpha) \ln(1-\alpha) + \alpha$	$(-\ln(1 - \alpha))^{-1}$
D3 three-dimensional	$[1 - (1 - \alpha)^{1/3}]^2$	$3(1-\alpha)^{2/3}/2[1-(1-\alpha)^{1/3}]$
D4 Ginstling-Brounshtein	$(1 - 2\alpha/3)-(1-\alpha)^{2/3}$	$3 / 2[(1-\alpha)^{-1/3} - 1]$
order of reaction		
F1 first order	$-\ln (1 - \alpha)$	$1 - \alpha$
F2 second order	$1 / (1 - \alpha)$	$(1 - \alpha)^2$
F3 third order	$[1 / (1 - \alpha)]^2$	$(1 - \alpha)^3$
Fn n-th order	$[1 / (1 - \alpha)]^n$	$(1 - \alpha)^n$

Kinetics of dehydration

Cuox

Copper oxalate is anhydrous.

Feox.$2H_2O$

Mu and Perlmutter [60] studied the kinetics of the dehydration of Feox, by applying the n-th order equation (Fn) (see Table 1.4) to programmed temperature runs done in N_2, at 1°C min^{-1} over the temperature range 20-350°C. They obtained an activation energy of 106.3 $\pm$ 1.6 kJ mol^{-1}, for α = 0.04-0.99, with n = ⅔ (i.e. R3) and A = 3.33×10^9 s^{-1}.

Coox.$2H_2O$

Mu and Perlmutter [60] used the same reaction conditions and method as discussed for Feox to examine the kinetics of dehydration of Coox.$2H_2O$. They obtained an activation energy of 157.7 $\pm$ 1.2 kJ mol^{-1} and A = 5.37×10^{15} s^{-1}, for α = 0.04-0.94 and n = 1.

Venkataraman *et al* [61] studied the kinetics of the dehydration of Coox in air, at a heating rate of 10°C min^{-1}, employing the equation:

$\ln(g(\alpha)/T^2) = \ln(AR / \phi E_a) - (E_a / RT)$

and substituting different mechanism-dependent equations into $g(\alpha)$. The activation energies obtained from these calculations were compared with values obtained using the mechanism-independent Coats and Redfern equation (C-R). The kinetic models which gave similar values to those obtained from the C-R equation, with E_a = 91.7 kJ mol^{-1}; A = 7.47×10^8, were the first-order equation (F1), E_a = 92.0 kJ mol^{-1} and A = 1.72×10^9 s^{-1}, the contracting-area equation (R2), E_a = 89.5 kJ mol^{-1} and A = 4.22×10^8 s^{-1}, and the contracting-volume equation (R3), E_a = 90.0 kJ mol^{-1} and A = 3.25×10^8 s^{-1}.

Niox.$2H_2O$

Mu and Perlmutter [60] used the same reaction conditions and method discussed for Feox, to examine the kinetics of dehydration of Niox.$2H_2O$. They obtained an activation energy of 252 $\pm$ 1 kJ mol^{-1} and A = 7.93×10^{24} s^{-1}, for α = 0.06-0.95 and n = 2.

Kinetics of decomposition

Cuox

Broadbent *et al* [57] obtained sigmoid α - time curves, based on accumulatory gas pressure measurements in an initially evacuated, constant volume apparatus, for the isothermal decomposition of Cuox (248 - 272°C). The Avrami-Erofe'ev equation, with n=3 (A3) gave the best fit over $0.2 < \alpha < 0.95$. The contracting-volume equation (R3), also gave a reasonable fit over $0.68 < \alpha < 0.93$. The initial acceleratory period could be described by the power law (P1) with n=2.9. The final section ($\alpha > 0.80$) fitted the first-order equation (F1). The overall activation energy was found to be 136 kJ mol^{-1}. Kinetic measurements made using a vacuum microbalance, gave α - time curves with a marked acceleratory period, and a maximum rate at $\alpha = 0.50$. The Prout-Tompkins equation (B1) fitted the data well, giving different slopes for α above and below 0.5. The Avrami-Erofe'ev equation (An) gave a better fit for n = 3.57, again with different slopes for α above and below 0.5. Above $\alpha = 0.5$ the contracting-area equation (R2) also fitted well. An overall activation energy of 128 kJ mol^{-1} agreed well with the value obtained from the constant volume apparatus.

Dollimore *et al* [62] reported that the results of isothermal TG experiments on Cuox in N_2 and in air could be described by the Avrami-Erofe'ev equation, with n = 2 (A2). They obtained activation energies of 193 kJ mol^{-1} in N_2 and 184 kJ mol^{-1} in air with respective pre-exponential factors of 2.83×10^{14} s^{-1} and 7.14×10^{13} s^{-1}. For a mechanism independent investigation they combined the integral kinetic equation ($g(\alpha)$) with the Arrhenius equation, and took natural logarithms on both sides to get: $\ln t = \ln g(\alpha) - \ln A - E/(RT)$, where t = time (sec); T = temperature (K); R is the gas constant and E and A are the Arrhenius parameters. By plotting ln t against 1/T, and assuming that $\ln g(\alpha)$ is negligibly small compared to ln A, they obtained an average activation energy of 214 kJ mol^{-1} with $A = 1.53 \times 10^{17}$ s^{-1}, in the range $\alpha = 0.1$-0.9, for the experiments in N_2.

Mu and Perlmutter [60] obtained kinetic information on the decomposition of Cuox, using the same reaction conditions and method (Fn) as discussed for the dehydration of Feox. They obtained an activation energy of 665 $\pm$ 4 kJ mol^{-1} and $A = 1.39 \times 10^{67}$ s^{-1},for α =

0.03-0.94 and n = 2. These values are much higher than the activation energies and pre-exponential factors reported in other studies mentioned above.

Feox

Mu and Perlmutter [60] used the same reaction conditions and method as discussed for dehydration of Feox to examine the kinetics of decomposition of Feox. The activation energy was 113 $\pm$ 1.2 kJ mol^{-1} and A = $2.50x10^{8}$ s^{-1}, for α = 0.03-0.98 and the apparent order, n = 2.

Coox

Broadbent *et al* [63] studied the decomposition of Coox using isothermal TG (297 to 315°C) in vacuum. For Coox which had been dehydrated at 150°C, a long induction period to decomposition was observed with an activation energy of 204 kJ mol^{-1}. Up to α = 0.50 the main reaction could be described by the exponential law (E1). Above α = 0.50 the reaction was linear, and beyond α = 0.90-0.95 the first-order decay (F1) applied. For Coox dehydrated at 200°C, the activation energy for the induction period was 225 kJ mol^{-1}. The main decomposition (α= 0.25-0.95) fitted the Prout-Tompkins equation (B1) and over the acceleratory region the exponential law (E1) gave a good fit. An activation energy of 165 kJ mol^{-1} was obtained.

The decomposition of coarse-grained Coox [64] (317 to 427°C) fitted the Avrami-Erofe'ev equation (An), with n = 2. Activation energies were 159 kJ mol^{-1} (below 352°C) and 57 kJ mol^{-1} (above 352°C). For finer-grained Coox, kinetic data were fitted by the Avrami-Erofe'ev equation with n = 3, and the activation energies measured were 120 kJ mol^{-1} (below 392°C) and 59 kJ mol^{-1} (above 392°C).

Mu and Perlmutter [60] used the same reaction conditions and method as discussed for the dehydration of Feox, to examine the kinetics of decomposition of Coox. They obtained an activation energy of 198 $\pm$ 2.8 kJ mol^{-1} and A = $1.11x10^{15}$ s^{-1},for α = 0.02-0.97 and apparent order, n = 2.

Niox

Jacobs and Kureishy [65] compared isothermal accumulatory and differential experiments on the hydrate (Niox.$2H_2O$) and dehydrated Niox. Dehydration (172-223°C) was a first-order process (F1) with an activation energy of 77 kJ mol^{-1}. Isothermal accumulatory experiments on the hydrate (245-260°C), showed an initial reaction (α = 0 - 0.0085) which could be fitted by the contracting-area equation (R2), and gave an activation energy of 141 kJ mol^{-1}. An acceleratory region followed (α = 0.10 - 0.85) which was fitted by the Avrami-Erofe'ev equation, with n = 2 and had an activation energy of 210 kJ mol^{-1}. For the differential experiments, the gas was removed at set intervals. The Avrami-Erofe'ev equation with n = 2 fitted the data for α = 0.20 - 0.88. The activation energy of 130 kJ mol^{-1} was less than that for the accumulatory run, but was close to that found for the initial process.

Dominey *et al* [66] did isothermal experiments on dehydrated Niox (230-260°C) in vacuum. The contracting-area equation (R2) fitted the initial reaction (α < 0.016) with an activation energy of 159 kJ mol^{-1}. The acceleratory reaction overlapped the initial reaction, so corrections were made by extrapolation of the initial reaction. The acceleratory region consists of an induction period (activation energy of 216 kJ mol^{-1}) followed by a region fitted by the power law with n = 3 initially, and later n = 2, with an activation energy of 151 kJ mol^{-1}.

Broadbent *et al* [67] used the Avrami-Erofe'ev equation (n = 2), followed by a first-order decay (F1) to describe the isothermal (270-380°C) decomposition of Niox in nitrogen.

Jach *et al* [68] did isothermal studies on Niox (253-360°C) in vacuum and obtained sigmoidal α - time curves with a gradual approach to an acceleratory region. The first slow linear region had an activation energy of 197 kJ mol^{-1}. The acceleratory region was fitted to the power law (P1) with n approaching 2 and the activation energy was 121 kJ mol^{-1}. This was followed by a first-order decay with an activation energy of 136 kJ mol^{-1}.

Prout and Brown [69] obtained sigmoidal α - time curves for the decomposition of Niox in vacuum, with an initial reaction fitted by the contracting-area equation (R2) and an activation energy of 138 kJ mol^{-1}. The Avrami-Erofe'ev equation fitted the sigmoid region for α = 0.17 - 0.80 and the first-order equation gave a good fit over α = 0.75 - 0.95. The acceleratory region (α = 0.013 - 0.5) was best described by the Prout-Tompkins equation (E_a = 141 kJ mol^{-1}), and the decay period (α = 0.5 - 0.98) by the contracting-volume equation (R3) (E_a = 148 kJ mol^{-1}).

Mu and Perlmutter [60] used the same reaction conditions and method as discussed for the dehydration of Feox, to examine the kinetics of decomposition of Niox. They obtained an activation energy of 766 $\pm$ 1.6 kJ mol^{-1} and A = 1.45×10^{65} s^{-1}, for α = 0.01-0.97 and n = 1. These values are much higher than those reported by other authors .

Literature values of the kinetic parameters for the individual oxalates are summarised in Table 1.5.

Table 1.5.
KINETIC PARAMETERS FOR THE DEHYDRATION AND DECOMPOSITION OF THE INDIVIDUAL OXALATES

T range /°C	Conditions	Models	α-range	E_a/ kJ mol^{-1}	A/s^{-1}	ref
Cuox						
prog. T 1°C min^{-1}	N_2	F2	0.03-0.94	665	1.39×10^{67}	60
247-272						
	accum-	A3	0.2-0.95	136		57
	ulatory	R3	0.68-0.93			
		P1	<0.5			
		(n=2.9)				
		F1	>0.80			
235-261		B1				
	vacuum	An				
		(n=3.57)		128		
		R2				
		A2				
	N_2			193	2.83×10^{14}	62
	air	independent		184	7.14×10^{13}	
	N_2		0.1-0.9	214	1.53×10^{17}	
Feox						
dehydr	N_2	F2/3	0.04-0.99	106	3.33×10^{9}	60
decomp		F2	0.03-0.98	113	2.5×10^{8}	
prog 1°Cmin^{-1}						

Table 1.5 continue

T range /°C	Conditions	Models	α-range	E_a/ kJ mol^{-1}	A/s^{-1}	ref
Coox						
dehydr	air	C-R		91	7.47×10^{8}	61
		F1		92	1.72×10^{9}	
		R2		89	4.22×10^{8}	
		R3		90	3.25×10^{8}	
	N_2	F1	0.04-0.94	158	5.37×10^{15}	60
decomp		F2	0.02-0.97	198	1.11×10^{15}	
prog T 1°Cmin^{-1}						
297-315	vacuum	induction period		204		63
dehydr. at 150°C		E1	0.0-0.50			
		linear	0.50-0.90			
		F1	0.90-0.95			
dehydr. at 200°C		induction period		225		
		E1	0.0-0.50			
		B1	0.25-0.95	165		
317-427						
coarse		A2				
<352°C				195		64
>352°C				57		
fine		A3				
<392°C				120		
>392°C				59		
Niox						
dehydr	N_2	F2	0.06-0.95	253	7.93×10^{24}	60
decomp		F1	0.01-0.97	766	1.45×10^{65}	
prog T 1°Cmin^{-1}						
245-260	accum-	R2	0.0-0.0085	141		65
hydrate	ulatoty	A2	0.10-0.85	210		
	differential	A2	0.20-0.88	130		
			0.05-0.80	138		
dehydr	vacuum					
230-260		R2	<0.016	159		66
		induction period		216		
		P1		151		

The variety of kinetic models found to be applicable and the range of Arrhenius parameters derived illustrate the problems discussed above of defining reactant preparations and reaction conditions. Physical variability is further complicated by the mathematical problems of deciding on adequacy of fit of a kinetic model.

1.9 AIMS OF THE RESEARCH

Previous investigations [70-72] have shown that mixed metal oxalates generally decompose endothermically in inert atmospheres even when copper is one of the metals present, in contrast to the decomposition of Cuox which is exothermic, in inert atmospheres. The structure of copper oxalate is reported to differ from that of iron, cobalt and nickel oxalates, so the thermal behaviour of mixed metal/copper oxalates, $FeCu(ox)_2$, $CoCu(ox)_2$ and $NiCu(ox)_2$, should be of interest because these mixed oxalates apparently adopt the same structure as iron, cobalt and nickel oxalate, rather than that of Cuox.

The investigation was also aimed at determining the effects of varying M in $MCu(ox)_2.xH_2O$ on the thermal stability of the mixed oxalate.

CHAPTER 2 EXPERIMENTAL

2.1 PREPARATION

Individual oxalates

The individual oxalates, $Mox.2H_2O$ (where M= Zn, Co and Ni) and Cuox were prepared by dissolving 0.01 mole of the metal sulphate in 50 mL deionised water, and then adding, dropwise from a burette, a dilute solution of 0.01 mole of potassium oxalate in 80 mL of water. The oxalate was added very slowly to obtain the maximum particle size and product purity. During addition the solution was constantly stirred and heated. The precipitate was filtered, washed with water, and left to dry at room temperature.

For the preparation of $Feox.2H_2O$, the same procedure as for the other oxalates was followed, using 0.01 mole of $(NH_4)_2Fe(SO_4)_2$. The whole reaction was done under nitrogen, to prevent the iron from oxidising to Fe(III).

Mixed oxalates

$FeCu(ox)_2.3H_2O$

0.02 mole of potassium oxalate was dissolved in 2 L of water. Nitrogen was bubbled through the solution for 5 minutes to remove all oxygen trapped in the reaction vessel. The rest of the reaction was done under nitrogen. A solution of 0.01 mole of copper sulphate in 50 mL of water was slowly added, dropwise from a burette. The reactants were constantly stirred and heated, to form an aqueous solution of dioxalato cuprate ($[Cu(ox)_2]^{2-}$). Subsequently a solution of 0.01 mole of iron sulphate in 50 mL of water was also added dropwise. A green precipitate formed and the mixture was allowed to cool to room temperature. It was then filtered, washed with water and left to dry.

$CoCu(ox)_2.3H_2O$

The same procedure was followed as for $FeCu(ox)_2.3H_2O$, except that it was not necessary to do the preparation under N_2. It is important to note that a very dilute

solution of potassium oxalate was used, otherwise a product containing excess copper was obtained.

$NiCu(ox)_2.3.5H_2O$

The same procedure was followed as above, but in this case a solution of 0.01 mole of $CuSO_4.5H_2O$ in 50 mL of water was added to an aqueous solution (approximately 0.01 mole in 2L) of dioxalato nickelate ($[Ni(ox)_2]^{2-}$).

Physical mixtures

Physical mixtures of the individual oxalates were prepared by gently grinding equimolar quantities of Cuox and one of the other oxalates ($Feox.2H_2O$, $Coox.2H_2O$ or $Niox.2H_2O$) together.

2.2 COMPOSITIONAL ANALYSIS

Atomic Absorption Spectroscopy

The amounts of metal in the samples were determined by atomic absorption spectroscopy (AAS). The samples were dissolved in dilute H_2SO_4 and heated until fuming. 10 mL of concentrated HNO_3 was then added, to destroy the oxalate ion, which was found by Spears [71] to interfere with the analysis. The solution was then diluted for atomic absorption analysis.

The results obtained from the use of calibration curves were found to be consistently high. This was thought to be due to matrix effects. To overcome these effects a standard addition method was used. Measured volumes of standard solutions were added directly to known quantities of the sample solution and the sample concentrations were determined by extrapolation. These results compared favourably with other results, obtained from titrimetric and electrogravimetric determinations.

Titrimetric analysis

The copper oxalate was titrated with a 0.02 mol L^{-1} $KMnO_4$ solution, which was standardised with a sodium oxalate solution. This titration gave the amount of oxalate present in copper oxalate. The same procedure was used to determine the amount of oxalate in $Coox.2H_2O$, $Niox.2H_2O$, $Znox.2H_2O$, $CoCu(ox)_2.3H_2O$ and $NiCu(ox)_2.3.5H_2O$.

Since Fe(II) is oxidised to Fe(III) by $KMnO_4$, the oxalate determination of $Feox.2H_2O$ and $FeCu(ox)_2.3H_2O$ could not be done directly. Instead, the $Feox.2H_2O$ sample was first titrated with $KMnO_4$ to obtain the total amount of Fe^{2+} and $C_2O_4^{2-}$. The Fe^{3+} formed through oxidation by $KMnO_4$ was then reduced to Fe^{2+}, using the tin(II) chloride method. The amount of iron in solution was then obtained by titration with a standardised $K_2Cr_2O_7$ solution. The amount of oxalate present could be determined by difference. Tin(II) chloride reduces Cu^{2+} to Cu^+ and hence, for the $FeCu(ox)_2.3H_2O$ sample, the copper was first removed by electrodeposition and then the tin(II) chloride method was applied, followed by $K_2Cr_2O_7$ titration of the remaining iron-containing solution.

Electrogravimetric analysis

A sample of $FeCu(ox)_2.3H_2O$ was dissolved in a hot mixture of concentrated sulphuric acid and concentrated nitric acid. After dissolution, about 1 g of urea was added to remove oxides of nitrogen. Platinum gauze electrodes were used and the electrolysis was done at an applied voltage of about 2 to 4 V to obtain a current of 2 to 4 A. The electrolysis was continued for about 1 h, until all the copper was deposited onto the cathode. The electrode was weighed and the percentage copper was determined. The remaining solution was analysed for iron, as described above.

The water content of all the samples was calculated by difference.

2.3 STRUCTURAL ANALYSIS

Infrared Spectroscopy

The infrared spectra of the compounds, using the KBr technique, in the range 4000 cm^{-1} to 200 cm^{-1} were recorded on a Perkin Elmer IR180 Spectrophotometer. Spectra recorded on the same samples, using the Nujol Mull method did not show any differences.

2.4 X-RAY POWDER DIFFRACTION

X-ray powder diffraction photographs were obtained by exposing samples of Cuox, $Niox.2H_2O$, $NiCu(ox)_2.3.5H_2O$, $Feox.2H_2O$ and $FeCu(ox)_2.3H_2O$ to copper K_α radiation for four hours. Co absorbed copper K_α radiation, so cobalt K_α radiaton was used for $Coox.2H_2O$ and $CoCu(ox)_2.3H_2O$. The samples were packed in 0.6 mm borosilicate tubes, and placed in a Phillips camera, with a radius of 29 mm, lined with AFGA CURIX X-ray film. X-ray powder diffractometer traces were also obtained, using a Philips automatic diffractometer, and a Co source with a Fe filter. The source was set on 20 mA and 40 kV, with a range of $4x10^3$ counts s^{-1} and a time constant of 1 second. The chart speed was 10 mm min^{-1}. A layer of about 1 mm of sample was packed in an aluminium tray with a Perspex backing. The samples were scanned over a 2θ range of 19-90°.

2.5 THERMAL ANALYSIS

The oxalate samples were examined using thermogravimetry (TG), thermomagnetometry (TM) and differential scanning calorimetry (DSC), on Perkin Elmer Delta Series 7 instruments, in nitrogen or oxygen atmospheres.

The TG furnace was calibrated using the Curie point method. Alumel(163°C) and Nickel(354°C) were used in a two-point calibration for runs up to 500°C and Nickel and Iron (780°C) for runs up to 800°C.

Platinum sample pans with sample masses of 1 - 5 mg were used for TG, and aluminium sample pans, covered but not crimped, for DSC. The possibility of catalysis of any of the processes studied, by the materials of the sample containers was not ruled out. Unless otherwise stated, the heating rate was maintained constant at 20°C min^{-1}. The magnet used for the Curie point calibration of the TG furnace was similarly positioned for TM experiments. The temperature range for most of the TG experiments was 50 - 500°C and this was extended to 850°C for some of the TM experiments on Fe-containing compounds. The main magnetic transitions of interest are the Curie transitions of Fe (780°C), Fe_3O_4 (580°C), and Ni (354°C).

2.6 EVOLVED GAS ANALYSIS

Quadrupole mass spectrometry

Samples of each oxalate (1.0 - 2.5 mg) were first dehydrated and then decomposed at low pressure ($3x10^{-5}$ - $2x10^{-4}$ torr) in a continuously-pumped glass vacuum system linked directly to a quadrupole mass spectrometer (Anavac-2). The peaks 16 through 46 amu were continuously scanned, in the 10^{-5} torr range. The furnace temperatures were kept constant until the rate of gas evolution, with continuous pumping, decreased to low levels. The furnace temperature was then slowly increased until no further gas evolution was detected.

Thermal Conductivity Detection

Additional programmed temperature (20°C min^{-1}) and isothermal DSC experiments in N_2 were done using a thermal conductivity detector (TCD) on the exit gas stream, combined for some experiments with a liquid nitrogen trap to condense the CO_2 from the CO. Similar experiments were carried out using CO_2 as the carrier gas so that any evolution of CO, in the presence of an excess of CO_2, could be detected more clearly. Zinc oxalate was used as a reference material in the TCD experiments, on the assumption that equimolar quantities of CO and CO_2 are likely to be formed under non-oxidising

conditions [1].

Since Znox decomposes to form equimolar quantities of CO and CO_2, the percentages of CO and CO_2 evolved, during decomposition in N_2, could be estimated. The relative peak area obtained in the TCD experiments in the presence of a cold trap was related to one molar quantity of CO, and after removal of the cold trap to CO_2. Peak areas obtained without the presence of a cold trap were related to equimolar quantities of CO and CO_2. In a CO_2 atmosphere the amount of CO evolved by a sample was estimated by comparing the peak area obtained for the sample with that found for Znox (i.e. one mole of CO evolved).

CHAPTER 3 COMPOSITIONAL AND STRUCTURAL INVESTIGATION

3.1 COMPOSITIONAL ANALYSIS

The results obtained from the compositional analysis are compared with the calculated percentages in Table 3.1.

Table 3.1.
COMPOSITIONAL ANALYSIS OF THE INDIVIDUAL AND MIXED OXALATES

COMPOUND	%M where M= Fe, Co, Ni, Zn	%Cu	%ox	%H_2O by difference
Cuox calc.		43.9 41.9	56.2 58.1	
Feox.$2H_2O$ calc.	30.9 31.1		47.8 48.9	21.1 20.0
$FeCu(ox)_2.3H_2O$ calc.M=Fe	15.6 15.9	17.4 18.2	51.8 50.4	15.2 15.4
Coox.$2H_2O$ calc.	31.6 32.2		47.2 48.1	21.2 19.7
$CoCu(ox)_2.3H_2O$ calc.M=Co	16.7 16.7	18.1 18.0	49.9 49.9	15.3 15.3
Niox.$2H_2O$ calc.	30.8 32.1		45.9 48.2	23.3 19.7
$NiCu(ox)_2.3.5H_2O$ calc.M=Ni	16.7 16.2	16.6 17.5	48.4 48.7	18.3 17.4
Znox.$2H_2O$ calc.	35.0 34.5		46.4 46.5	18.6 19.0

3.2 INFRARED ANALYSIS

There was no indication of residual SO_4^{2-} from the method of preparation in any of the spectra recorded. C-O stretching bands were observed at ~1325 cm^{-1} and 1375 cm^{-1}.

These closely spaced bands indicate the presence of bridging oxalates, with all four oxygens coordinated to metal ions, in all the oxalates. Terminal oxalates would show peaks at 1317 cm^{-1} and 1420 cm^{-1} corresponding to the C=O and C-O-M stretching frequencies [73]. A summary of the peaks obtained for the different oxalates appears in Table 3.2.

Table 3.2.
INFRARED BAND FREQUENCIES (cm^{-1}) OBTAINED FOR THE INDIVIDUAL AND MIXED OXALATES

band	Feox	Coox	Niox	Cuox	Znox	FeCu	CoCu	NiCu
ν7+ν1	1640	1620	1640	1670	1640	1650	1670	1620
ν2	1365	1360	1370	1370	1370	1370	1370	1360
ν8	1325	1315	1330	1330	1320	1325	1325	1320
ν9	830	830	840	830	825	835	830	825
ν4	500	495	500	510	495	515	515	490
ν10					450	500	500	
ν11	385	380	370	390				
ν5	375		340					

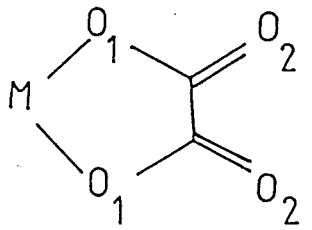

Nakamoto [74] investigated some di- and trivalent metal oxalato- complexes. He found that a linear relationship exists between ν4 (predominantly M-O stretch) and the average of ν1 and ν7 (both are C-O_2 stretching) and between ν4 and either ν2 or ν8 (both are predominantly C-O_1 stretching). For some divalent oxalato-complexes (Zn, Cu, Pt and Pd) the average of ν1 + ν7 increased as ν4 increased, and ν8 decreased as ν4 increased. These results supported the theory that as the M-O bond becomes stronger, the C-O_1 becomes weaker and the C-O_2 and C-C bonds become stronger. In the metal oxalates (Mox) C-O_1 and C-O_2 cannot be so clearly distinguished, since the metal oxalates have polymeric structures, where the oxalate ion is bound to two metal ions.

For the individual oxalates, under investigation in our research, it was found that ν4 increased in the order Co = Zn < Fe = Ni < Cu. From Table 3.2 it is clear that the

average of $\nu 1 + \nu 7$ increased as $\nu 4$ increased, and $\nu 8$ increased as $\nu 4$ increased. In both cases a roughly linear relationship was observed. Looking at the mixed oxalates, $\nu 4$ for $NiCu(ox)_2.3.5H_2O$ was much lower than that observed for $FeCu(ox)_2.3H_2O$ and $CoCu(ox)_2.3H_2O$ (which were equal). This is the same trend as that observed for the covalent radii and first ionization potentials of Ni, Fe and Co, see Table 3.3.

Table 3.3.
PROPERTIES OF THE METALLIC ELEMENTS, M IN Mox [77]

M	Covalent radius / nm	1st ionisation energy / kJ mol^{-1}
Co	0.126	758
Ni	0.121	737
Fe	0.125	759

3.3 X-RAY POWDER DIFFRACTION

From the X-ray powder photographs, $Feox.2H_2O$, $FeCu(ox)_2.3H_2O$, $Coox.2H_2O$, $CoCu(ox)_2.3H_2O$, $Niox.2H_2O$ and $NiCu(ox)_2.3.5H_2O$, appear to be isomorphous and are presumably isostructural. The pattern for Cuox was different, which suggests that Cuox has a different structure from the structure of the oxalates of other transition metal elements under investigation, and that copper takes up the more usual structure when it is coprecipitated with Fe, Co or Ni. This observation was confirmed by examination of the X-ray powder diffractometer traces. From Table 3.4 it is clear that the same d-spacings are observed for $Feox.2H_2O$, $Coox.2H_2O$, $Niox.2H_2O$ and $Znox.2H_2O$, with different intensities of the peaks (see Appendix for traces of d-spacings). This means that the coordination geometry of the different metal oxalates are the same, but that the atomic coordinates in the unit cells differ. The line at d = ~3.6 Å was not observed for $Niox.2H_2O$ and had a maximum intensity for $Znox.2H_2O$ of 14%. The pattern for Cuox was very different from that of the other oxalates, with its maximum occurring at a lower d-spacing (d = ~3.9 Å) than the other oxalates (d = 4.8 Å).

$FeCu(ox)_2.3H_2O$ seems to have coprecipitated Cuox present as an impurity (see also section 4.2, Thermal Analysis). This is evident from a very strong peak (intensity

83.6%) at d = 3.9 Å, and the presence of peaks at d = 2.14, 2.32, 2.50, 2.43, 2.82 and 2.99 Å. Other than these peaks, $FeCu(ox)_2.3H_2O$ exhibits the same peaks as $Feox.2H_2O$ and it can be concluded that $Feox.2H_2O$ and $FeCu(ox)_2.3H_2O$ are isomorphous. $CoCu(ox)_2.3H_2O$ also contains some Cuox as an impurity, but much less than in $FeCu(ox)_2.3H_2O$. The peaks corresponding to Cuox are d= 2.14, and 2.98 Å. All the other peaks correspond to those observed in $Coox.2H_2O$ and the other individual oxalates. $NiCu(ox)_2.3.5H_2O$ exhibits peaks at exactly the same d-spacing as $Niox.2H_2O$. It is therefore isomorphous with $Niox.2H_2O$ and probably isostructural.

The X-ray powder diffraction data for the different oxalates are summarised in Table 3.4.

Table 3.4.
X-RAY POWDER DIFFRACTION DATA FOR THE INDIVIDUAL OXALATES

Feox		Coox		Niox		Znox	
d/Å	I/I_o	d/Å	I/I_o	d/Å	I/I_o	d/Å	I/I_o
4.87	100	4.82	100	4.74	100	4.76	100
		4.19	5				
3.92	14	3.91	19	3.89	22	3.95	25
3.64	1	3.57	2			3.60	15
3.34	3						
3.12	24	3.00	17	2.94	24	2.98	41
						2.72	6
				2.66	2	2.67	12
2.59	13	2.58	20	2.52	10	2.57	20
2.39	4	2.39	4	2.38	2	2.36	3
2.26	3	2.29	2				
		2.23	5	2.20	6	2.24	13
						2.16	4
2.12	9	2.08	9	2.06	9	2.09	12
						2.05	4
1.99	7					2.00	4
1.94	2	1.94	6	1.94	2	1.97	3
				1.90	7	1.92	11
1.89	8	1.88	10	1.86	8	1.89	14
1.83	2	1.79	6			1.80	6
				1.79	3	1.78	9
						1.69	2
						1.64	3
1.62	3	1.59	3	1.57	5	1.59	5
1.52	2			1.51	2		
		1.48	2	1.46	3	1.48	4
						1.43	2

X-RAY POWDER DIFFRACTION DATA FOR THE MIXED OXALATES

FeCu		CoCu		NiCu	
d/Å	I/I_o	d/Å	I/I_o	d/Å	I/I_o
4.78	100	4.78	100	4.80	100
3.91	84	3.91	46	3.94	21
3.60	19	3.59	4	3.60	3
3.15	3	2.98	38	3.00	24
(2.99)	(58)				
(2.82)	(3)				
2.75	4				
2.66	19	2.68	4	2.67	3
2.59	14	2.56	13	2.54	10
(2.50)	(9)	(2.55)	(6)		
2.43	4	2.41	4	2.40	3
2.38	3				
2.32	5	2.32	5		
2.25	12	2.22	11	2.21	5
2.18	3				
(2.14)	(4)	(2.14)	(4)		
2.10	8	2.08	9	2.08	8
2.04	6				
2.00	4				
1.94	11	1.93	9	1.94	7
1.89	13	1.88	9	1.87	7
1.81	13	1.79	9	1.78	4
1.72	3	1.76	8	1.76	3
1.65	4				
		1.59	4	1.59	4
		1.48	3	1.48	3

Values in brackets indicate d-spacings due to coprecipitated Cuox.

X-RAY POWDER DIFFRACTION DATA FOR Cuox

Cuox	
d/Å	I/I_o
3.91	100
2.84	6
2.51	14
2.42	5
2.32	8
2.14	5
1.95	7
1.79	11
1.76	12
1.52	4
1.46	3

CHAPTER 4 THERMAL ANALYSIS

4.1 PRELIMINARY DEHYDRATION

All of the oxalates, individual and mixed, except for Cuox, contain water (Table 4.1) which is lost on heating in N_2 or O_2, or under reduced pressure (10^{-5} torr), at temperatures below the onset of decomposition. The composition of copper oxalate has been given as Cuox.0.5H_2O and Cuox.0.3H_2O [51]. It appears that small non-stoichiometric quantities of water may be entrained in the crystal lattice depending on the method of preparation. In this investigation no evidence of appreciable quantities of water was found in the elemental analysis or thermal analysis of the Cuox sample prepared. The characteristics of the dehydration stages for the oxalates studied, obtained from TG and DSC measurements, and in the continuously evacuated system, are summarised in Table 4.1.

Table 4.1

DEHYDRATION OF THE INDIVIDUAL AND MIXED OXALATES

Compound Mox.$2H_2O$	Onset /°C	%Mass loss	ΔH /kJ mol^{-1}	T range/ °C low pressure
M = Fe				
N_2	162	19.4	100 ± 1	125 - 135
O_2	173	20.7	128 ± 7	
-$2H_2O$ calc.		20.0		
M = Co				
N_2	175	18.3	102 ± 3	145 - 150
O_2	181	18.0	141 ± 5	
-$2H_2O$ calc.		19.7		
M = Ni				
N_2	214	19.4	131 ± 2	120 - 140
O_2	215	19.1	144 ± 6	
-$2H_2O$ calc.		19.7		
M = Zn				
N_2	142	18.6	125 ± 1	
O_2	147	17.8	122 ± 3	
-$2H_2O$ calc.		19.0		
$MCu(ox)_2.nH_2O$				
M = Fe				
N_2	139	14.4	227 ± 2	110 - 150
O_2	138	14.2	149 ± 3	
-$3H_2O$ calc.		15.5		
M = Co				
N_2	141	14.6	226 ± 5	140 - 150
O_2	142	14.2	197 ± 15	
-$3H_2O$ calc.		15.5		
M = Ni				
N_2	202	17.3	204 ± 5	170 - 180
O_2	179	17.2	180 ± 4	
-$3.5H_2O$ calc.		17.5		

4.2 DECOMPOSITION

Individual oxalates

Cuox

Thermogravimetry

Copper oxalate is anhydrous and the TG curve at 20°C min^{-1} (Figure 4.1) shows only one decomposition step of 55.9% in nitrogen, with onset at ~260°C. The calculated mass loss for formation of copper metal = 58.0%. In oxygen, the mass loss was 51.8%, with onset at ~297°C. This corresponds to formation of Cu_2O (calculated residue = 47.2%). This is in agreement with the findings of Broadbent *et al* [32].

Differential scanning calorimetry

The DSC curves for Cuox heated in N_2 and O_2 at 20°C min^{-1} are shown in Figure 4.2. In N_2, there is a strong exotherm with onset at ~290°C with ΔH = -33 kJ mol^{-1}. In O_2, this exotherm is in the same temperature range, but the ΔH value has increased to -138 kJ mol^{-1}. These results are similar to those obtained by Dollimore and Griffiths [19].

Evolved gas analysis

Under reduced pressure, decomposition of Cuox took place between 300-330°C. A small amount of H_2O was detected. Cuox is usually reported as evolving only CO_2. The ratio of CO_2:CO, however, was found to range between 3:2 at the start of decomposition (300°C) and 2:1 towards the end (325°C). Overall, between 33-40% of the evolved gas is CO, while CO_2 constitutes the other 60-67%.

TCD results confirmed the evolution of CO during decomposition in N_2 and the proportion was 52% CO. In CO_2, the proportion dropped to about 2%. Thermochemical calculations on the DSC results (section 5.1) suggest formation of some Cu_2O.

Figure 4.1. TG of Cuox (a) in N_2 (b) in O_2 at 20°C min^{-1}

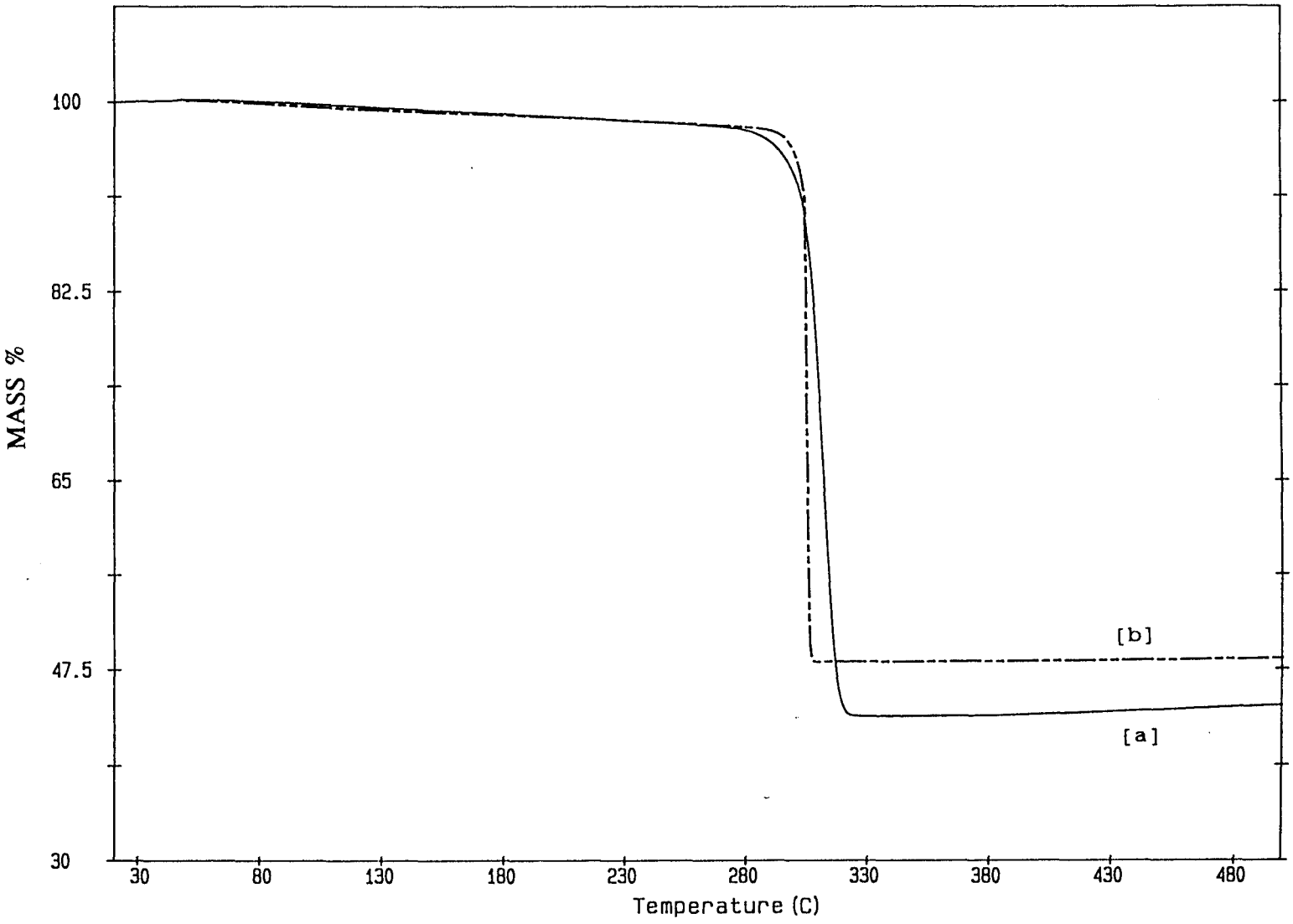

Figure 4.2. DSC of Cuox (a) in N_2 (b) in O_2 at 20°C min^{-1}

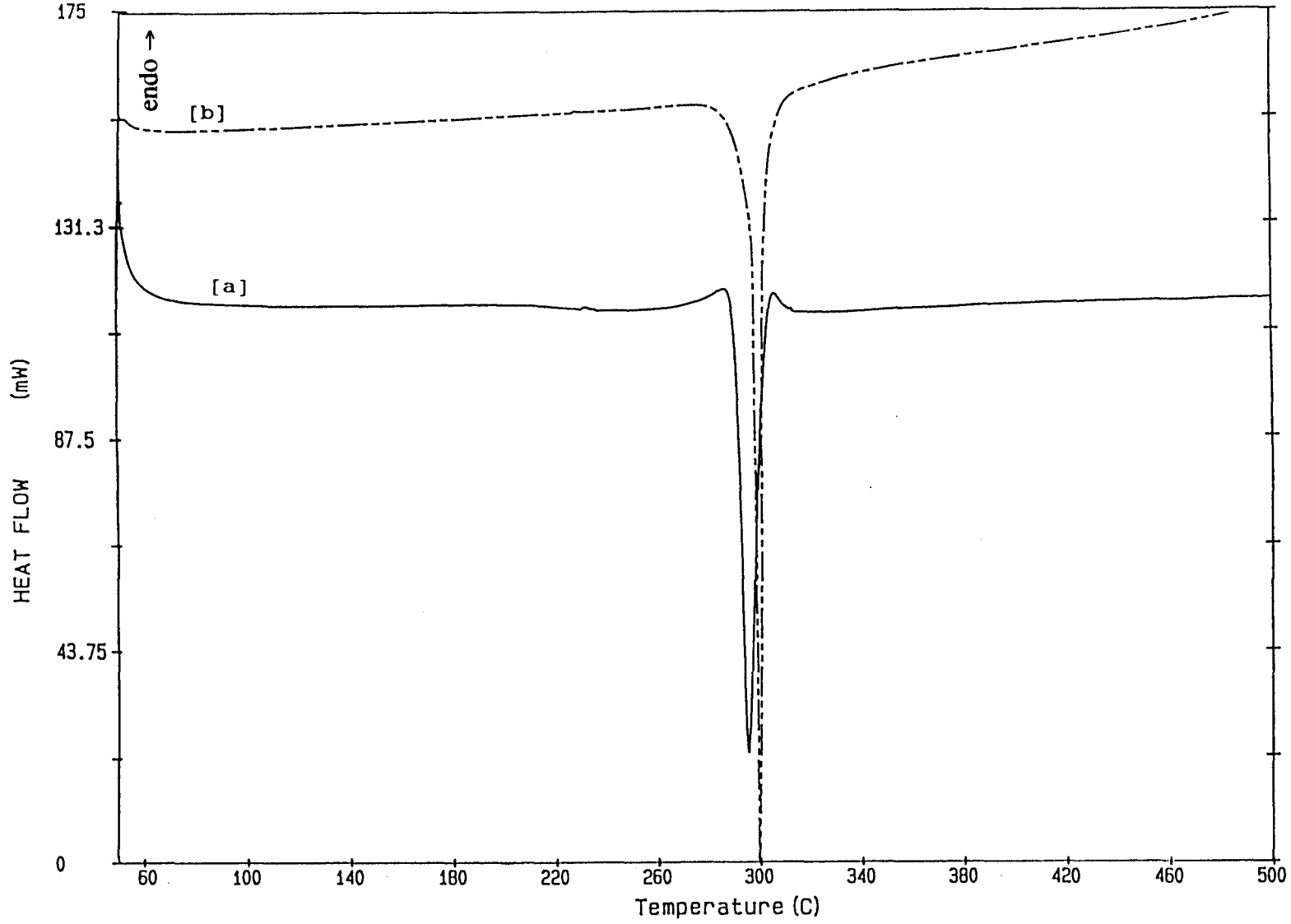

Feox

Thermogravimetry

TG curves (Figure 4.3) in N_2 at 20°C min^{-1} showed that dehydration began at 162°C and resulted in a mass loss of 19.4%. In O_2, dehydration occurred at 173°C with a loss mass of 20.7%. The calculated mass loss for $2H_2O$ is 20.0%. Decomposition in N_2 began at ~310°C and was complete by 435°C. The residue was 39.6% of the original sample mass, which corresponds most closely to the formation of FeO (calculated residue 40.0%) with the loss of CO and CO_2. In O_2, the onset temperature is ~210°C and the residue is Fe_2O_3 (mass found 46.0%, calculated 44.4%).

Differential scanning calorimetry

The corresponding DSC curves at 20°C min^{-1} for Feox are shown in Figure 4.4. The dehydration endotherm varied slightly: onset 162°C, ΔH = 100 kJ mol^{-1} in N_2, and onset 173°C, ΔH = 128 kJ mol^{-1}, in O_2. Dehydration was followed by a decomposition endotherm with onset ~367°C and ΔH = 130 kJ mol^{-1} in nitrogen. In O_2, the reaction is strongly exothermic, ΔH = -250 kJ mol^{-1}, with onset temperature lowered to ~226°C.

Thermomagnetometry

The TM curve (Figure 4.5) of the decomposition product of Feox in N_2 shows a sharp weight loss, onset ~605°C, which is assumed to correspond to the Curie transition of Fe_3O_4 (580°C). There was no sign of the Curie transition of Fe at 780°C. FeO is reported [47,49,75] to disproportionate ($4FeO \rightarrow Fe_3O_4 + Fe$) on cooling.

Evolved gas analysis

Under reduced pressure at 334°C, initially three times more CO_2 than CO was evolved. The rate of evolution of CO then increased and the ratio of CO_2:CO was 2:1 at maximum evolution (340°C). Overall, CO formed 25-30% of the gaseous product and CO_2 70-75%.

TCD results in CO_2 gave similar proportions (28%) of CO, but in N_2 the proportion of CO increased to 70%.

Figure 4.3. TG of Feox.$2H_2O$ (a) in N_2 (b) in O_2 at 20°C min^{-1}

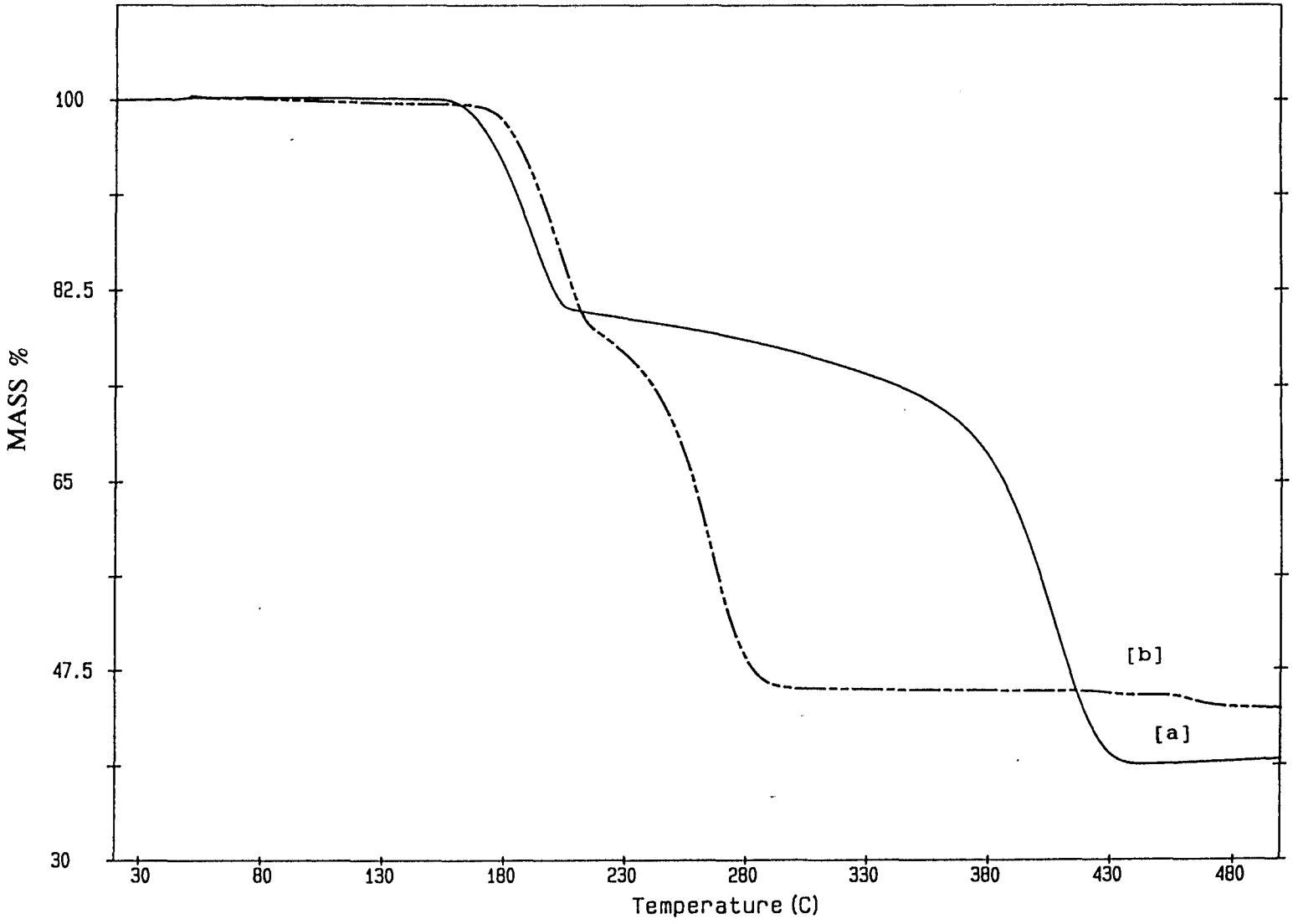

Figure 4.4. DSC of Feox.$2H_2O$ (a) in N_2 (b) in O_2 at 20°C min^{-1}

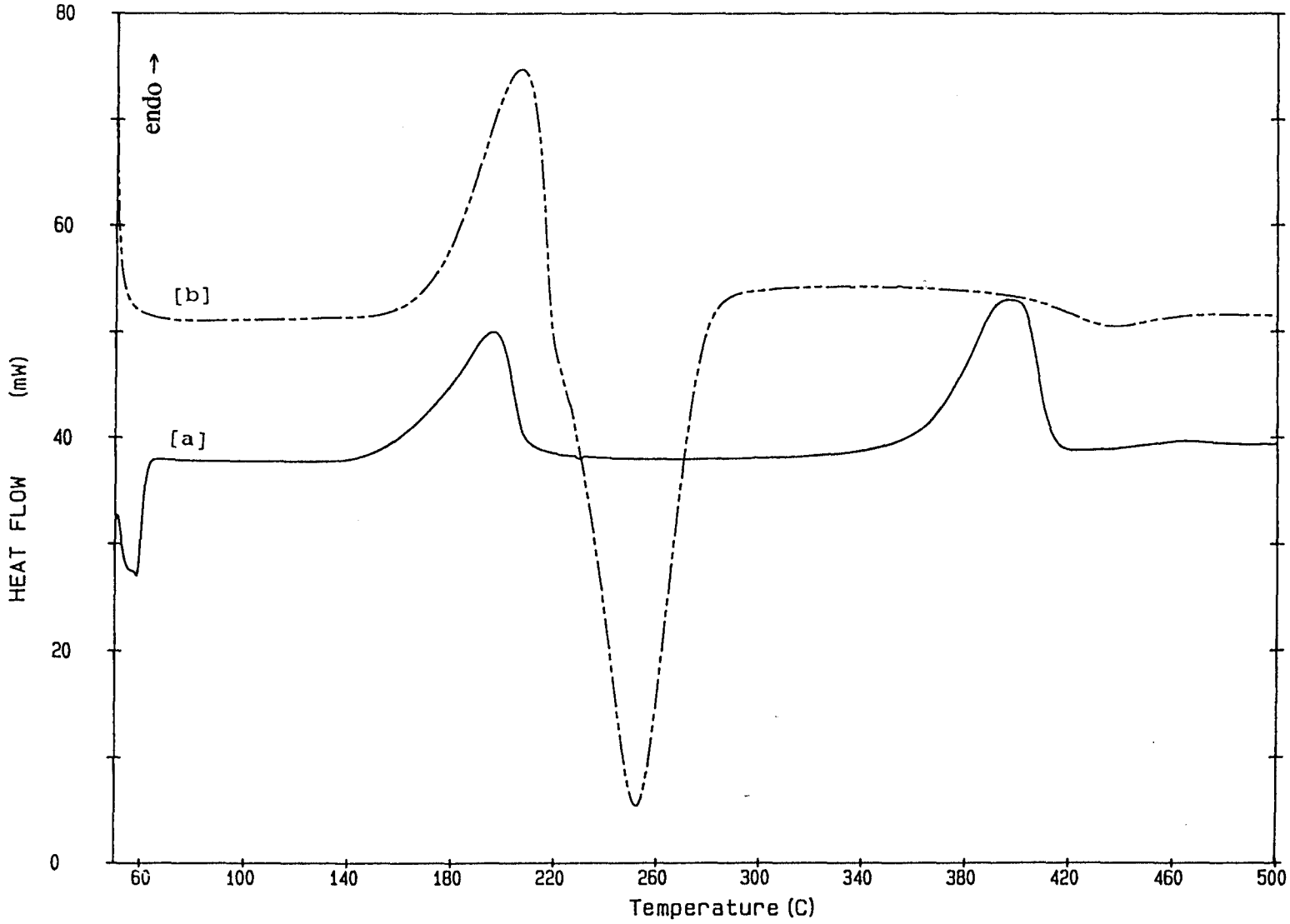

Figure 4.5. TM of Feox.$2H_2O$ in N_2 at 20°C min^{-1}

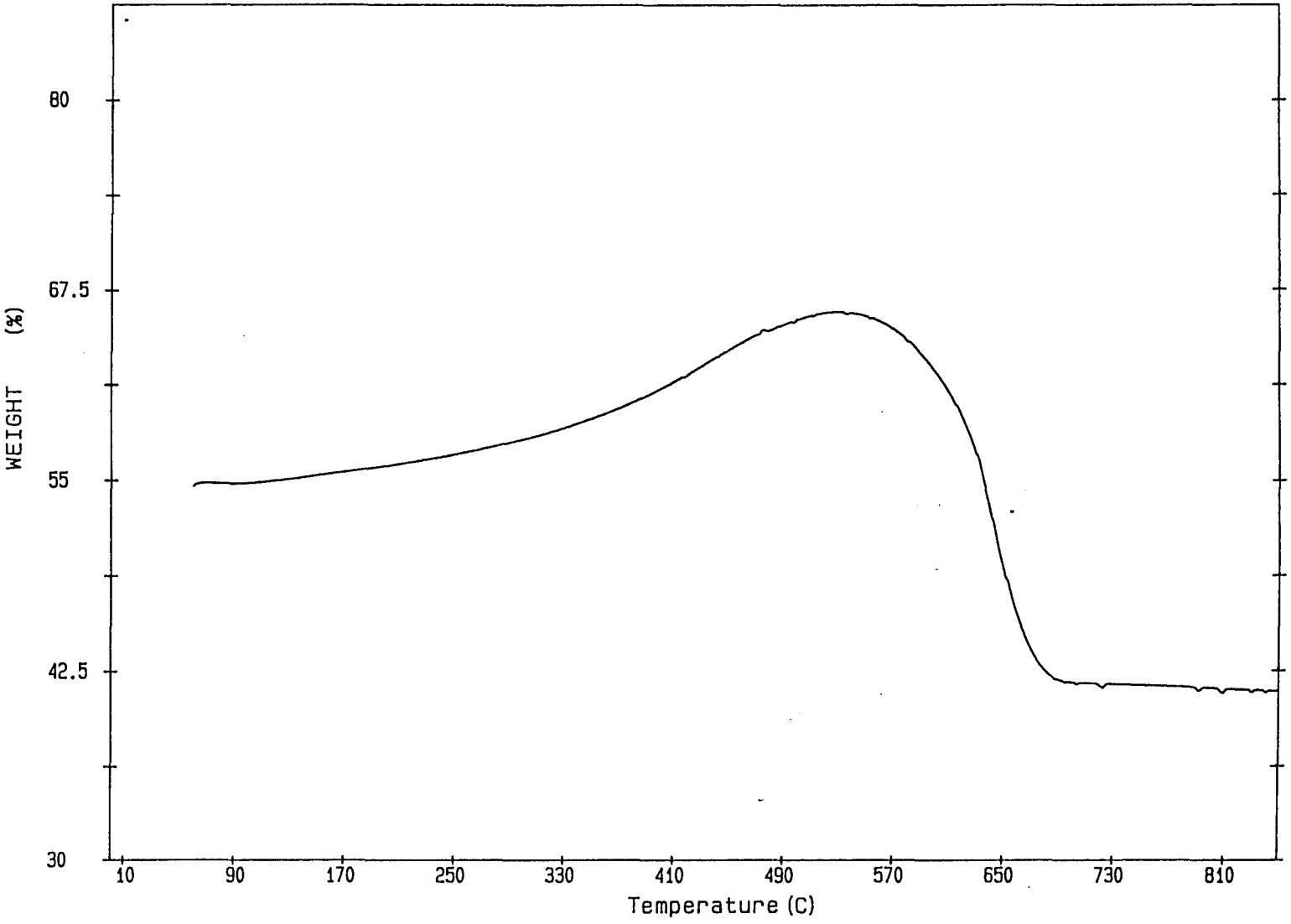

Coox

Thermogravimetry

The TG curves for Coox heated at 20°C min^{-1} are shown in Figure 4.6. A dehydration step at 175°C of 18.3% in N_2, and at 181°C of 18.0% in O_2, was observed. In nitrogen, decomposition started at about 340°C and was complete by 430°C. The mass of the residue was 34.8% which corresponds to the formation of Co (calculated residue 32.2%) with loss of $2CO_2$. In oxygen the onset is about 280°C and the residue is Co_3O_4 (mass found 46.2%, calculated 43.9%).

Differential scanning calorimetry

The DSC curves for Coox heated at 20°C min^{-1} are shown in Figure 4.7. The dehydration endotherm in N_2 of 102 kJ mol^{-1} has an onset of 175°C. In oxygen the dehydration endotherm has an onset of 181°C and ΔH = 141 kJ mol^{-1}. In nitrogen, in addition to the dehydration endotherm, an endotherm with onset 355°C and ΔH = 97.5 kJ mol^{-1} was observed for the decomposition step. In oxygen the reaction is strongly exothermic, ΔH = -265 kJ mol^{-1}, with onset temperature lowered to 286°C.

Evolved gas analysis

Decomposition, under reduced pressure, of previously dehydrated Coox commenced at about 330°C. Both the partial pressures of CO and CO_2 rose to a maximum at 338°C and then dropped until the end of decomposition at 342°C. Between 334 and 340°C the ratio of CO_2:CO ranged between 3:1 and 5:1. By the end of decomposition the ratio was 1:2. CO_2 is thus the major decomposition product, but CO constitutes between 15 and 20% of the evolved gas.

TCD results in N_2 and in CO_2 showed no detectable CO.

Figure 4.6. TG of Coox.$2H_2O$ (a) in N_2 (b) in O_2 at 20°C min^{-1}

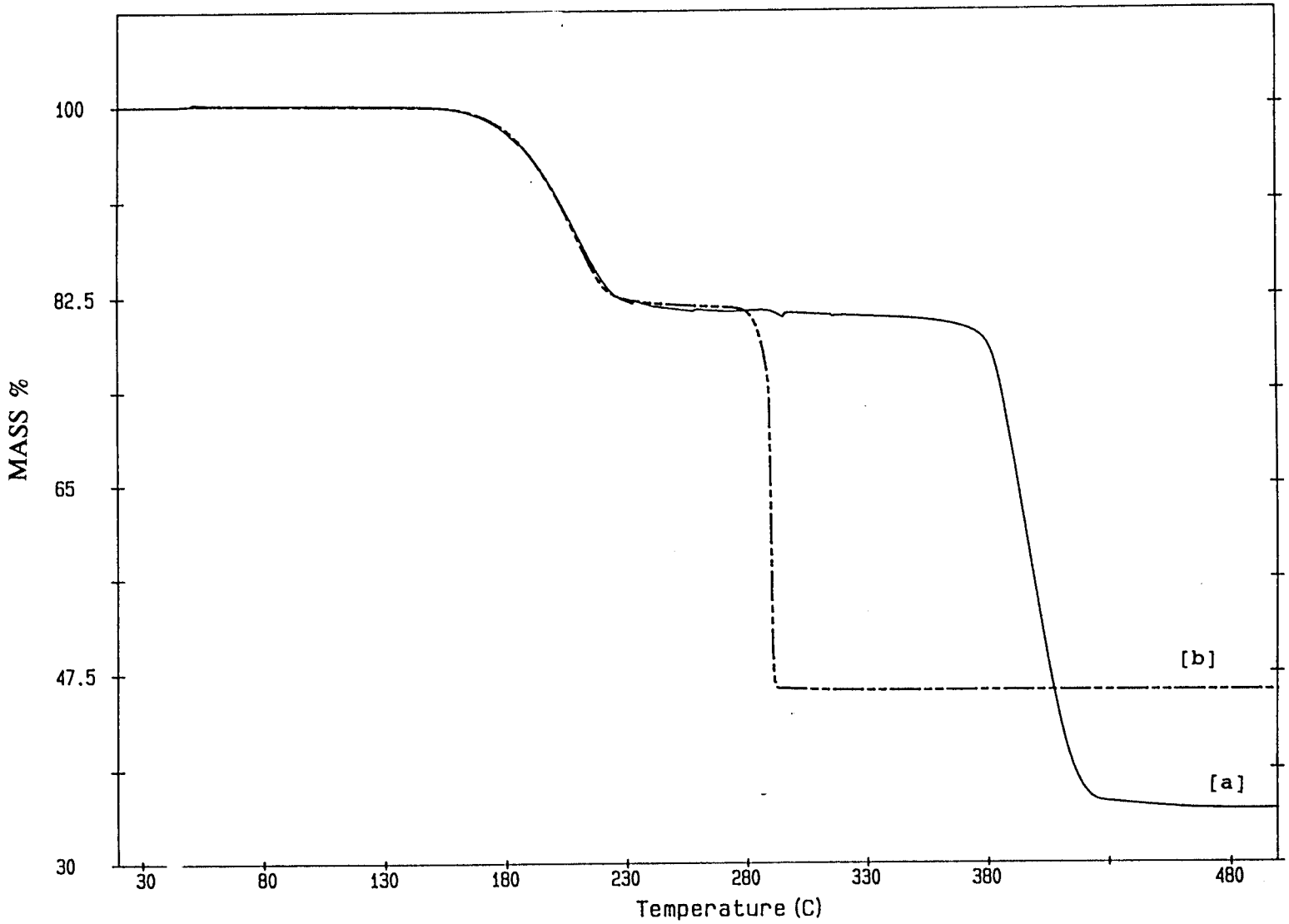

Figure 4.7. DSC of Coox.$2H_2O$ (a) in N_2 (b) in O_2 at 20°C min^{-1}

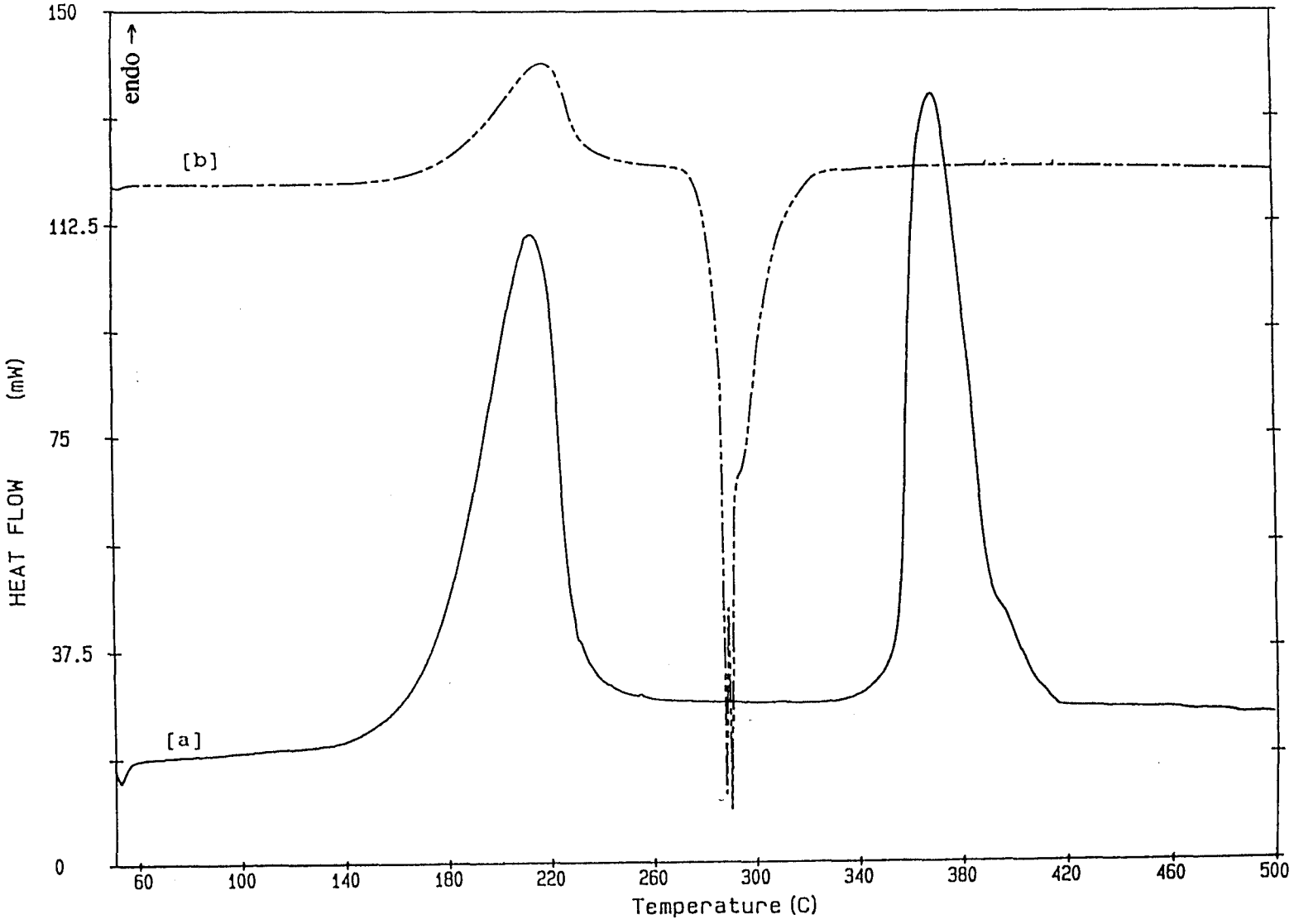

Niox

Thermogravimetry

The TG curves for Niox heated at 20°C min^{-1} in N_2 and O_2 can be seen in Figure 4.8. Dehydration occurs at ~ 215°C with a mass loss of 19.4% in nitrogen and 19.1% in oxygen. In nitrogen, decomposition started at about 330°C and was complete by 410°C. The mass of the residue, 32.5%, corresponds to the loss of $2CO_2$ to form Ni (calculated residue 32.1%). In oxygen the onset is about 338°C and the residue is NiO (mass found 38.2%, calculated 41.0%).

Differential scanning calorimetry

The DSC curves for Niox heated at 20°C min^{-1} are shown in Figure 4.9. A dehydration endotherm of 131 kJ mol^{-1} in N_2 and 144 kJ mol^{-1} in O_2 was observed at about 215°C. In nitrogen, the dehydration endotherm is followed by an endotherm with overlap from a weak exotherm (onset 331°C and ΔH = 71.0 kJ mol^{-1}). In oxygen, reaction is strongly exothermic, ΔH = -193 kJ mol^{-1}, with onset at 338°C.

Thermomagnetometry

The TM curve (Figure 4.10) for the product residue of Niox in N_2 showed a sharp weight loss at ~360°C. This is due to the presence of Ni in the residue (Curie point of Ni 354°C).

Evolved gas analysis

Under reduced pressure, decomposition started at about 298°C and the ratio of CO_2:CO was found to be 1:2. The rate of evolution of CO_2 rapidly increased, while the partial pressure of CO remained constant, so that a 1:1 relation held at 300°C and 2:1 at 302°C. At the maximum gas evolution 85 - 90% of the gas was CO_2. The main gaseous decomposition product of Niox is thus CO_2.

TCD results in N_2 and in CO_2 showed no detectable CO.

Figure 4.8. TG of Niox.$2H_2O$ (a) in N_2 (b) in O_2 at 20°C min^{-1}

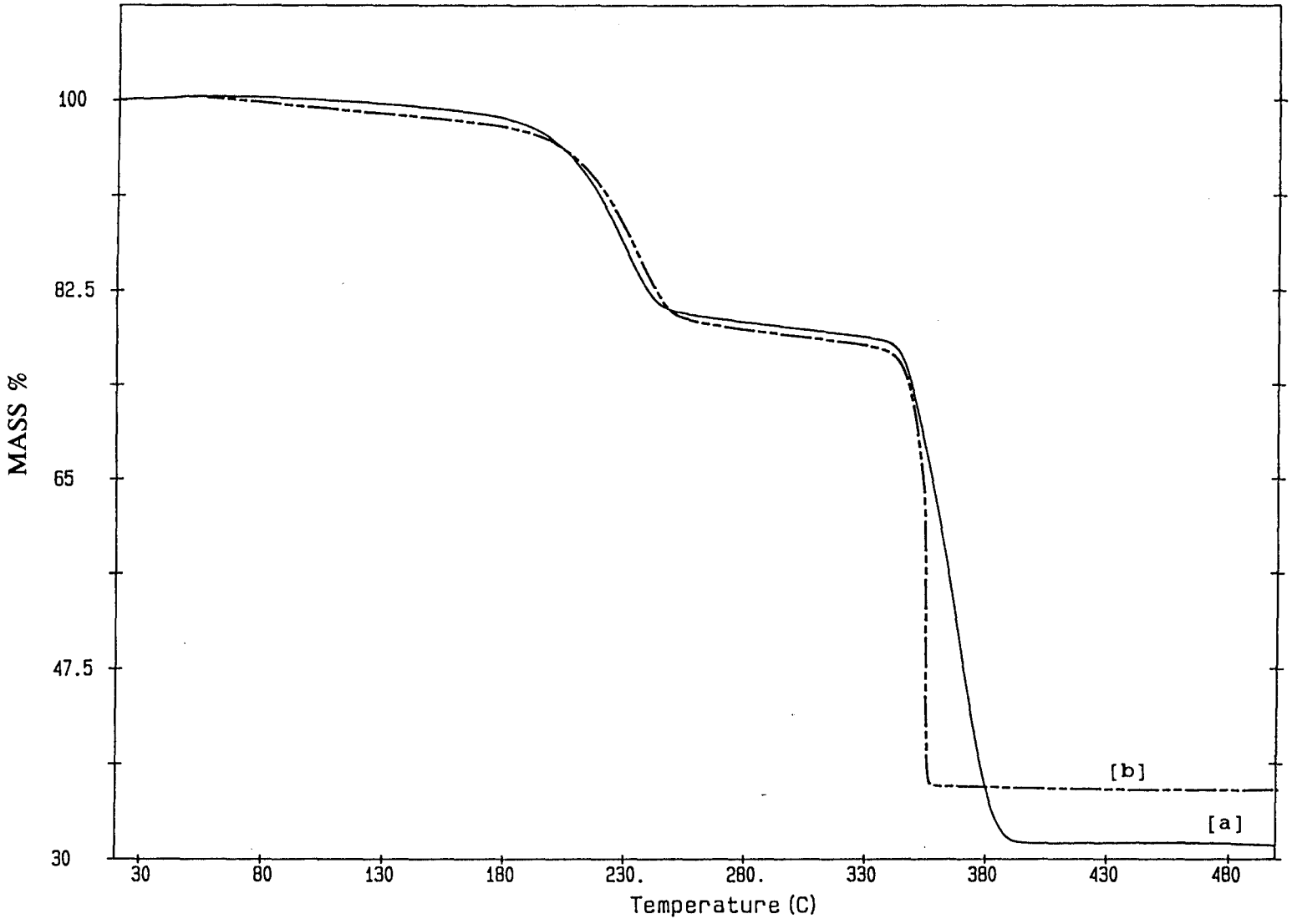

Figure 4.9. DSC of Niox.$2H_2O$ (a) in N_2 (b) in O_2 at 20°C min^{-1}

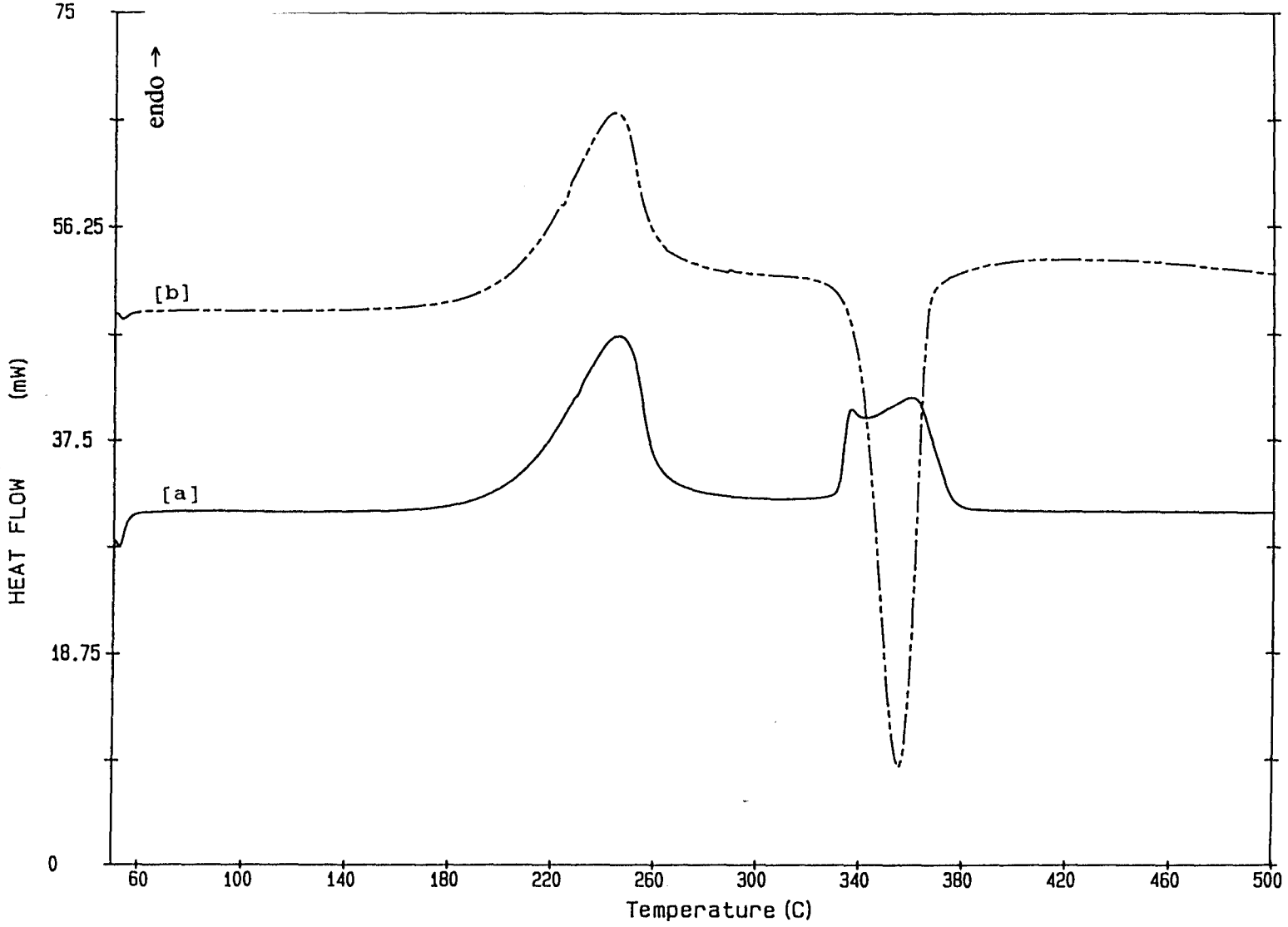

Figure 4.10. TM of Niox.$2H_2O$ in N_2 at 20°C min^{-1}

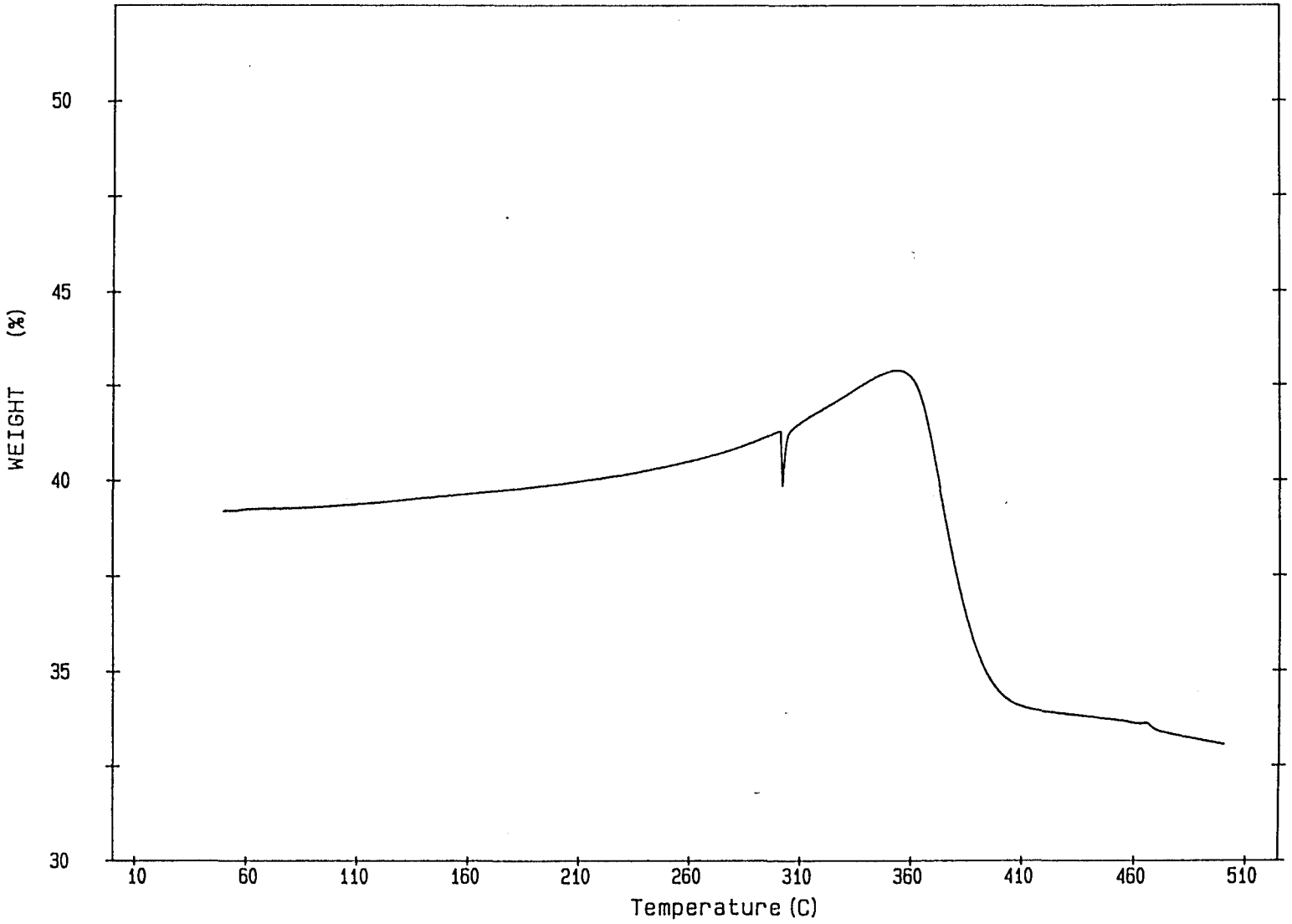

Znox

Thermogravimetry

The TG traces for Znox heated at 20°C min^{-1} in N_2 and O_2 are shown in Figure 4.11. In both atmospheres dehydration occurred from about 145°C, with a mass loss of 18.2 ± 0.4%, corresponding to the loss of 2 moles of H_2O (calculated 19.0%) In nitrogen and oxygen, decomposition started at about 355°C and was completed by 460°C. The mass loss of 39%, corresponds to the loss of CO_2 and CO to form ZnO (calculated residue 42.97%, observed 42.4% in N_2 and 43.6% in O_2).

Differential scanning calorimetry

The DSC curves of Znox.$2H_2O$ in O_2 and N_2 at 20°C min^{-1} are shown in Figure 4.12. The dehydration endotherm with onset ~140°C, has ΔH = 123 kJ mol^{-1} in both N_2 and O_2 atmospheres. The DSC curve in N_2 then shows a decomposition endotherm with an onset of 355°C and ΔH = 114 kJ mol^{-1}.

The DSC curve in O_2 (Figure 4.12, curve b) shows a strong exotherm (ΔH = -99 kJ mol^{-1}) at an onset temperature of 354°C owing to the oxidation of CO to CO_2.

TCD results showed that the evolution of CO and CO_2 coincides with the decomposition endotherm, in both N_2 and CO_2 atmospheres. These peaks could be used as a standard for calculation of the percentage CO and CO_2 evolved by other oxalates.

Figure 4.11. TG of Znox.$2H_2O$ (a) in N_2 (b) in O_2 at 20°C min^{-1}

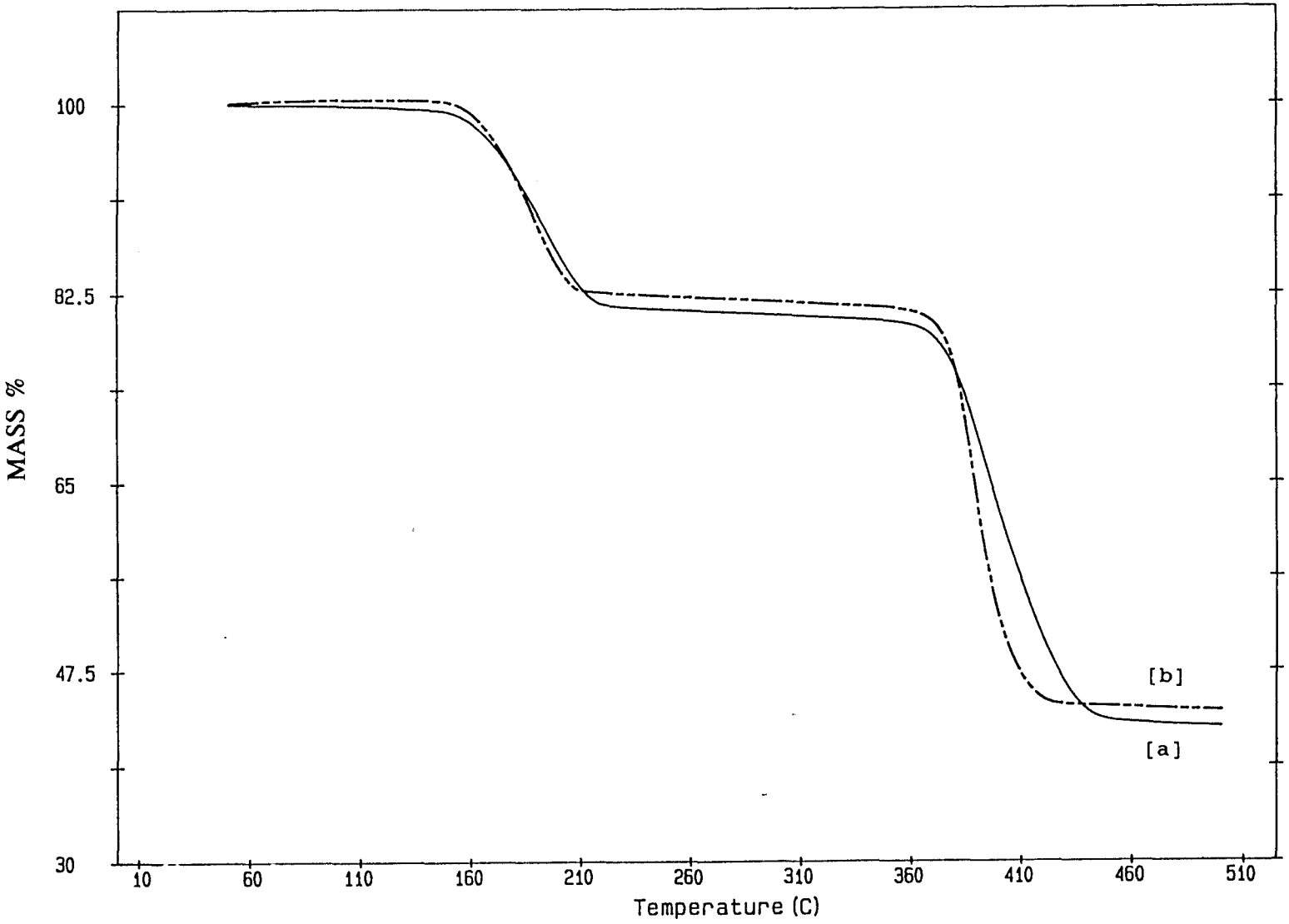

Figure 4.12. DSC of Znox.$2H_2O$ (a) in N_2 (b) in O_2 at 20°C min^{-1}

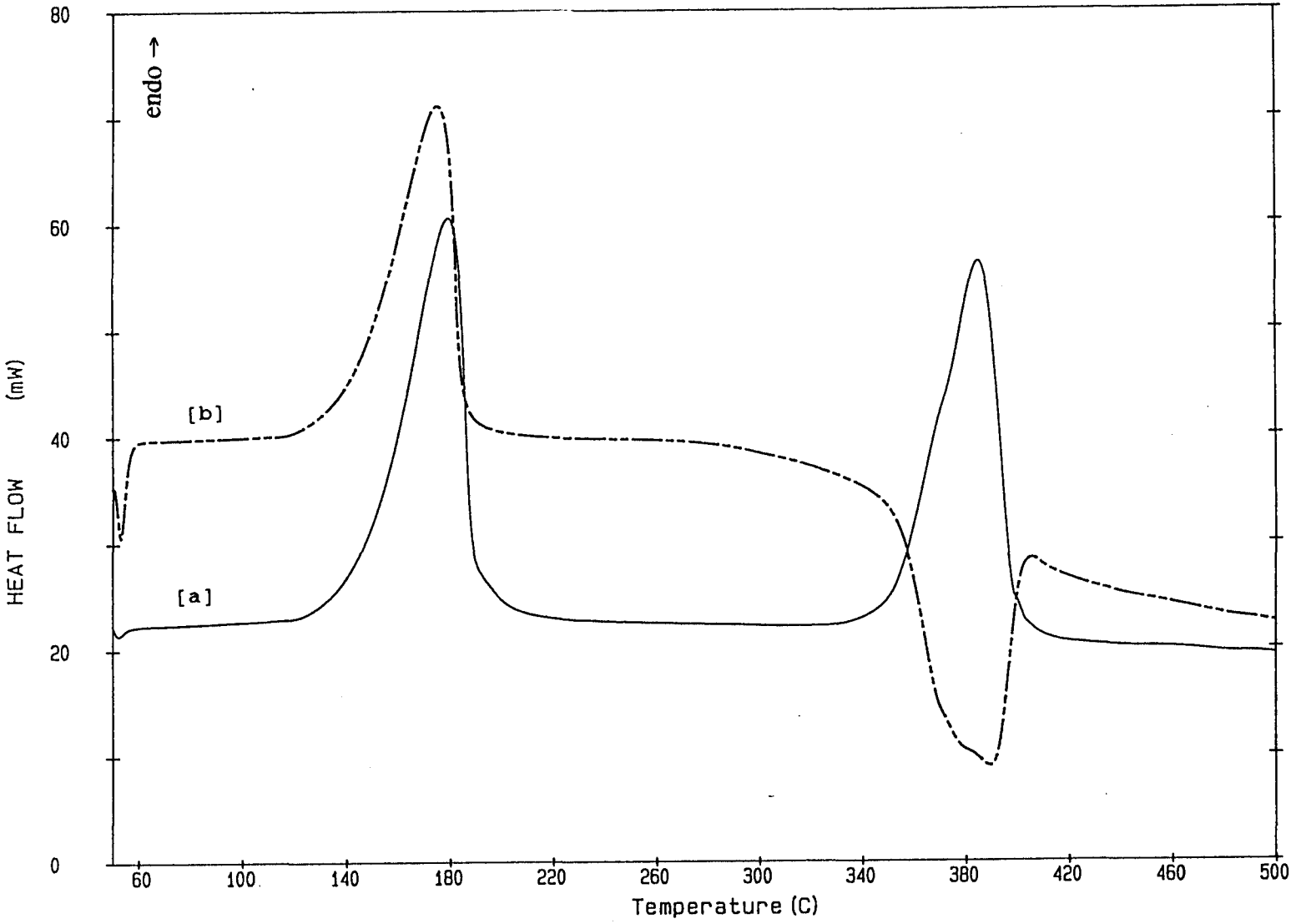

Data for the decompositions in N_2, in CO_2, and under reduced pressure, and for reactions in oxygen of the individual oxalates are summarised in Table 4.2.

Table 4.2

INDIVIDUAL OXALATES: DECOMPOSITION IN NITROGEN AND REACTION IN OXYGEN

(a) Mass loss and enthalpy change

Compound	Onset /°C	% Mass loss	ΔH/ kJ mol^{-1}
Cuox			
N_2	291	55.9	-32.6 ± 0.1
O_2	297	51.8	-138 ± 4
[-2CO_2] calc.		58.0	
Feox			
N_2	367	41.0	130 ± 2
O_2	226	33.3	-251 ± 11
[-CO,CO_2] calc.		40.0	
Coox			
N_2	355	45.5	97.5 ± 1.3
O_2	286	35.9	-265 ± 1
[-2CO_2] calc.		48.1	
Niox			
N_2	331	48.1	71.0 ± 4.9
O_2	338	42.6	-193 ± 1
[-2CO_2] calc.		48.2	
Znox			
N_2	355	39.0	144 ± 1
O_2	355	38.6	-99.5 ± 0.3
[-CO,CO_2] calc.		38.0	

(b) Residue and expected products

Compound	%Residue	EXPECTED PRODUCTS CO_2 as % of gas	solid product as % of original solid	
Cuox				
N_2	44.1	100	Cu	: 42.0
O_2	48.2	75	Cu_2O	: 47.2
		50	CuO	: 52.5
Feox				
N_2	39.6	39.6	FeO	: 40.0
O_2	46.0	46.0	Fe_2O_3	: 44.4
Coox				
N_2	36.1	36.1	Co	: 32.2
O_2	46.2	46.2	CoO	: 41.0
			Co_3O_4	: 43.9
Niox				
N_2	32.5	32.5	Ni	: 32.1
O_2	38.2	38.2	NiO	: 41.0

(c) Evolved gas analysis

Compound	T Range/ °C	Range of CO_2:CO	$\%CO_2$ under reduced pressure	$\%CO_2$ in N_2	$\%CO_2$ in CO_2
Cuox	300 - 330	3:2 - 2:1	60 - 67	48	98
Feox	334 - 340	2:1 - 3:1	70 - 75	30	72
Coox	330 - 340	2:1 - 5:1	80 - 85	100	100
Niox	298 - 302	1:2 - 8:1	85 - 90	100	100

Physical mixtures

Cuox + Feox.$2H_2O$

Thermogravimetry

The TG curves for a physical mixture of equimolar quantities of Cuox and Feox.$2H_2O$ heated at 20°C min^{-1} in N_2 and O_2 are shown in Figure 4.13. The first stage of the reaction was the dehydration of Feox.$2H_2O$. Decomposition in N_2 takes place in two steps with mass losses of 32.2% at 280°C and 17.5% at 340°C. In O_2, reaction of the mixture was accompanied by mass losses of 32.2% at 280°C and 17.5% at 340°C.

Differential scanning calorimetry

The DSC scans for the mixture at 20°C min^{-1} are shown in Figure 4.14. Dehydration of Feox.$2H_2O$ in N_2 is followed by an exotherm with ΔH = -25.1 kJ mol^{-1} at 290°C and an endotherm at 354°C with ΔH = 102 kJ mol^{-1}. These temperatures and enthalpy values correspond closely to those for the decompositions of the individual oxalates, Cuox and Feox. In O_2, three overlapping exotherms are observed; the first with its onset at about 240°C. (Overall ΔH = -390 kJ mol^{-1}).

Figure 4.13. TG of Cuox + Feox.$2H_2O$ (a) in N_2 (b) in O_2 at 20°C min^{-1}

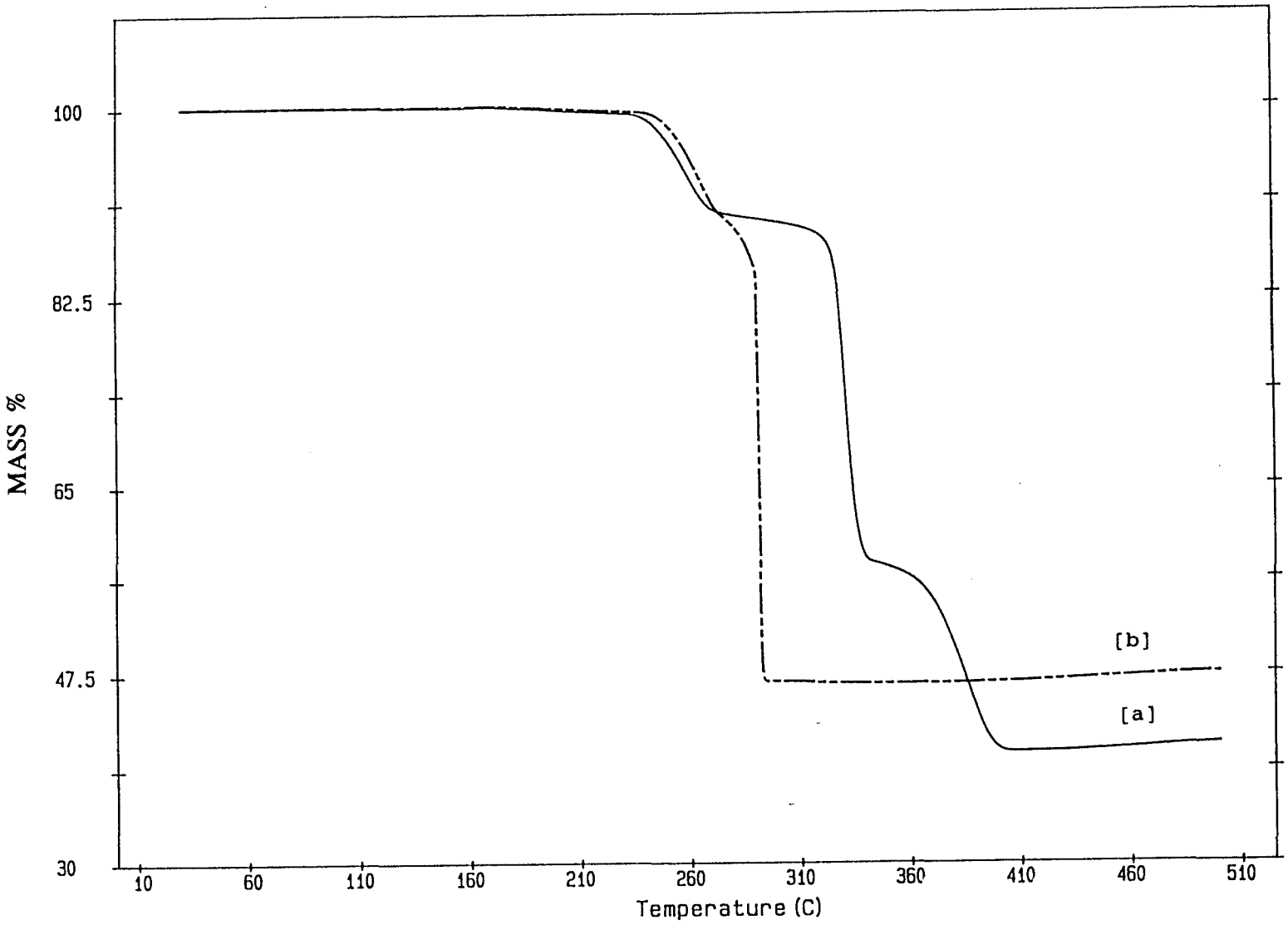

Figure 4.14. DSC of Cuox + Feox.$2H_2O$ (a) in N_2 (b) in O_2 at 20°C min^{-1}

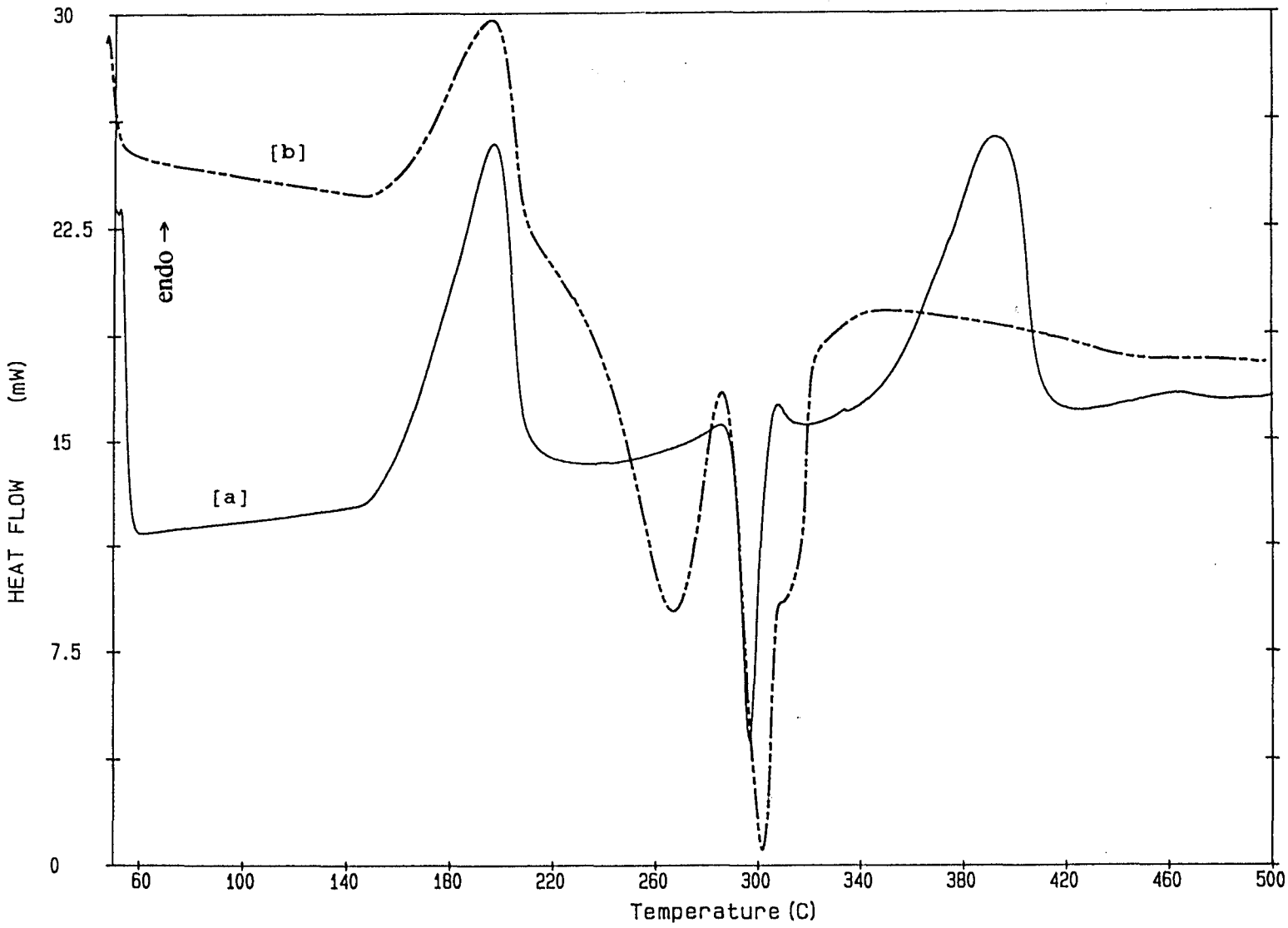

Cuox + Coox.$2H_2O$

Thermogravimetry

The TG curves for a physical mixture of equimolar quantities of Cuox and Coox.$2H_2O$ heated at 20°C min^{-1} in N_2 and O_2 are shown in Figure 4.15. The first stage of the reaction was the dehydration of Coox.$2H_2O$. Decomposition in N_2 takes place in two steps with mass losses of 27.4% at 280°C and 22.9% at 345°C. In O_2, reaction of the mixture was accompanied by a single step of 41.8% at 290°C.

Differential scanning calorimetry

The DSC scans for the mixture at 20°C min^{-1} are shown in Figure 4.16. Dehydration of Coox.$2H_2O$ in N_2 is followed by an exotherm with ΔH = -24.3 kJ mol^{-1} at 285°C and an endotherm at 361°C with ΔH = 78.2 kJ mol^{-1}. These temperatures and enthalpy values correspond closely to those for the decompositions of the individual oxalates, Cuox and Coox. In O_2, two overlapping exotherms are observed at 288°C (ΔH = -516 kJ mol^{-1}).

Figure 4.15. TG of Cuox + Coox.$2H_2O$ (a) in N_2 (b) in O_2 at 20°C min^{-1}

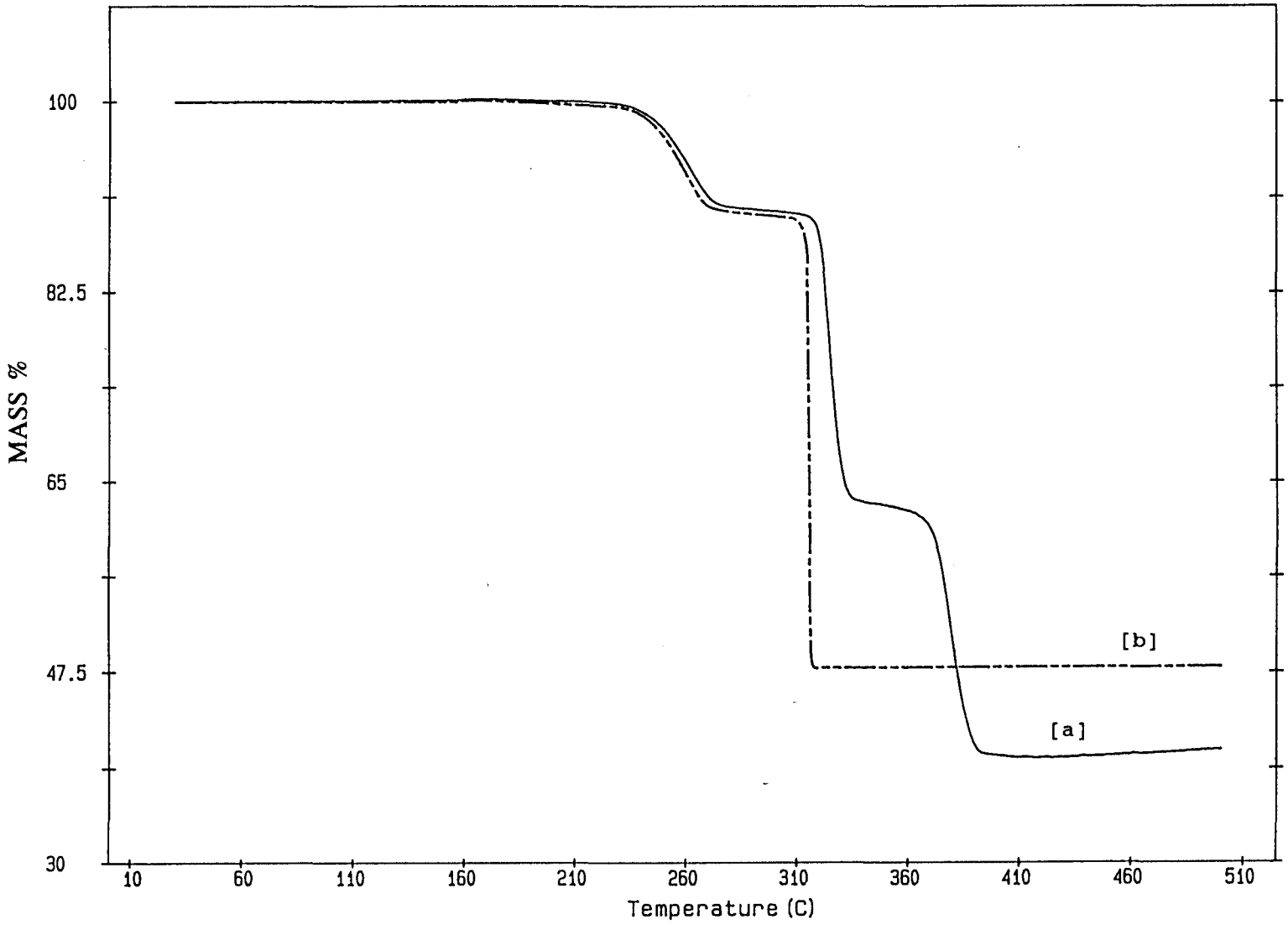

Figure 4.16. DSC of Cuox + Coox.$2H_2O$ (a) in N_2 (b) in O_2 at 20°C min^{-1}

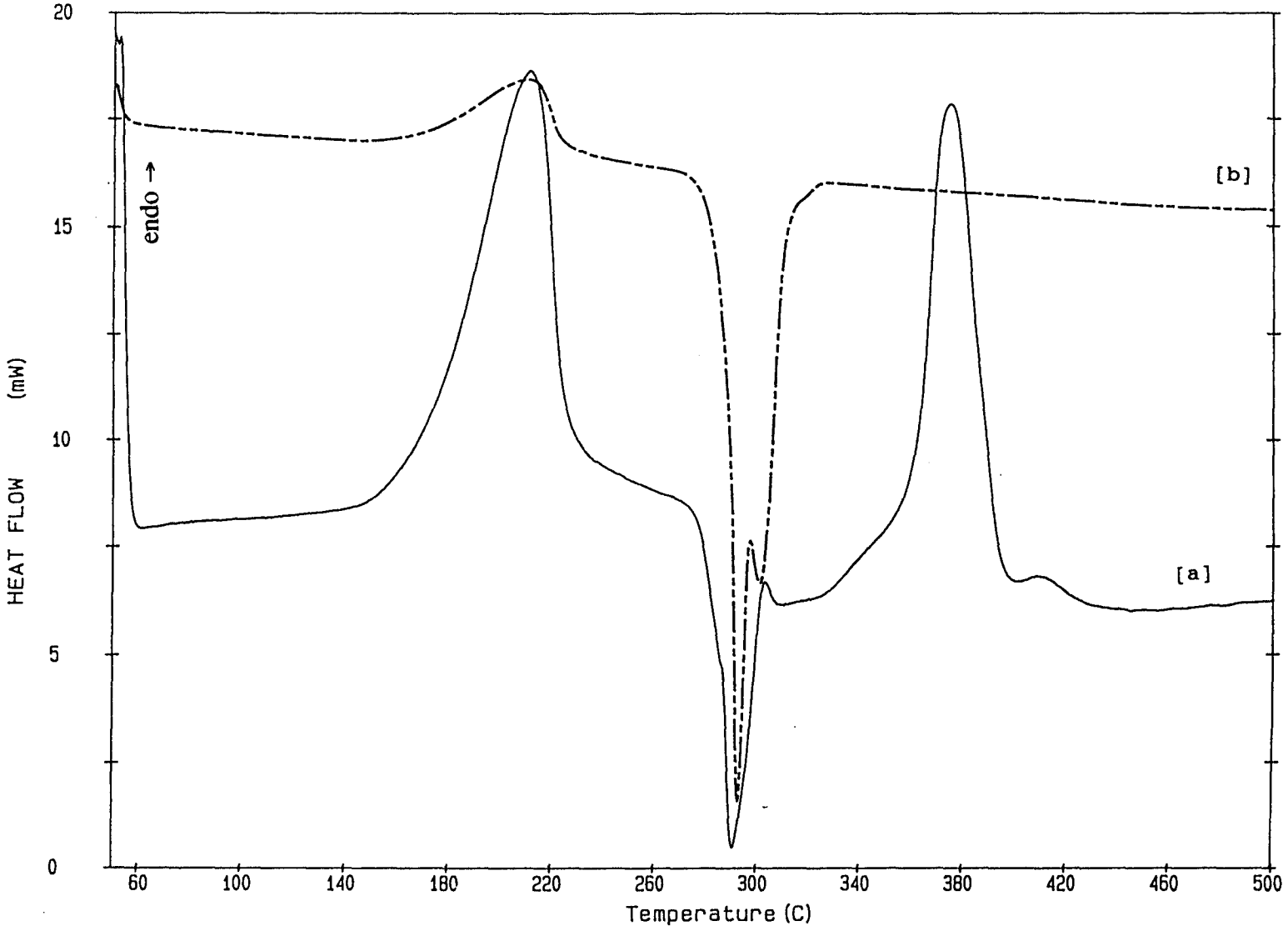

Cuox + Niox.$2H_2O$

Thermogravimetry

The TG curves for the physical mixture of equimolar quantities of Cuox and Niox.$2H_2O$ heated at 20°C min^{-1} in N_2 and O_2 are shown in Figure 4.17. The first stage of the reaction was the dehydration of Niox.$2H_2O$. Decomposition in N_2 takes place in two steps with mass losses of 25.9% at 300°C and 26.6% at 348°C. In O_2, reaction of the mixture was accompanied by a single mass loss of 44.3% at 300°C.

Differential scanning calorimetry

The DSC scans for the mixture at 20°C min^{-1} are shown in Figure 4.18. Dehydration of Niox.$2H_2O$ in N_2 is followed by an exotherm with ΔH = -24.9 kJ mol^{-1} at 303°C and an endotherm (with overlap from a weak exotherm, similar to that found in Niox) at 342°C with ΔH = 116 kJ mol^{-1}. These temperatures and enthalpy values correspond closely to those for the decompositions of the individual oxalates, Cuox and Niox. In O_2 two exotherms are observed. The first at onset 304°C with ΔH = -94 kJ mol^{-1}, and the second at 347°C with ΔH = -127 kJ mol^{-1}.

Figure 4.17. TG of Cuox + Niox.$2H_2O$ (a) in N_2 (b) in O_2 at 20°C min^{-1}

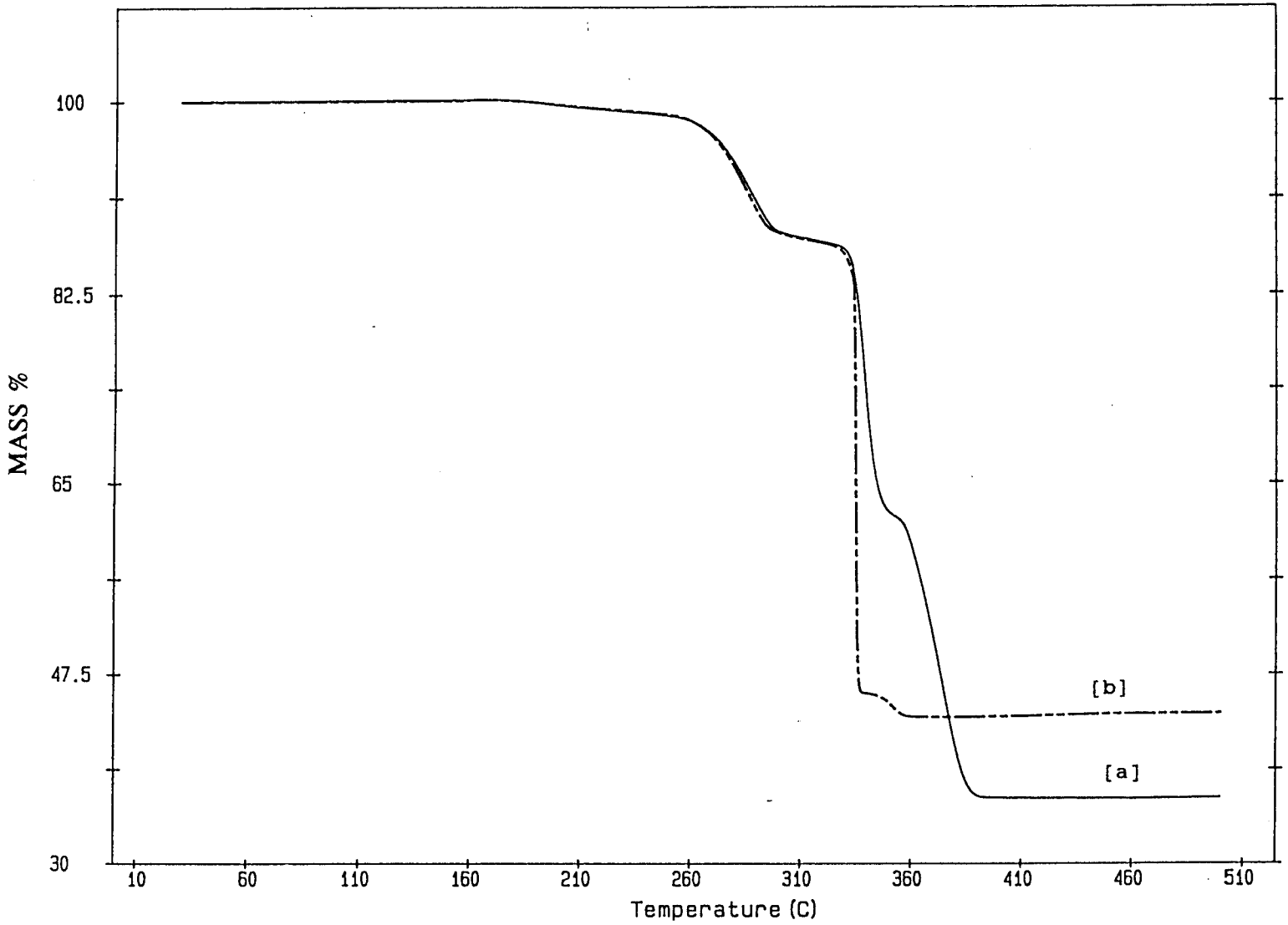

Figure 4.18. DSC of Cuox + Niox.$2H_2O$ (a) in N_2 (b) in O_2 at 20°C min^{-1}

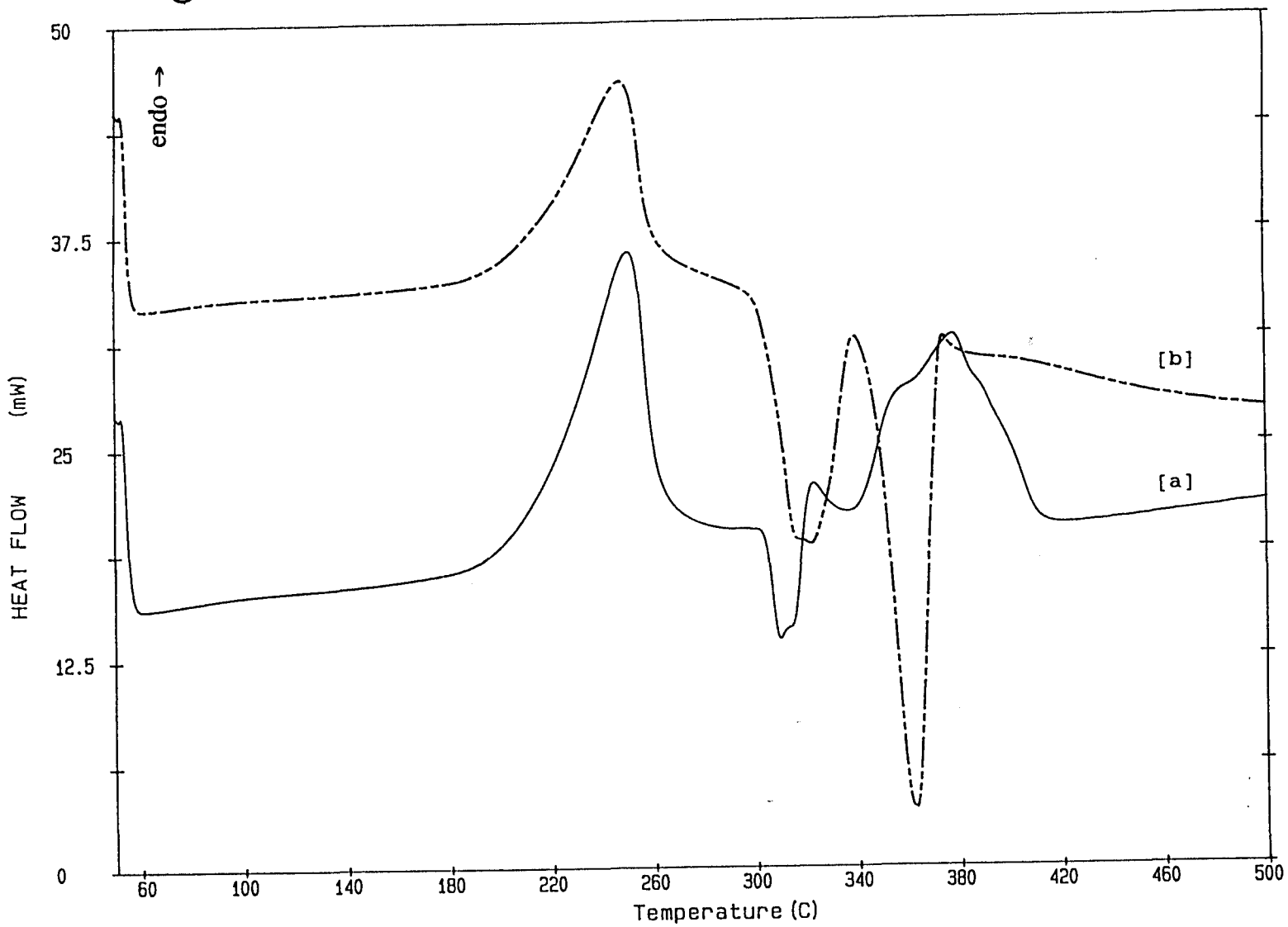

The TG and DSC results for the physical mixtures are summarised in Table 4.3 and compared with the values expected for the individual oxalates (in brackets).

Table 4.3

PHYSICAL MIXTURES OF INDIVIDUAL OXALATES WITH Cuox

Compound Cuox + Mox.2H_2O	Onset /°C	% Mass loss	ΔH /kJ mol^{-1}	Residue %	EXPECTED PRODUCT (calc. %)
M = Fe					
N_2	290	32.2	-25 (-33)	40.1	FeO+Cu
	354	17.5	102 (130)		(40.9)
total		49.7			
-3CO_2-CO		(48.3)			
O_2	240	44.4	-390 (-389)	47.4	Fe_2O_3+2CuO (48.1)
M = Co					
N_2	285	27.4	-24 (-33)	40.0	Cu+Co
	361	22.9	78 (98)		(36.6)
total		50.3			
-4CO_2		(52.6)			
O_2	288	41.8	-514 (-403)	48.2	CoO+CuO (46.2)
M = Ni					
N_2	303	25.9	-25 (-33)	36.5	Ni+Cu
	342	26.6	116 (71)		(36.6)
total		52.5			
-4CO_2		(52.6)			
O_2	304	44.3	-94(-138)	44.1	NiO+CuO
	347		-127 (-193)		(46.2)

The TG and DSC results thus suggest that the dehydrations, the decompositions in N_2, and the reactions in O_2 of the physical mixtures are the same as those of the individual oxalates.

Mixed oxalates

$FeCu(ox)_2.3H_2O$

Thermogravimetry

The TG curves for the decomposition of $FeCu(ox)_2.3H_2O$ at 20°C min^{-1} are shown in Figure 4.19. A dehydration step at ~110°C of 14.4% in N_2 and 14.2% in O_2 confirmed that each mole of compound contains three moles of water (Table 4.1). On further heating in N_2, decomposition took place, commencing at 200°C, in two overlapping steps, resulting in a mass loss of 45.6%. The percentage residue of ~40% in N_2 is closest to that calculated (41.0%) for the formation of FeO and Cu_2O by loss of CO and CO_2. The percentage residue calculated for formation of FeO and CuO is 43.3%. The product residue was reheated in O_2 and an overall mass increase of ~5% of the initial mass was observed. This increase suggests the oxidation of FeO to Fe_2O_3 and Cu_2O to CuO (calculated increase 4.6%).

The TG scan in O_2 (Figure 4.19, curve b) showed one decomposition step (onset ~200°C), resulting in a mass loss of 41.6%. The residue of 44.1% is close to that for the formation of $\frac{1}{2}Fe_2O_3$ and CuO (calculated 45.6%).

Differential scanning calorimetry

The DSC curves of $FeCu(ox)_2.3H_2O$ heated at 20°C min^{-1} in O_2 and N_2 are shown in Figure 4.20. The dehydration endotherm with onset ~139°C, has ΔH = 227 kJ mol^{-1}. The DSC curve in N_2 then shows a weak exotherm (ΔH = -10.6 kJ mol^{-1}) with onset temperature of 300°C. This corresponds with the onset temperature of the strong exotherm in the decomposition of Cuox and it is possible that a small proportion of Cuox is present as a physical mixture with the mixed oxalate (see also section 3.3, X-ray powder diffraction). This exotherm is followed by an endotherm (onset ~350°C, ΔH = 160 kJ mol^{-1}).

The DSC curve in O_2 (Figure 4.20, curve b) shows that reaction (to form Fe_2O_3 and CuO) occurs in two strongly exothermic stages which overlap slightly.

The decomposition of $FeCu(ox)_2$ in N_2 is thus suggested to occur via the following reactions:

$$FeCu(ox)_2.3H_2O(s) \rightarrow FeCu(ox)_2(s) + 3H_2O(g)$$

$$2FeCu(ox)_2(s) \rightarrow 2FeO(s) + Cu_2O(s) + 3CO_2(g) + 5CO(g)$$

It is assumed that, for the reaction in O_2, decomposition (as above) is followed by oxidation:

$FeO \rightarrow Fe_2O_3$ [-140 kJ mol^{-1}]

$CO \rightarrow CO_2$ [-283 kJ mol^{-1}]

$Cu_2O \rightarrow CuO$ [-73.0 kJ mol^{-1}]

Thermomagnetometry

The TM curve of the decomposition product of $FeCu(ox)_2$ at 20°C min^{-1} in N_2 (Figure 4.21, curve a) shows a slight mass increase up to 470°C, resulting from some oxidation by residual oxygen, and a sharp weight loss at approximately 580°C, indicating that Fe_3O_4 is present in the residue.

The TM curve in O_2 (Figure 4.21, curve b) showed a continuous loss of weight with two rate maxima at approximately 440°C and 550°C. The TG curve in O_2 showed a mass increase of 1.8%, onset ~450°C, owing to oxidation. The TM results thus suggest the formation of some ferromagnetic γ-Fe_2O_3 which converts to paramagnetic α-Fe_2O_3 above about 340°C, while the main reaction is formation of Fe_3O_4.

Evolved gas analysis

Decomposition of $FeCu(ox)_2$ under reduced pressure started at 192°C, with a CO_2:CO ratio of 2:1. The evolution of CO_2 increased rapidly, until the ratio was nearly 6:1 (226°C). The partial pressure of CO then rose and reached a ratio of 1:1 at 336°C. Towards the end of decomposition, the CO_2 partial pressure exceeded the partial pressure of CO and a ratio of 3:2 was maintained. About 35% of the evolved gas was CO during the earlier stages of decomposition (260-320°C), about 45% at 320-336°C and 50-56% towards the final stages of decomposition (338-342°C). Both CO and CO_2 are thus evolved during the decomposition of $FeCu(ox)_2$.

Programmed temperature DSC runs on $FeCu(ox)_2$, heated in CO_2 or in N_2, showed a strong TCD response due to CO, coinciding with the decomposition endotherm in Figure 4.20. Evolution of CO_2 only, was detected during the exothermic stage. An isothermal experiment at 300°C, in N_2 (in the presence of a cold trap) showed no evolution of CO during the exothermic decomposition step. CO was detected during a further programmed temperature run from 300-440°C. Thus only CO_2 is evolved initially and some CO is evolved during the later stages of decomposition. The overall proportion of CO was 30% both in N_2 and in CO_2.

Figure 4.19. TG of $FeCu(ox)_2.3H_2O$ (a) in N_2 (b) in O_2 at 20°C min^{-1}

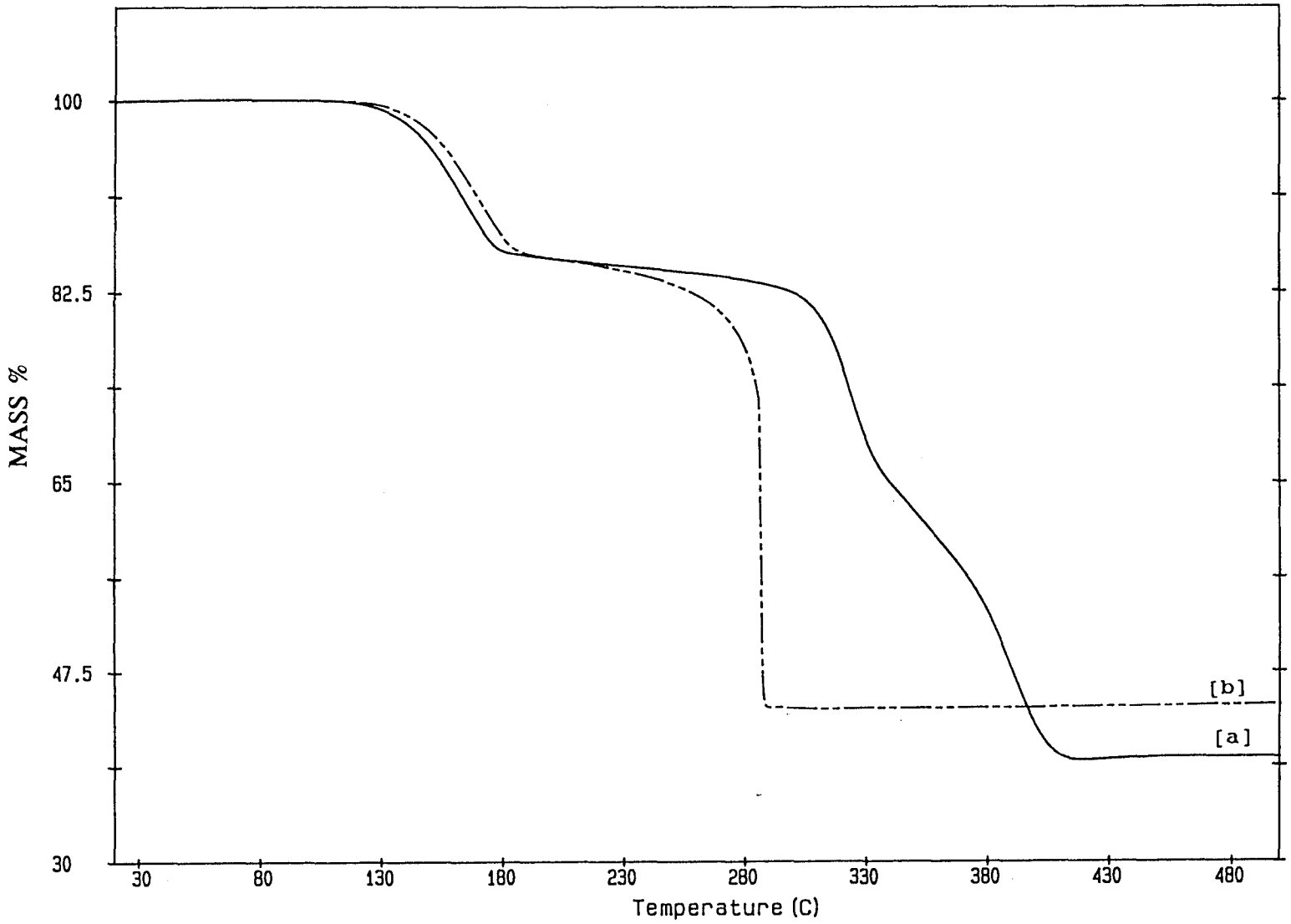

Figure 4.20. DSC of $FeCu(ox)_2.3H_2O$ (a) in N_2 (b) in O_2 at 20°C min^{-1}

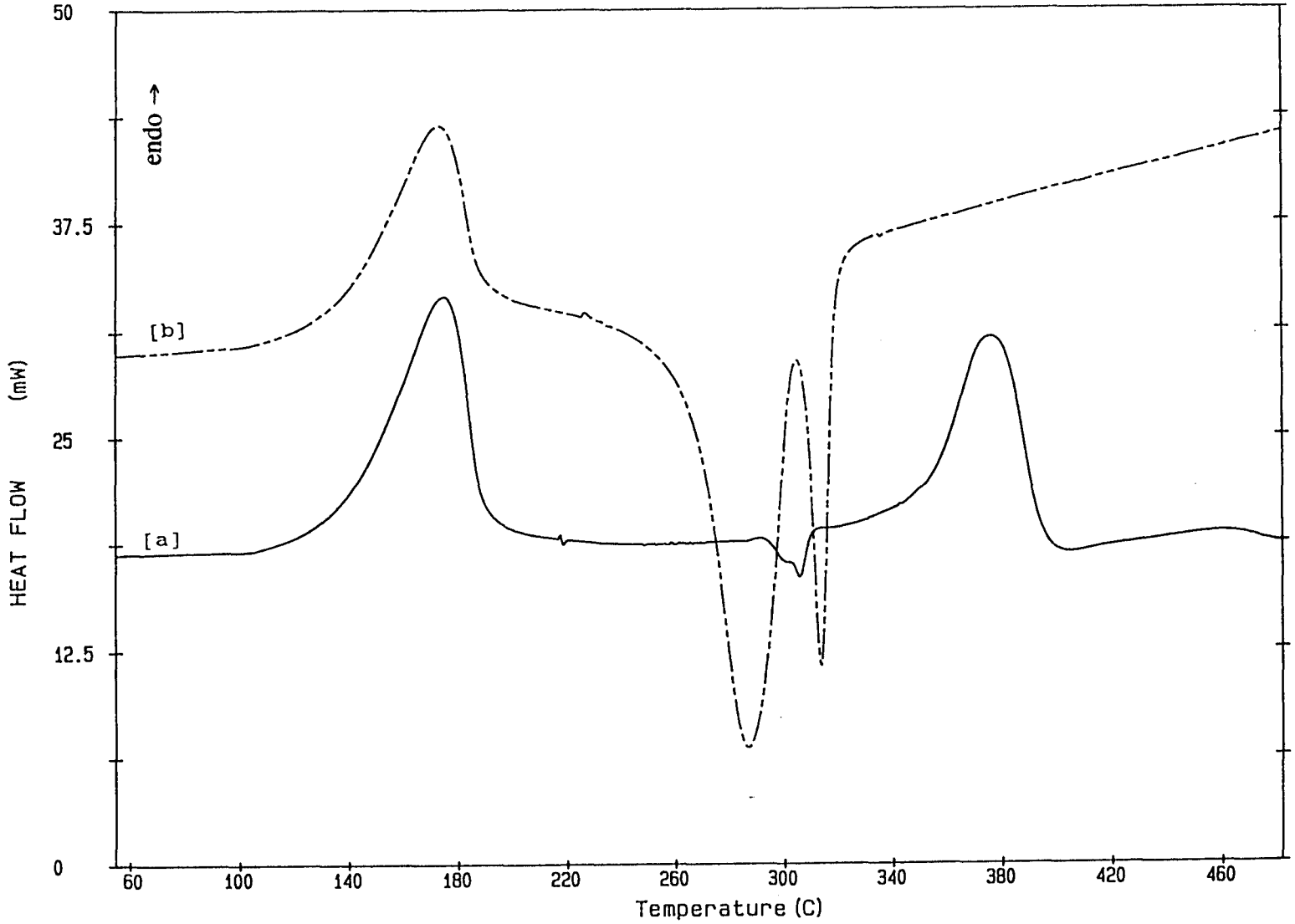

Figure 4.21. TM of $FeCu(ox)_2.3H_2O$ (a) in N_2 (b) in O_2 at 20°C min^{-1}

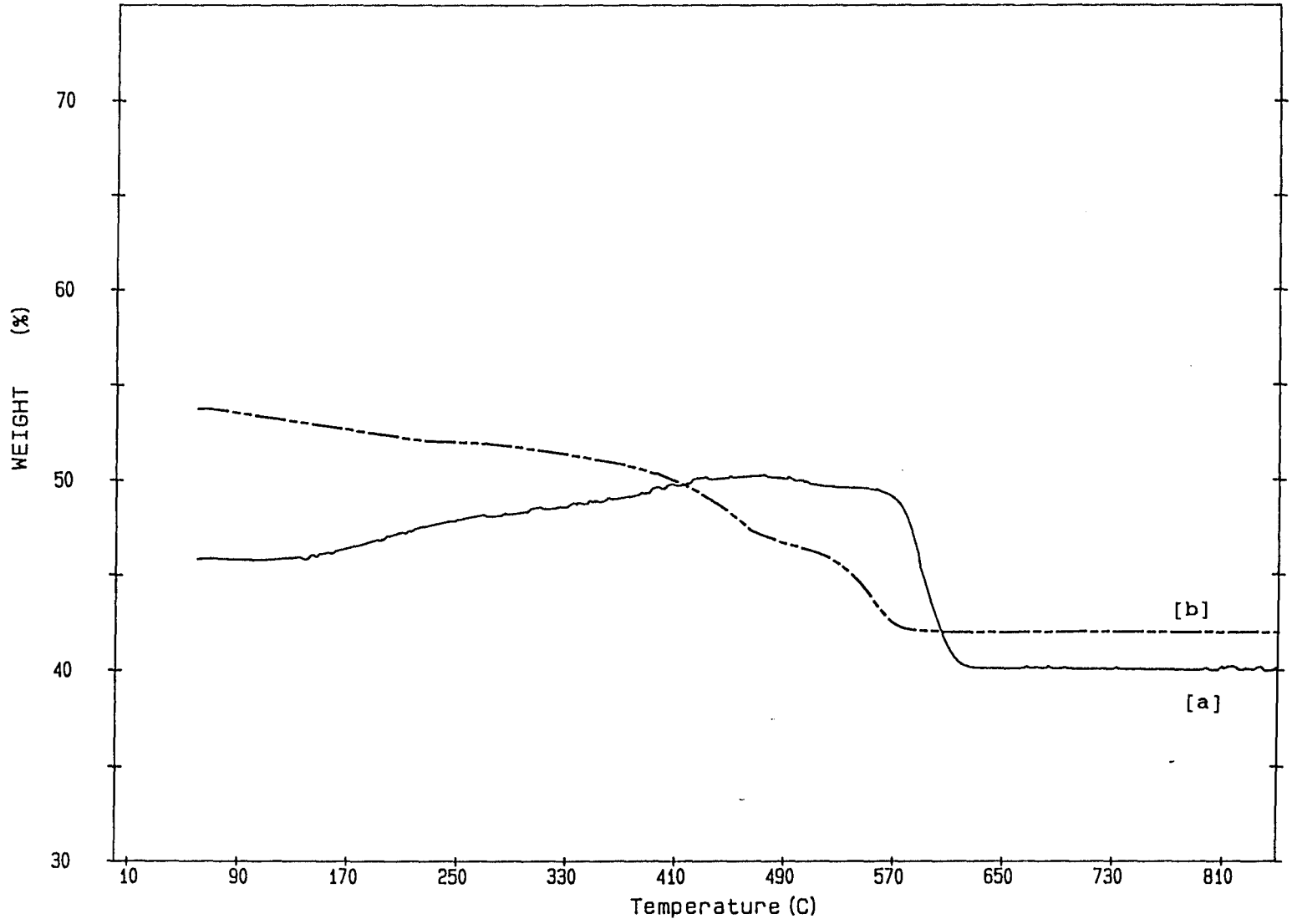

$CoCu(ox)_2.3H_2O$

Thermogravimetry

A TG curve for $CoCu(ox)_2.3H_2O$ heated in N_2 at 20°C min^{-1} is shown in Figure 4.22, curve a. Dehydration occurs at ~140°C with a mass loss of 14.6% in N_2 and 14.2% in O_2. The mass loss calculated for loss of three moles of water per mole of reactant is 15.4% (Table 4.1). Decomposition commences at 280°C in two overlapping stages, with an overall mass loss of 50.3%. This mass loss corresponds well with the calculated value (49.9%) for the loss of $4CO_2$. The percentage residue of 35.1% suggests that the decomposition products are Cu and Co (calculated 34.7%):

$CoCu(ox)_2(s) \rightarrow Cu(s) + Co(s) + 4CO_2$

In oxygen (Figure 4.22, curve b) decomposition commences at about 290°C, with a mass loss of 41.2%. The percentage residue of 44.6% suggests the formation of CuO and CoO as decomposition products (calculated 43.8%):

$CoCu(ox)_2(s) \rightarrow CuO(s) + CoO(s) + 4CO_2$

Differential scanning calorimetry

The DSC curves for $CoCu(ox)_2$ in nitrogen and oxygen at 20°C min^{-1} are shown in Figure 4.23 (curves a and b, respectively). The dehydration endotherm in N_2 of 227 kJ mol^{-1} has an onset temperature of ~140°C. In oxygen, the dehydration endotherm has an onset of 142°C and ΔH = 197 kJ mol^{-1}. Again, a weak exotherm of -2.2 kJ mol^{-1} in nitrogen, onset 316°C, indicates coprecipitation of a small amount of copper oxalate in the mixed oxalate. The next feature of the DSC curve is an endotherm of 97 kJ mol^{-1} with onset 345°C. In oxygen (Figure 4.23, curve b), a strong exotherm with onset 293°C and ΔH = -511 kJ mol^{-1} is observed.

The decomposition of $CoCu(ox)_2$ in N_2 is thus suggested to occur via the following reactions:

$CoCu(ox)_2.3H_2O(s) \rightarrow CoCu(ox)_2(s) + 3H_2O(g)$

$CoCu(ox)_2(s) \rightarrow Co(s) + Cu(s) + 4CO_2(g)$

It is assumed that, for the reaction in O_2, decomposition (as above) is followed by

oxidation:

$Co \rightarrow CoO$ [-237.9 kJ mol^{-1}]

$Cu \rightarrow CuO$ [-156.1 kJ mol^{-1}]

Evolved gas analysis

A sample of $CoCu(ox)_2$ which had been dehydrated under reduced pressure at 140-150°C, was re-introduced into the furnace at 290°C and gradually heated to 348°C. The evolution of H_2O was detected from 290-300°C. Dehydration was thus not complete at 150°C, which suggests that some of the water molecules are more strongly bound in the mixed oxalate than in $Coox.2H_2O$. Water vapour is thus also present during decomposition. At 290°C mostly CO_2 was detected. The CO concentration rose slowly, so that the CO_2:CO ratio varied between 2:1 and 3:1 from 290-296°C and between 3:2 and 2:1 from 300-310°C. By 310°C the partial pressure of CO_2 dropped to less than half of its maximum (at 296°C) while the partial pressure of CO remained constant. The partial pressure of CO increased faster than that for CO_2 between 310-320°C, so that the partial pressures were equal at 320°C. Between 320 and 336°C the ratio of CO_2:CO remained roughly 3:2 and increased to about 2:1 at 338-342°C. Towards the end of decomposition the rate of CO_2 evolution decreased until it was half that of CO. Between 290 and 300°C, the overall composition of the evolved gases was H_2O: 10-25%, CO: 20-35%, CO_2: 50-55%, and above 300°C, CO: 33-50%, CO_2: 50-67%.

Programmed temperature DSC runs on $CuCo(ox)_2$ with a TCD showed that hardly any CO is evolved during the decomposition of $CoCu(ox)_2$. Evolution of CO_2 takes place in two stages, with the amount evolved during the exothermic reaction (shown in Figure 4.23) being less (about 1/6) of that evolved during the endothermic process. An isothermal DSC experiment at 340°C in N_2 also did not show up any CO, but the two stages of evolution of CO_2 were observed.

Figure 4.22. TG of $CoCu(ox)_2.3H_2O$ (a) in N_2 (b) in O_2 at 20°C min^{-1}

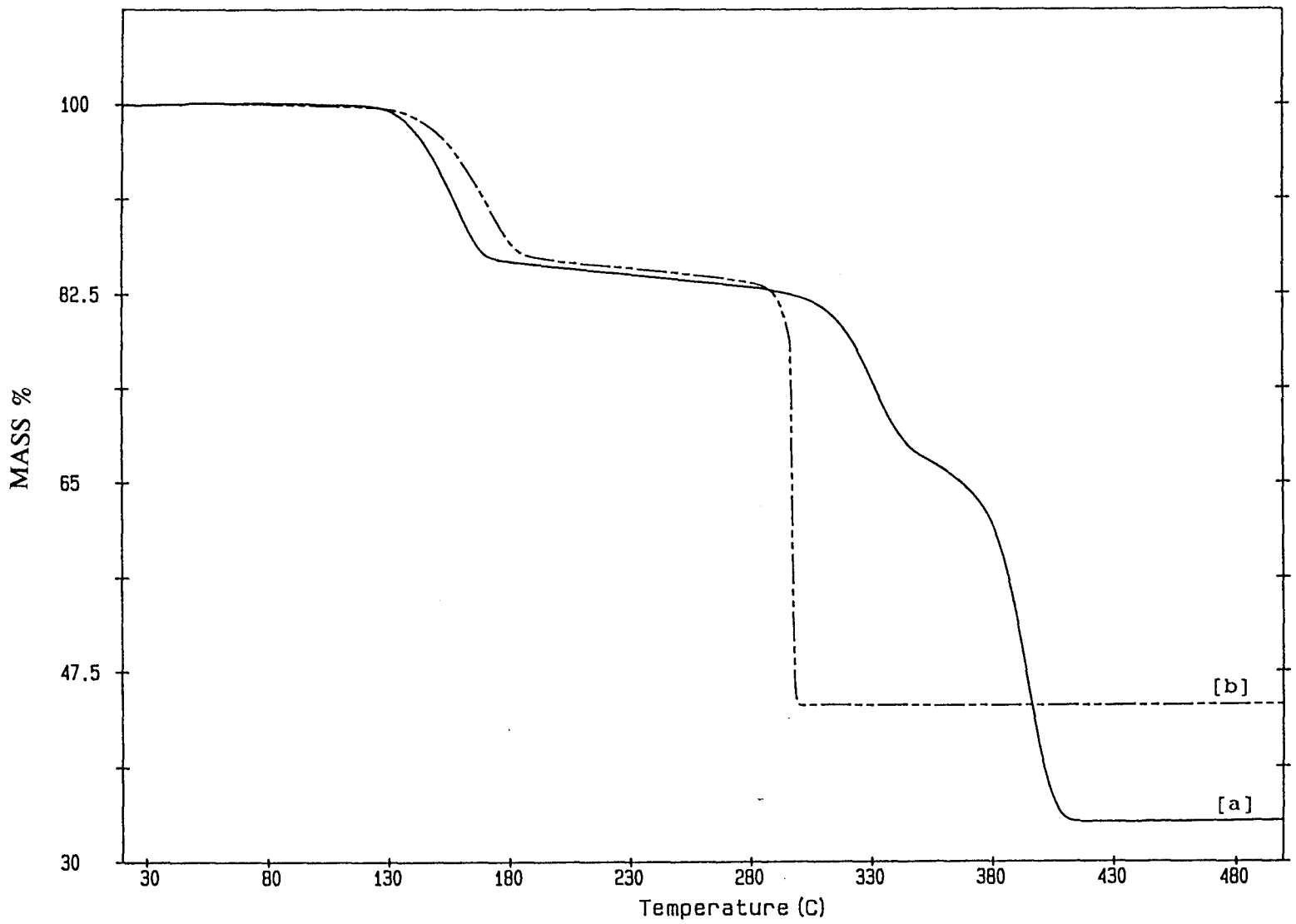

Figure 4.23. DSC of $CoCu(ox)_2.3H_2O$ (a) in N_2 (b) in O_2 at 20°C min^{-1}

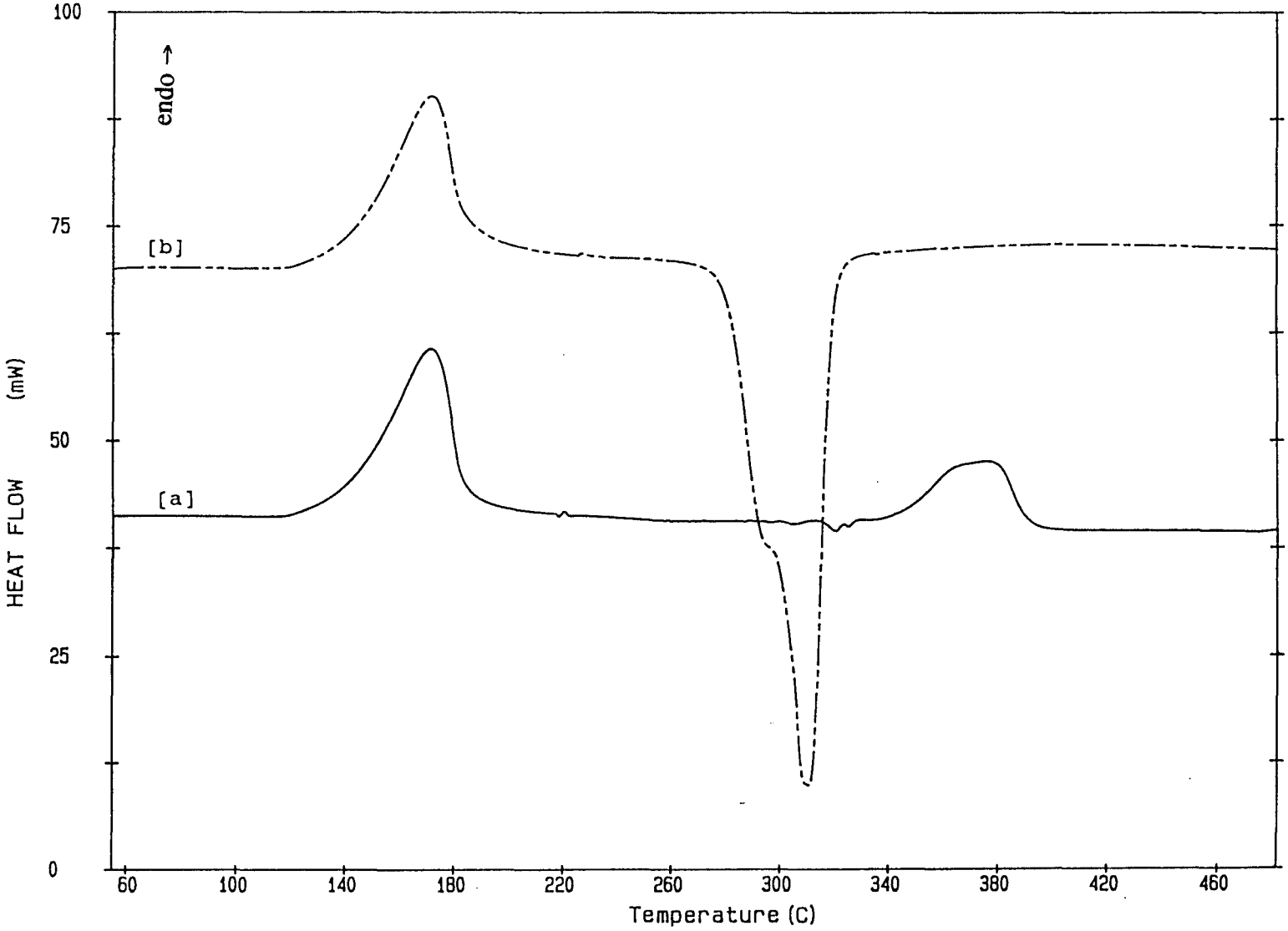

$NiCu(ox)_2.3.5H_2O$

Thermogravimetry

The TG curves for $NiCu(ox)_2.3.5H_2O$, heated in nitrogen and oxygen at 20°C min^{-1}, are shown in Figure 4.24 (curves a and b, respectively). Dehydration occurs in N_2 and in O_2 at about 190 ± 10 °C with a mass loss of 17.3 ± 0.1%. This mass loss suggests the loss of 3.5 moles of water for each mole of reactant (calculated 17.5%) (Table 4.1).

Decomposition in N_2 starts at ~360°C in two overlapping stages. The overall mass loss is 50.4%. The calculated mass loss for evolution of $4CO_2$ is 48.7%. The residue of 32.3% is closest to formation of Cu and Ni (calculated 33.9%).

$NiCu(ox)_2(s) \rightarrow Cu(s) + Ni(s) + 4CO_2(g)$

In oxygen (Figure 4.24, curve b), reaction occurs at about 300°C with a mass loss of 44.6%. The percentage residue of 38.2% suggests the formation of NiO and CuO (calculated 42.7%).

Differential scanning calorimetry

DSC curves for $NiCu(ox)_2$ in nitrogen and oxygen, at 20°C min^{-1}, are shown in Figure 4.25 (curves a and b, respectively). The dehydration endotherm varied slightly, onset ~200°C, ΔH = 204 kJ mol^{-1} in nitrogen, and onset ~180°C, ΔH = 180 kJ mol^{-1} in oxygen. Dehydration was followed at higher temperatures in nitrogen (onset ~360°C) by endothermic decomposition (ΔH = 158 kJ mol^{-1}). In oxygen, strongly exothermic reaction occurs with onset at ~310°C and ΔH = -274 kJ mol^{-1}.

Thermomagnetometry

The TM curve (Figure 4.26) for the product residue of $NiCu(ox)_2$ in N_2 showed some ferromagnetism of the initial residue which was lost on heating from 50°C to 270°C. The Curie transition of Ni was not observed. This suggests some alloying of Ni and Cu in the decomposition product. For an alloy of Ni and Cu to show ferromagnetic properties, more than 55% Ni has to be present [76]. The TG curve in oxygen showed onset of

oxidation at ~300°C.

Evolved gas analysis

A sample of $NiCu(ox)_2$ which had been dehydrated under reduced pressure at 170-180°C, was re-introduced into the furnace at 290°C and gradually heated. The presence of H_2O was detected up to 300°C. The CO_2:CO ratio was about 3:2 during the first stages of decomposition (292-298°C). The rate of CO_2 evolution increased and reached a ratio of 2:1 from 295°C until the end of decomposition (330°C). CO_2 was the major product of decomposition (56% at temperatures below 300°C and 67% above 300°C), while the amount of CO present varied from 44% to 33%.

DSC runs on $NiCu(ox)_2$ in N_2 with the TCD and a cold trap showed that about 48% of the gas evolved during decomposition is CO, but in CO_2, the proportion of CO was decreased to about 1%. The isothermal decomposition of $NiCu(ox)_2$ at 345°C, in N_2 (in the presence of a cold trap) showed the evolution of a small amount of CO at the beginning of decomposition. This was followed by a two-stage evolution of CO_2.

Figure 4.24. TG of $NiCu(ox)_2.3H_2O$ (a) in N_2 (b) in O_2 at 20°C min^{-1}

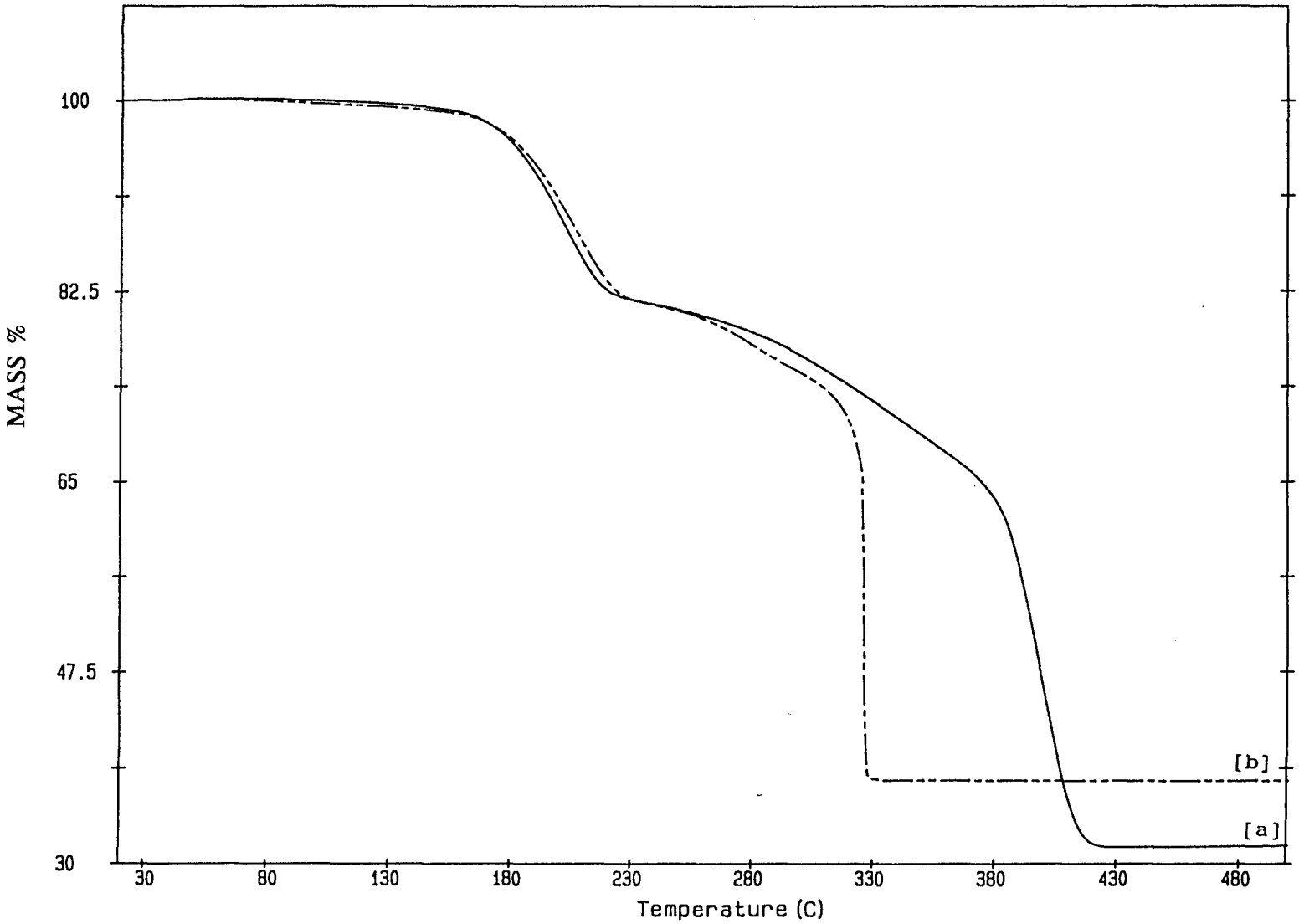

Figure 4.25. DSC of $NiCu(ox)_2.3H_2O$ (a) in N_2 (b) in O_2 at 20°C min^{-1}

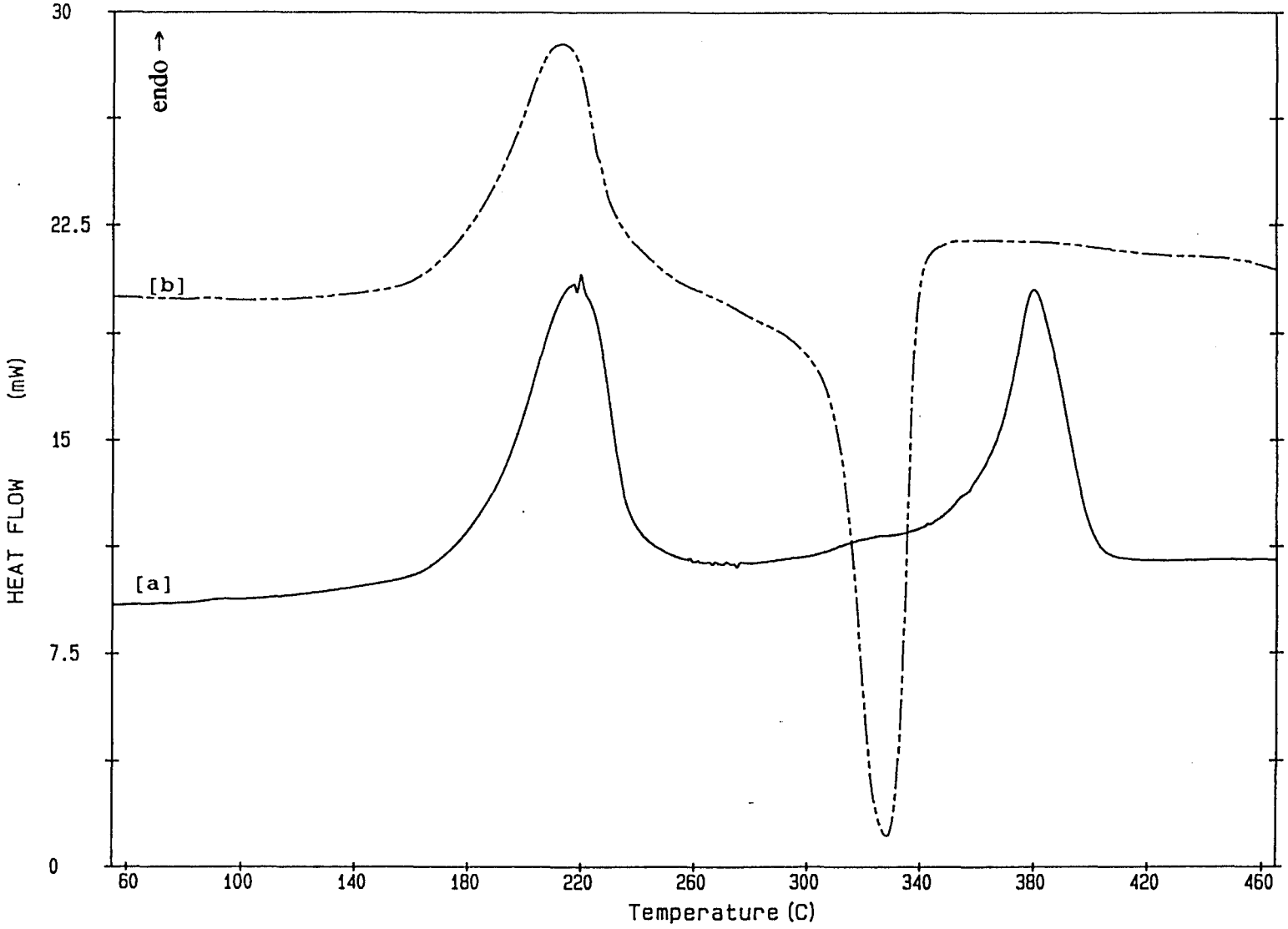

Figure 4.26. TM of $NiCu(ox)_2.3H_2O$ in N_2 at 20°C min^{-1}

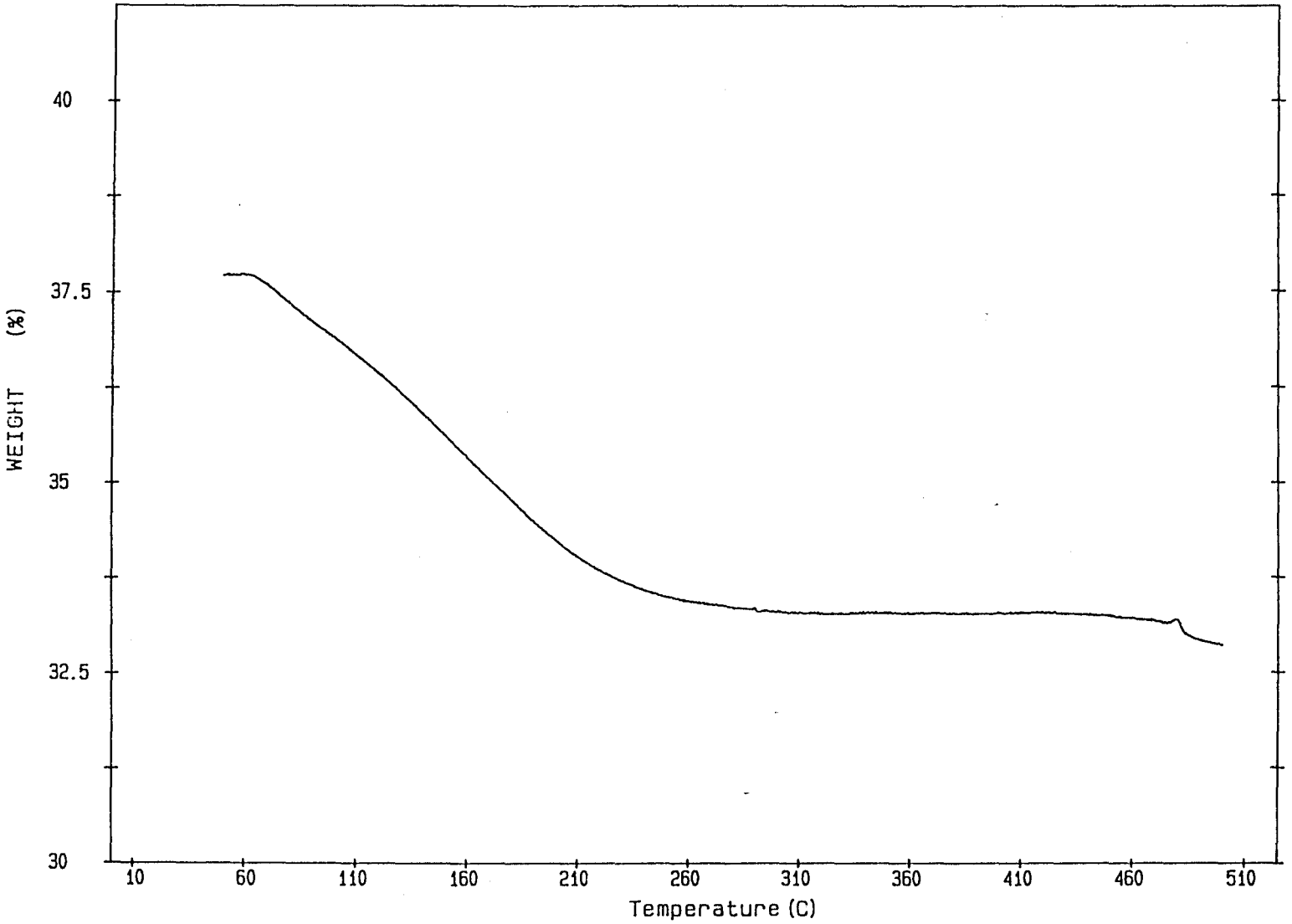

Data for the decompositions in N_2, in CO_2, and under reduced pressure, and for reactions in oxygen of the mixed oxalates are summarised in Table 4.4.

Table 4.4

MIXED OXALATES: DECOMPOSITION IN NITROGEN AND REACTION IN OXYGEN

(a) Mass loss and enthalpy change

Compound	Onset/°c	% Mass loss	ΔH / kJ mol^{-1}
$FeCu(ox)_2$			
N_2	299	45.6	-10.6 ± 1.1
	351		160 ± 6
O_2	264	41.6	-417 ± 8
$CoCu(ox)_2$			
N_2	316	50.3	-2.2 ± 0.3
	345		97.1 ± 9.7
O_2	293	41.2	-511 ± 1
$NiCu(ox)_2$			
N_2	362	50.4	158 ± 5
O_2	308	44.6	-274 ± 16

(b) Residue and expected products

Compound	% Residue	EXPECTED PRODUCT CO_2 as % of gas	solid product as % of original solid	
$FeCu(ox)_2$				
N_2	40.0	100	Fe+Cu	: 34.2
		75	FeO+Cu	: 38.8
O_2	44.1	67	FeO+½Cu_2O	: 41.0
			FeO+CuO	: 43.3
		50	Fe_2O_3+CuO	: 45.6
$CoCu(ox)_2$				
N_2	35.1	100	Cu+Co	: 34.7
O_2	44.6	50	CuO+CoO	: 43.8
$NiCu(ox)_2$				
N_2	32.3	100	Cu+Ni	: 33.9
O_2	38.2	50	CuO+NiO	: 42.7

(c) Evolved gas analysis

Compound	T range/ °C	Range of CO_2:CO	%CO_2 under reduced pressure	%CO_2 in N_2	%CO_2 in CO_2
$FeCu(ox)_2$	192-226	2:1 - 6:1	65	70	70
	336-340	1:1 - 3:2	44-55		
$CoCu(ox)_2$	290-300	3:2 - 3:1	50-55 (H_2O 10-25)	100	100
	310-340	1:1 - 2:1	50-66		
$NiCu(ox)_2$	292	3:2	56	52	99
	330	2:1	67		

CHAPTER 5 THERMOCHEMISTRY

5.1 INDIVIDUAL OXALATES

Znox.$2H_2O$

The decomposition of Znox in N_2 is known to proceed as follows [1]:

$Znox.2H_2O(s) \rightarrow Znox(s) + 2H_2O(g)$

$Znox(s) \rightarrow ZnO(s) + CO_2(g) + CO(g)$ ....(1)

and in oxygen:

$Znox(s) + \frac{1}{2}O_2(g) \rightarrow ZnO(s) + 2CO_2(g)$ ....(2)

This has been confirmed by the TG and DSC results discussed in Chapter 4.

The difference between (1) and (2) corresponds to the reaction:

$CO(g) + \frac{1}{2}O_2(g) \rightarrow CO_2(g)$ ....(3)

The thermal decomposition of Znox was chosen as a reference reaction because formation of other oxides or the metal is highly unlikely. It was also used to determine whether the enthalpy of reaction (3), which is reported to be catalysed by ZnO [49] can be measured using DSC. The enthalpy of formation of Znox, ΔH_f(Znox), was calculated from the enthalpies of reaction in nitrogen, $\Delta H(N_2)$, and in oxygen, $\Delta H(O_2)$. The values found were -966 kJ mol^{-1} and -1035 kJ mol^{-1}, respectively, (ΔH_f(average) = -1000 $\pm$ 35 kJ mol^{-1}).

The enthalpy of reaction for (3), $\Delta H(3)$ was calculated from tabulated data [77] to be -283 kJ mol^{-1}, which is comparable to the measured difference in enthalpies of the reactions in oxygen and nitrogen in the DSC, ΔH(oxygen)-ΔH(nitrogen), of -214 kJ mol^{-1}.

Feox, Coox, Niox and Cuox

Approximate values of the enthalpies of formation of the anhydrous individual oxalates, ΔH_f(Mox), were estimated from the experimental values of the enthalpies of reaction *in oxygen*, ΔH(oxygen) (from Table 4.2), assuming that products were the various possible metal oxides and carbon dioxide.

Mox(s) + oxygen → MO(s) + $2CO_2$(g) ..... (4)

Mox(s) + oxygen → $0.5M_2O$(s) + $2CO_2$(g) ..... (5)

Mox(s) + oxygen → $0.33M_3O_4$(s) + $2CO_2$(g) ..... (6)

Mox(s) + oxygen → $0.5M_2O_3$(s) + $2CO_2$(g) ..... (7)

The estimates are given in Table 5.1.

Table 5.1
ENTHALPIES OF FORMATION OF THE INDIVIDUAL OXALATES ESTIMATED FROM REACTIONS IN OXYGEN

		ΔH_f /kJ mol^{-1}			
Reaction	Compound	Fe	Cu	Ni	Co
Literature values for oxides [91]					
(1)	MO	-272	-157	-240	-238
(2)	½M_2O		-85.5		
(3)	⅓M_3O_4	-373			-297
(4)	½M_2O_3	-412			
Experimental					
$\Delta H(N_2)$		130	-33	71	98
$\Delta H(O_2)$		-251	-138	-193	-265
Estimates for the oxalates					
(1)	Mox	-803	-805	-834	-760
(2)	Mox		-734		
(3)	Mox	-908			-819
(4)	Mox	-947			
Estimates of $\Delta H_{formation}$ of the oxalates in O_2 (solid product)		-949 (Fe_2O_3)	-807 (CuO) -734 (Cu_2O)	-835 (NiO)	-820 (Co_3O_4)

The estimates of ΔH_f(Mox) (Table 5.1) were then combined with the measured enthalpies of reaction in N_2, ΔH (nitrogen) (also from Table 4.2) to investigate the stoichiometry of reaction. The two main possibilities for the decomposition reactions of divalent metal oxalates in inert atmospheres are:

$Mox(s) \rightarrow xM(s) + (1-x)MO(s) + (1-x)CO(g) + (1+x)CO_2(g)$ ....(8)

with extremes, $x=1$, giving

$Mox(s) \rightarrow M(s) + 2CO_2(g)$

and $x=0$

$Mox(s) \rightarrow MO(s) + CO_2(g) + CO(g)$

or, if M^{2+} is reduced to M^+,

$2Mox(s) \rightarrow 2xM(s) + (1-x)M_2O(s) + (1-x)CO(g) + (3+x)CO_2(g)$ ....(9)

Generally, for both pathways, $0 < x < 1$, and x may also vary with extent of reaction, α, and/or reaction temperature. Estimates of x for the decomposition of the individual oxalates, based on experimental ΔH values obtained in DSC experiments in N_2, are given in Table 5.2.

Table 5.2

ESTIMATES OF x, THE FRACTION OF METAL FORMED DURING THE DECOMPOSITION OF THE INDIVIDUAL OXALATES IN NITROGEN

	ΔH Reaction (8) kJ mol^{-1}			ΔH Reaction (9) kJ mol^{-1}	
	Fe	Ni	Co	Cu	Cu
$\Delta H_{f,Mox}$ kJ mol^{-1}	-949	-835	-820	-807	-734
from Table 5.1 reaction in O_2					
x					
0	172	90	76	145	2.0
0.1	171	86	72	132	-3.6
0.2	170	81	67	120	-9.2
0.3	169	77	63	107	-15
0.4	168	73	58	95	-20
0.5	167	69	54	82	-26
0.6	165	64	49	69	-32
0.7	164	60	45	57	-37
0.8	163	56	40	44	-43
0.9	162	51	36	32	-48
1.0	161	47	31	19	-54
Experimental					
$\Delta H(N_2)$ kJ mol^{-1}	130	71	98	-33	-33
x	?	0.42 Ni	?		0.65Cu
1-x		0.58 NiO			0.35Cu_2O

From these results it is clear that Cuox decomposes according to reaction (9), with x = 0.65 to give:

$2Cuox(s) \rightarrow 1.3Cu(s) + 0.35Cu_2O(s) + 0.35CO(g) + 3.65CO_2(g)$

The results in Table 5.2 suggest a higher oxidation state than +2 for some of the Fe in the product formed in N_2. TM studies (section 4.2) indicate the formation of Fe_3O_4. Allowance has to be made for the reaction [47, 49, 75]:

$4FeO(s) \rightleftharpoons Fe_3O_4(s) + Fe(s)$

for which the calculated ΔH is -51 kJ mol^{-1}, which is reported to occur on cooling.

It is possible that oxidation of Co_3O_4 in O_2 is incomplete and that the value of $\Delta H_{formation}$ of Coox is too low (-851 kJ mol^{-1} is quoted in the literature [91] and -886 kJ mol^{-1} was calculated for Co + $2CO_2$ in N_2).

Niox decomposes according to reaction (8), with x = 0.42 to give:

$Niox(s) \rightarrow 0.42Ni(s) + 0.58NiO(s) + 0.58CO(g) + 1.42CO_2(g)$

The enthalpies of formation of the hydrated individual oxalates, $\Delta H_f(Mox.nH_2O)$, were estimated from the enthalpies of the dehydration reactions, $\Delta H(10)$, and the values of $\Delta H_f(Mox)$.

$Mox.nH_2O(s) \rightarrow Mox(s) + nH_2O(g)$ ..... (10)

Results for the individual oxalates are given in Table 5.3.

Table 5.3
THERMOCHEMICAL DATA FOR THE INDIVIDUAL OXALATES

Compound	$\Delta H_{formation}$ / kJ mol^{-1}
Cuox	-734 ± 30
Feox $Feox.2H_2O$	-949 ± 30 -1533 ± 50
Coox $Coox.2H_2O$	-820 ± 30 -1406 ± 50
Niox $Niox.2H_2O$	-835 ± 30 -1450 ± 50

5.2 MIXED OXALATES

Similar calculations were done to obtain estimates of the enthalpies of formation of the hydrated and anhydrous mixed oxalates, $\Delta H_f(MCu(ox)_2.nH_2O)$ and, $\Delta H_f(MCu(ox)_2)$. The reactions assumed to occur were:

$FeCu(ox)_2(s)\ (O_2) \rightarrow \frac{1}{2}Fe_2O_3(s) + \frac{1}{2}Cu_2O(s) + 4CO_2(g)$ ....(11)

$FeCu(ox)_2(s)\ (N_2) \rightarrow FeO(s) + \frac{1}{2}Cu_2O(s) + 2CO(g) + 2CO_2(g)$ ....(12)

$CoCu(ox)_2\ (O_2) \rightarrow CoO(s) + CuO(s) + 4CO_2(g)$ ....(13)

$CoCu(ox)_2\ (N_2) \rightarrow Co(s) + Cu(s) + 4CO_2(g)$ ....(14)

$NiCu(ox)_2\ (O_2) \rightarrow NiO(s) + CuO(s) + 4CO_2(g)$ ....(15)

$NiCu(ox)_2\ (N_2) \rightarrow Ni(s) + Cu(s) + 4CO_2(g)$ ....(16)

Results for the mixed oxalates are given in Table 5.4.

Table 5.4

THERMOCHEMICAL DATA FOR THE MIXED OXALATES

Compound	$\Delta H_{formation}$ / kJ mol^{-1}
$FeCu(ox)_2$	-1587 ± 67
$FeCu(ox)_2.3H_2O$	-2540 ± 70
$CoCu(ox)_2$	-1564 ± 107
$CoCu(ox)_2.3H_2O$	-2516 ± 110
$NiCu(ox)_2$	-1714 ± 18
$NiCu(ox)_2.3.5H_2O$	-2765 ± 20

Values for $FeCu(ox)_2$ and $CoCu(ox)_2$ are similar, while $NiCu(ox)_2$ has a slightly higher (by 150 kJ mol^{-1}) enthalpy of formation.

Values of $\Delta H_f(MCu(ox)_2)$ can then be compared with values of $\Delta H_f(Mox)$ and $\Delta H_f(Cuox)$ to determine the extent of any interaction e.g.

$$Mox(s) + Cuox(s) \rightarrow MCu(ox)_2(s) \quad .....(18)$$

Values of $\Delta H(18)$ are given in Table 5.5. The estimated enthalpies of interaction are small and, except for $NiCu(ox)_2$, are within the accumulated experimental errors.

Table 5.5
INTERACTION OF OXALATES ON MIXING

ΔH_f kJ mol^{-1}					
Cuox	M	Mox	Cuox + Mox	$MCu(ox)_2$	ΔH(interaction) kJ mol^{-1}
-744 ± 10	Fe	-949±30	-1683±60	-1587±67	-82±120
	Co	-820±30	-1554±60	-1564±107	-10±170
	Ni	-835±30	-1569±60	-1714±18	-124±80

CHAPTER 6 KINETICS

6.1 INTRODUCTION

Results from isothermal and programmed temperature experiments have been used to obtain kinetic parameters for the dehydration and decomposition stages, in nitrogen, of the mixed metal oxalates, $FeCu(ox)_2.3H_2O$, $CoCu(ox)_2.3H_2O$, and $NiCu(ox)_2.3.5H_2O$. Some information on the kinetics of dehydration and of decomposition of the individual oxalates is available in the literature (see Section 1.8), but very little [60] information was found on the dehydration of nickel oxalate and on the dehydration and decomposition of iron(II) oxalate. To enable a comparison to be made between kinetic parameters for the mixed and for the individual oxalates, series of isothermal TG experiments were done on $Feox.2H_2O$ and $Niox.2H_2O$ to obtain the missing information.

6.2 RESULTS

6.2.1 Thermal dehydration of the individual oxalates

The isothermal TG curves were converted to α - time curves. The α values were used to calculate $f(\alpha)$ against time curves for the contracting-area (R2), contracting-volume (R3) and first-order (F1) models (see Table 1.4). These curves were then examined for linearity over significant ranges of α. Rate coefficients at each isothermal temperature were calculated from the slopes of these linear regions and used in Arrhenius plots to estimate activation energies and pre-exponential factors.

$Niox.2H_2O$

The very early portions of the α - time curves included some irregularities as the sample reached the set isothermal temperature. The curves were then deceleratory and the contracting-area equation (R2) gave the best fit (α = 0.2 - 0.9) at all temperatures.

Feox.$2H_2O$

An isothermal α - time curve for the dehydration of Feox at 175°C is shown in Figure 6.1 together with plots of $f(\alpha)$ against time. The initial section of the α - time curve shows a brief acceleratory period, $0 < \alpha < 0.15$, followed by an approximately linear region, $0.15 < \alpha < 0.6$, and finally a deceleratory region. The R2 and R3 models gave approximately linear segments for $0.2 < \alpha < 0.9$, from which values of k' could be calculated. ($f(\alpha) = k't$, where $k' = k/2$ for the R2 model and $k' = k/3$ for the R3 model.)

A plot of $v = d\alpha/dt$ against time is shown in Figure 6.2. This plot shows an approximately linear segment from $0.3 < \alpha < 0.93$. This is a better test of the applicability of the R2 model, since for the R2 model:

$v = d\alpha/dt = 2k' (1 - k't)$

On this time scale, $v = 2k'$ when $t = 0$, and the slope of the plot of v against t is $-2(k')^2$. If a correction, t_o, to the time scale is required, i.e. $t' = t - t_o$ (where t is the actual time recorded and t' is the time elapsed since the onset of the process described by the R2 model), then t_o can be calculated from: t_o = (intercept - 2k') / slope.

As an additional test, a plot of ln v against $\ln(1 - \alpha)$ was prepared (Figure 6.3). $v = k(1 - \alpha)^n$, so $\ln v = n \ln(1 - \alpha) + \ln k$. This curve showed an approximately linear region from $-0.28 < \ln(1 - \alpha) < -2.98$ which corresponds to $0.24 < \alpha < 0.95$. The slope of this plot is the apparent order, $n = 0.81 \pm 0.02$. This value lies between the values expected for the R3 ($n = 0.67$) and F1 ($n = 1.00$) models. The intercept is ln k. Care has to be taken in comparison of k and k' on account of the usually neglected integration factors (see above).

Figure 6.1 The dehydration of Feox.$2H_2O$ from isothermal TG at 175°C

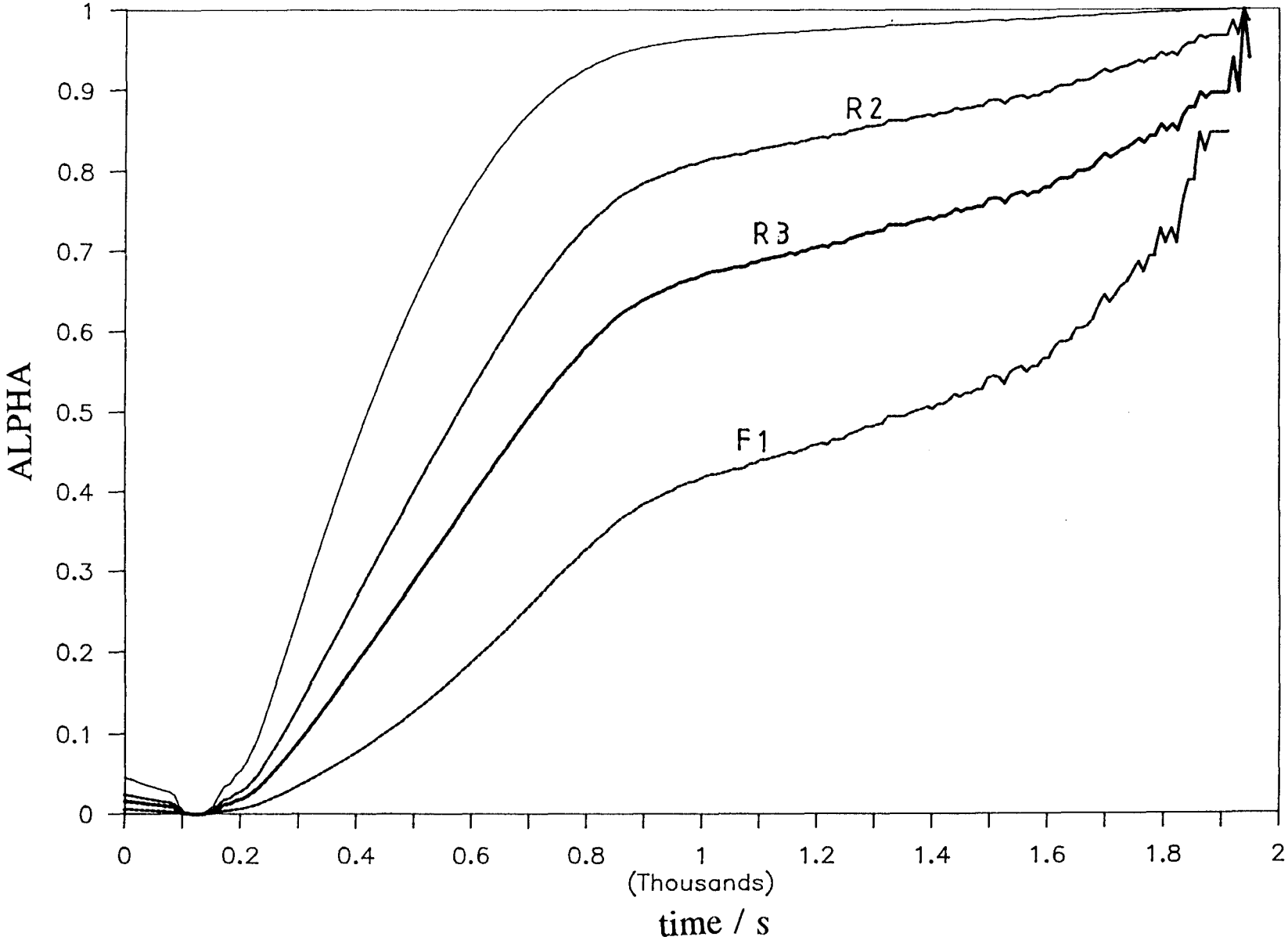

Figure 6.2 Rate of dehydration of Feox.2H_2O at 175°C from isothermal TG

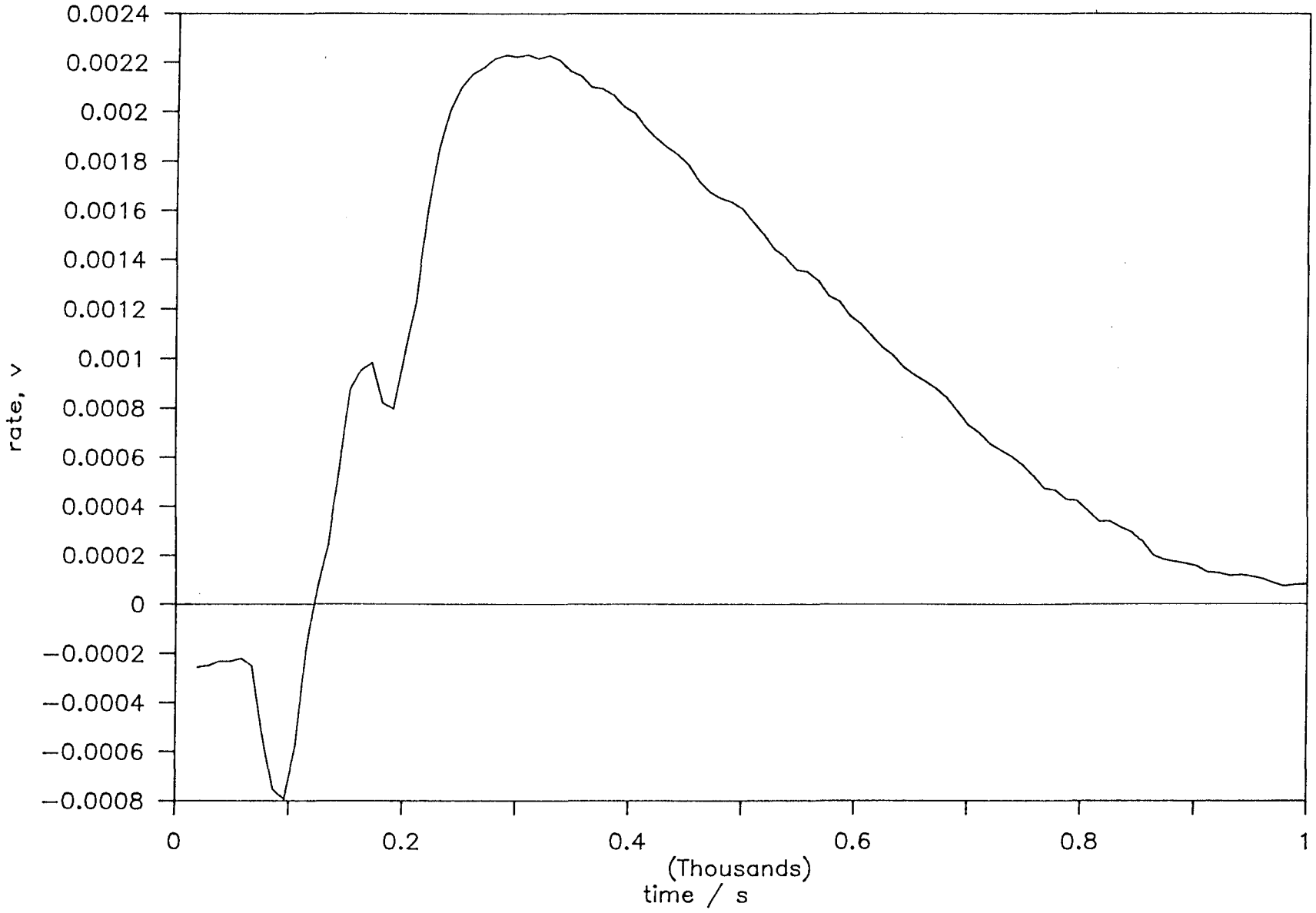

Figure 6.3 ln v vs ln (1 - α) plot for the dehydration of Feox.$2H_2O$ at 175°C

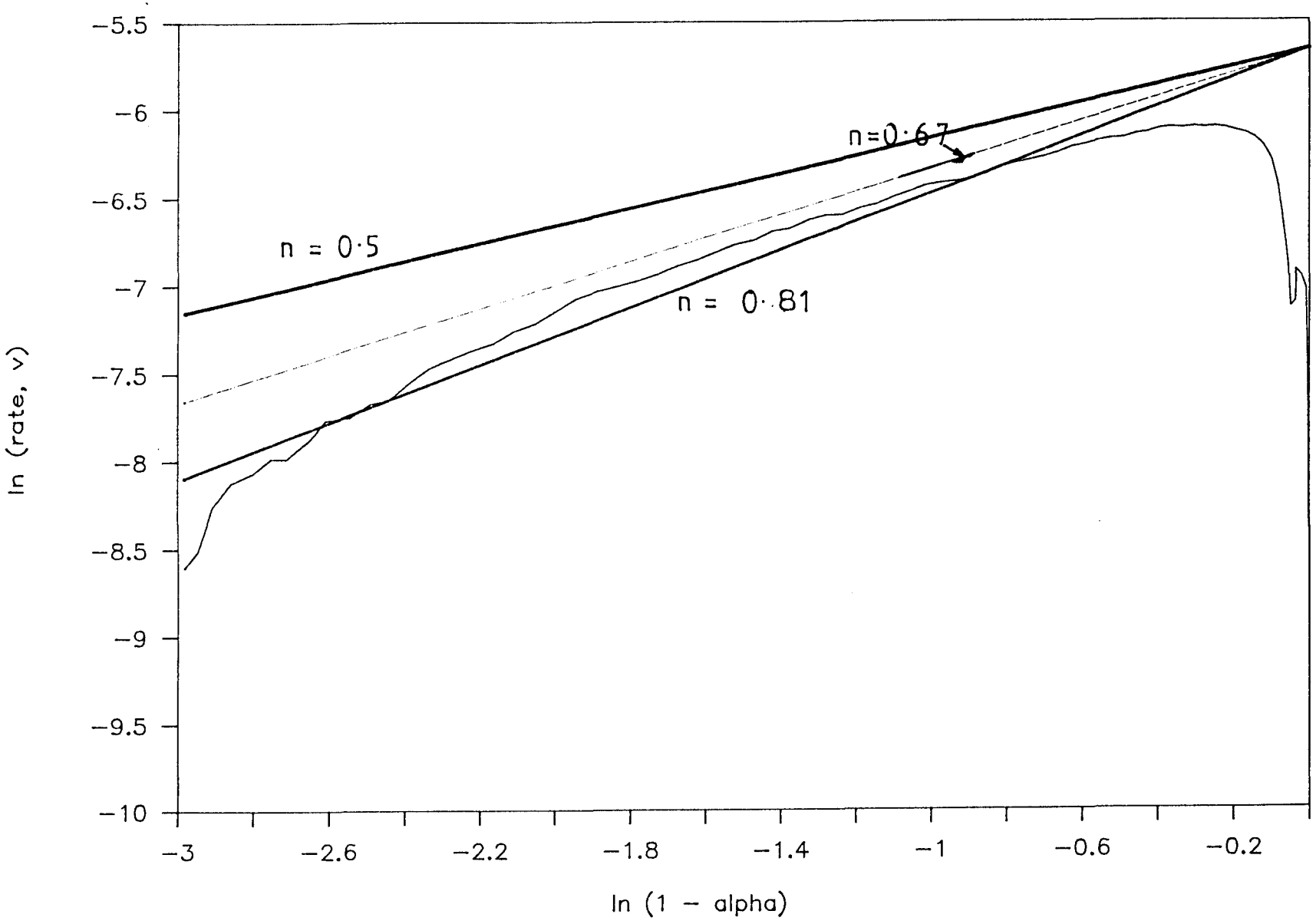

Similar calculations were done at the other temperatures and Table 6.1 contains a summary of the kinetic data obtained for the dehydration of Feox, using these methods.

Table 6.1.
KINETIC DATA FOR THE DEHYDRATION OF Feox

T/°C	α range	k'(R2) $x10^{-3}$	k'(R3) $x10^{-3}$	k $x10^{-3}$	n
165					
(1)	0.23-0.99	0.694	0.615		
(2)	0.36-0.99	0.746			
(3)	0.24-0.99			1.783	0.67
170					
(1)	0.08-0.95	0.882	0.718		
(2)	0.46-0.97	0.945			
(3)	0.40-0.95			2.141	0.65
175					
(1)	0.2-0.9	1.246	1.015		
(2)	0.24-0.95	1.406			
(3)	0.3-0.93			3.45	0.81
180					
(1)	0.15-0.90	1.276	1.015		
(2)	0.47-0.93	1.466			
(3)	0.25-0.89			2.933	0.64
185					
(1)	0.07-0.93	2.111	1.688		
(2)	0.43-0.93	2.405			
(3)	0.24-0.99			4.712	0.58

(1) From f(α) against t
(2) From v against t
(3) From ln v against ln (1 - α)

Results of the dehydration studies done on the individual oxalates are summarised in Table 6.2.

Table 6.2.
KINETIC PARAMETERS FOR THE DEHYDRATION OF THE INDIVIDUAL OXALATES

T-range /°C	Model	α-range	E_a/ kJ mol^{-1}	ln A /s^{-1}
Niox.$2H_2O$ 180-205	R2	0.2-0.9	68 ± 15	9.8 ± 0.16
Feox.$2H_2O$ 165-185	R2(1) R2(2) R3(1) (3)	0.23-0.9 0.47-0.93 0.23-0.9 0.3-0.89	87 ± 12 93 ± 12 79 ± 14 75 ± 17	16.5 ±0.12 18.2 ±0.11 14.2 ±0.13 14.4 ±0.16
prog. T 1°C min^{-1} [60]	R3	0.04-0.99	106 ± 2	21.9
Coox.$2H_2O$ prog. T 1°C min^{-1} [60]	F1	0.04-0.94	158 ± 1	36.2

(1) From f(α) against t
(2) From v against t
(3) From ln v against ln (1 - α)

An activation energy for the dehydration of Feox.$2H_2O$ [60] of 106.3 kJ mol^{-1} has been reported and is not too different from the values reported in Table 6.2. The activation energy for the dehydration of Niox.$2H_2O$ of 68 $\pm$ 15 kJ mol^{-1} is similar to values obtained for the dehydration of other oxalates, but is very different from the activation energy of 252 kJ mol^{-1} quoted by Mu and Perlmutter [60].

For many closely related reactions, a linear relationship is observed between the Arrhenius parameters (A and E_a) for the individual reactions, i.e.

$\ln A = B E_a + C$

where B and C are constants. This is called the compensation effect [78]. A plot of ln A against E_a for the dehydration of Feox, Coox and Niox, is shown in Figure 6.4. Although there are only three compounds, there is an apparent compensation effect for the dehydration of the individual oxalates.

Figure 6.4 Compensation effect for the dehydration of the individual oxalates

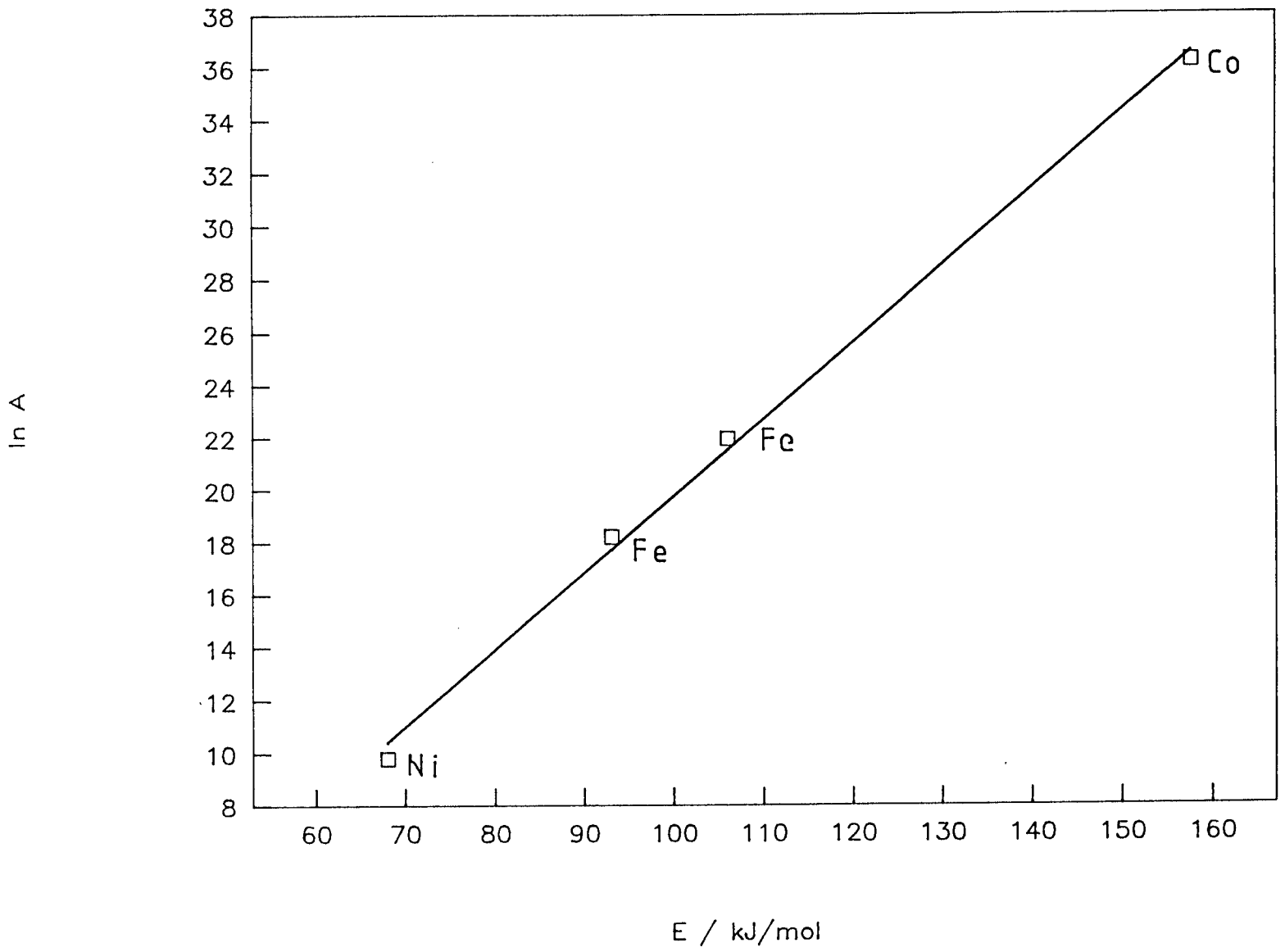

6.2.2 Thermal decomposition of the individual oxalates

Feox

Isothermal (330 - 350°C) TG decomposition curves for Feox were converted to α - time curves and an example is shown in Figure 6.5. The curves were best fitted by the contracting-volume equation (R3) over the range α = 0.1 - 0.9. An activation energy of 141 $\pm$ 22 kJ mol^{-1} and A = 1.2 x 10^8 s^{-1} were obtained for the decomposition. A value of 113 kJ mol^{-1} is quoted in the literature [60].

Reported values for activation energies of 665 kJ mol^{-1} for the decomposition of Cuox and 766 kJ mol^{-1} for the decomposition of Niox [60] are exceptionally high in comparison with values obtained by other authors [62, 66, 67, 68]. These values were therefore ignored in the investigation of a compensation effect for the decomposition.

The limited data gave a linear compensation plot (ln A against E_a) for the decomposition of Feox, Cuox and Coox (Figure 6.6). Niox was not included in the plot, since values of A, for decomposition in N_2 could not be obtained from the literature.

Figure 6.5 The decomposition of Feox from isothermal TG at 345°C

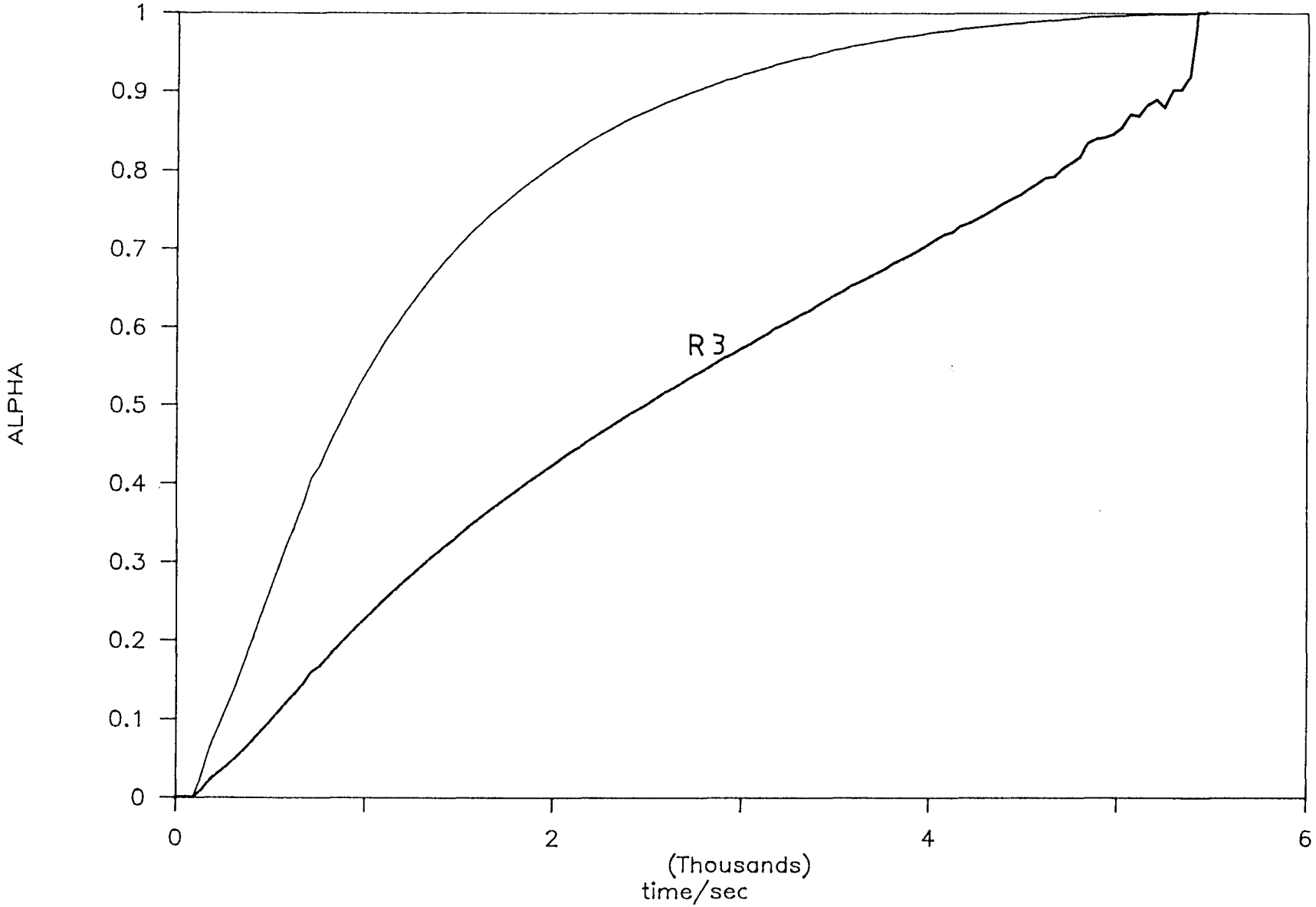

Figure 6.6 Compensation effect for the decomposition of the individual oxalates

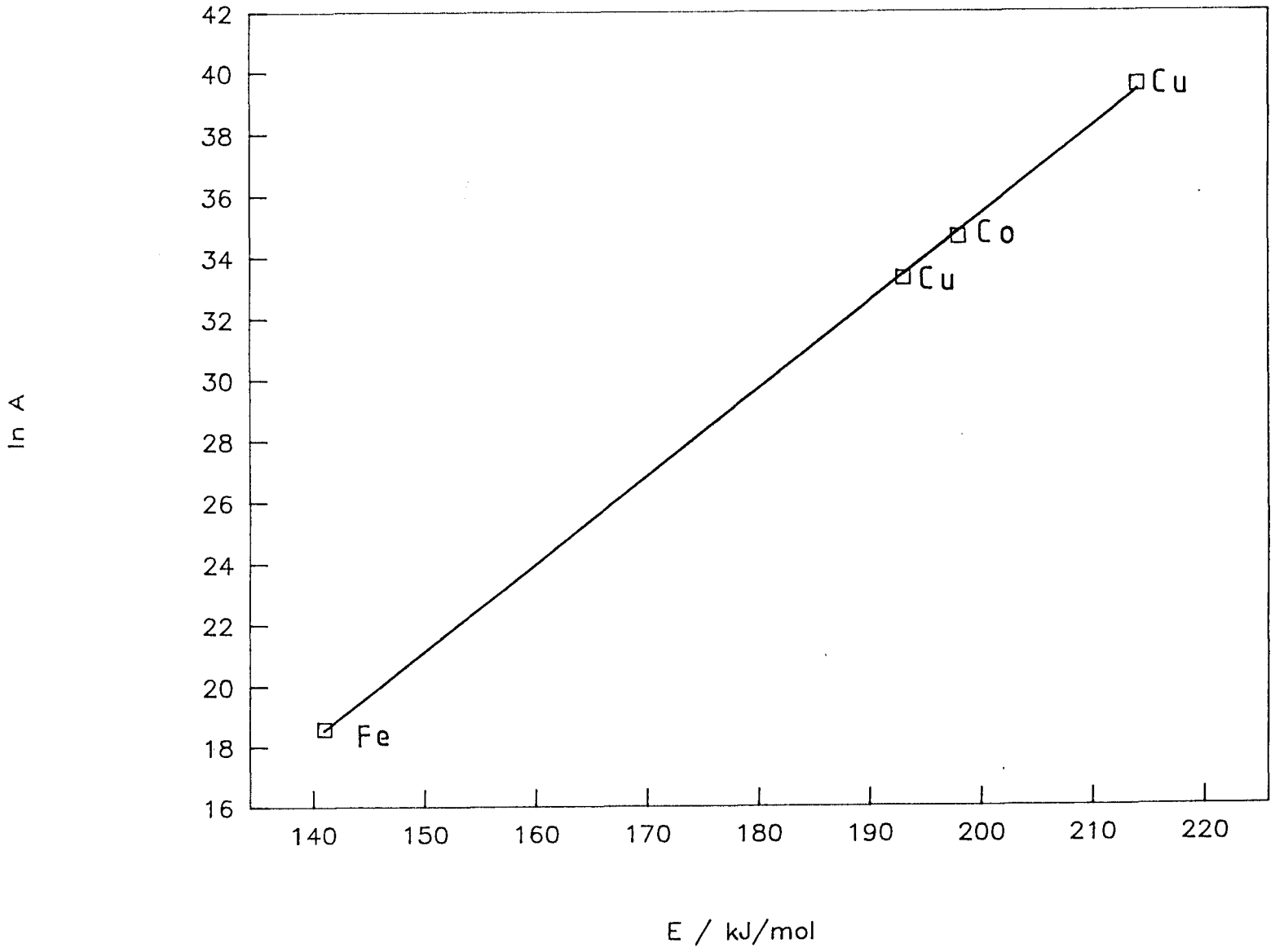

6.2.3 Thermal dehydration of the mixed oxalates

Isothermal TG and DSC curves were converted to α - time curves. The α - time curves included some irregularities as the samples reached the set isothermal temperatures. The curves obtained from the TG experiments were then deceleratory and the contracting-area equation (R2) generally gave the best fit over the widest α range. Some α - time curves ($FeCu(ox)_2$ and $CoCu(ox)_2$), obtained from DSC experiments, showed a linear region for $\alpha < 0.7$, followed by a deceleratory region, up to $\alpha = 0.99$.

Programmed temperature TG and DSC curves for the dehydration of the mixed oxalates were converted to α - temperature curves, and kinetic parameters were estimated, using the Borchardt and Daniels [79] method. The deviation of the DSC curve from the baseline is proportional to $(d\alpha/dt)$ and the ratio of the partial area (s) to the total area under the curve (S) is a measure of α. k can be obtained from $(d\alpha/dt) = k (1 - \alpha)^n$ if n is known. Values of n were substituted according to the models used for isothermal experiments. For programmed temperature TG experiments, α was taken to be the fractional mass loss, and $d\alpha/dt$ was obtained by differentiation of the TG curve, using a 9-point Savitsky-Golay [80] method.

The kinetic results for the dehydrations of the mixed oxalates are summarised in Table 6.3.

Table 6.3.
KINETIC PARAMETERS FOR THE DEHYDRATION OF THE MIXED OXALATES IN NITROGEN

T-range /°C	Models	α-range	E_a /kJ mol^{-1}	ln (A/s^{-1})
$FeCu(ox)_2.3H_2O$ isothermal TG 130-145	R2	0.3-0.8	47 ± 12	6.83±0.097
isothermal DSC 145-170	zero order	<0.7	80 ± 13	16.77±0.17
	R2	0.7-0.99		
programmed T TG	R2	0.1-0.8	92 ± 1	33.3±0.07
programmed T DSC	R2	0.1-0.8	90 ±0.1	33.95±0.003
$CoCu(ox)_2.3H_2O$ isothermal TG 115-135	R2	0.2-0.9	130 ± 9	32.9±0.11
isothermal DSC 125-150	zero order	0-0.8	89 ± 5	19.75±0.08
	R2	0.8-0.99		
programmed T TG	R2	0.1-0.7	118 ±2	41.38±0.05
programmed T DSC	R2	0.0-0.8	109 ± 0.2	39.15±0.01
$NiCu(ox)_2.3.5H_2O$ isothermal TG 165-185	R2	0.25-0.85	95 ± 17	18.94±0.17
isothermal DSC 165-185	R2	0.01-0.9	86 ± 16	15.59±0.12
programmed T TG	R2	0.1-0.85	98 ± 1	32.75±0.07
programmed T DSC	R2	0.1-0.8	101 ± 0.1	34.36±0.01

The activation energies obtained using programmed temperature TG and DSC runs were in good agreement. Isothermal TG results are probably the least reliable owing to temperature calibration problems, especially at lower temperatures. There was reasonable agreement between E_a values obtained from the programmed temperature and isothermal

DSC runs. Differences in the values of A obtained arise from the incorporation of various constants, including the heating rate, in this term, depending on the method of analysis.

Values of E_a for dehydration of the three mixed oxalates are very similar and are also similar to E_a values for the dehydration of the individual oxalates (Table 6.2).

THE COMPENSATION EFFECT AND THE MIXED METAL OXALATE DÈHYDRATIONS

A plot of ln A against E_a for the dehydration of $FeCu(ox)_2$, $CoCu(ox)_2$ and $NiCu(ox)_2$, is shown in Figure 6.7. Although there are only three compounds, there is an apparent compensation effect for the dehydration of the individual oxalates.

Figure 6.7 Compensation effect for the dehydration of the mixed oxalates

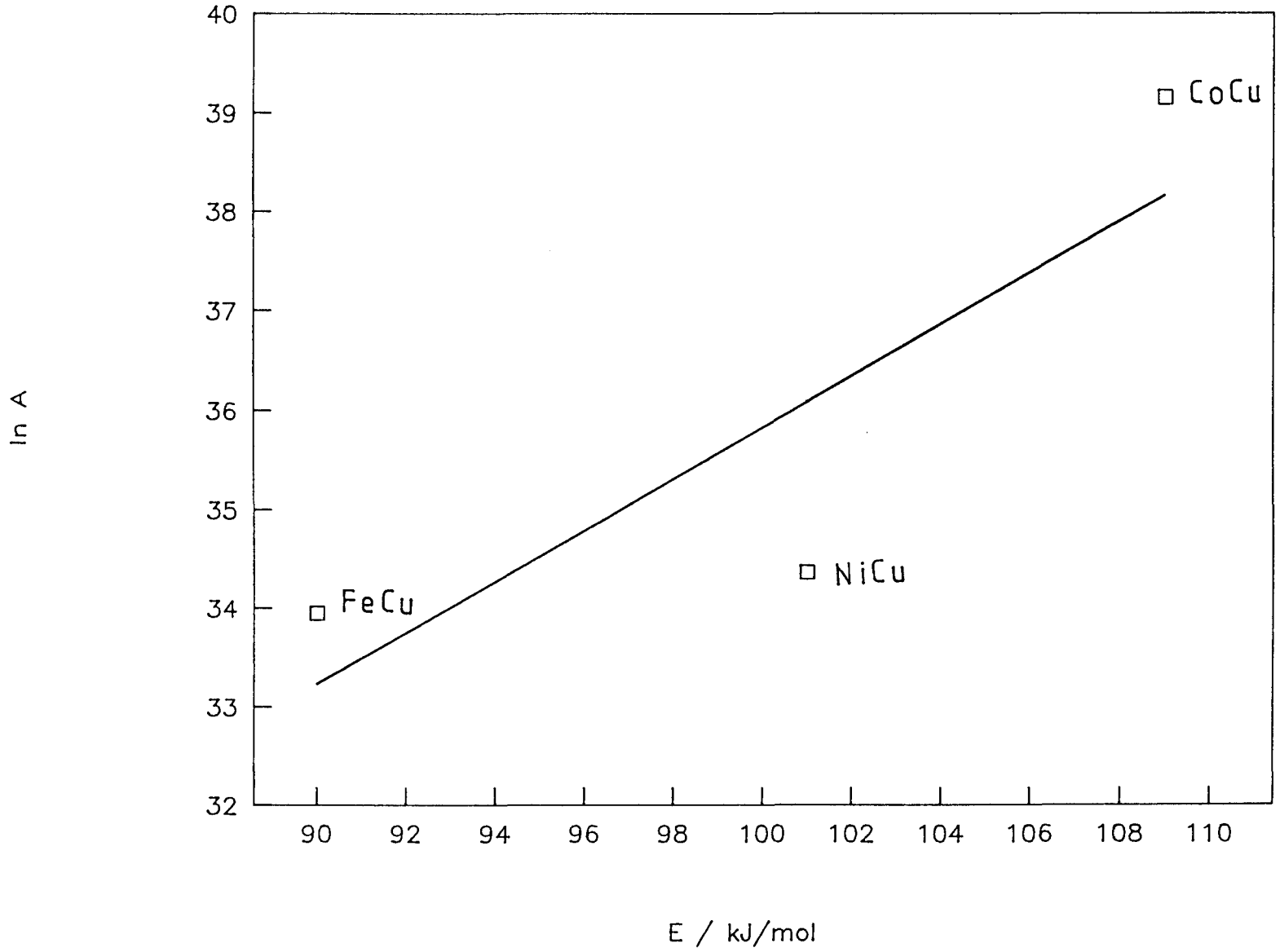

6.2.4 Thermal decomposition of the mixed oxalates

Kinetic analysis

Isothermal TG, DSC and TCD (except for $FeCu(ox)_2$) curves were converted to α - time and rate - time curves. Programmed temperature TG and DSC curves for the decomposition of the mixed oxalates were converted to α - temperature curves, and analyzed according to the Borchardt and Daniels [79] method.

Isothermal rate ($v = d\alpha/dt$) against time, t, curves, derived from isothermal TG experiments, for the decompositions of the mixed oxalates showed at least two overlapping rate processes. The shapes of the peaks indicated that both processes were initially acceleratory, passed through maxima (at different times) and then decelerated to completion (at different times). The Avrami-Erofe'ev equation (An), which is the most useful kinetic expression for describing such sigmoidal α-time relationships, leads to rate-time expressions of the form [81]:

$v = n\, k^n\, t^{(n-1)} \exp(- (kt)^n)$ ..... (1)

For concurrent processes, the overall isothermal rate, v, may be assumed to be made up of contributions $v_1, v_2,\ldots,v_i$ from the individual processes, combined with weighting factors, $w_1, w_2,\ldots,w_i$, so that:

$v = w_1v_1 + w_2v_2\ldots + w_iv_i$ ..... (2)

In this analysis, each of the contributions, v_i, was assumed to have the form of equation (1), with individual values k_i and n_i for each process i. Experimental v,t values (corrected if necessary for a time delay, t_o, so that $t' = t - t_o$) were then compared with v,t values calculated using suitable values of n_i, k_i and w_i, and the sums of the squares of the residuals,

$S_v = \Sigma R_v^2 = \Sigma (v_{exp} - v_{calc})^2$ and $S_\alpha = \Sigma R_\alpha^2 = \Sigma (\alpha_{exp} - \alpha_{calc})^2$ were minimised by adjustment of n_i, k_i, w_i and, if necessary, t_o, to give a reasonable visual match of experimental and calculated v,t and α,t curves. Values of n control the shapes of the peaks and values of k and t_o determine the height and position of the peak on the time scale.

Application of the above analysis showed that generally the earlier processes can be fitted

by sigmoidal models, but the final process is deceleratory. Information about the final decay process could be obtained by examining f(α) - time curves derived from the α - time curves obtained from the isothermal experiments.

For a single rate process involving both mass and enthalpy changes, α - time curves calculated from isothermal TG (α = fractional mass change) and isothermal DSC (α = fractional enthalpy change) experiments should be identical. Differences can arise from: (a) differences in the environment experienced by the sample in the two different instruments (as discussed in Section 1.6); or (b) different actual sample temperatures arising from the different calibration procedures in TG and DSC. When the rate process is complex, contributing processes will generally be accompanied by enthalpy changes of different magnitudes. Weighting factors for a complex DSC curve would then have to include enthalpy contributions for each process (and for DTA, contributions allowing for different heat capacities of the contributing reaction systems would have to be considered).

$FeCu(ox)_2$

An example of an α - time and rate - time curve, derived from isothermal TG (270 - 285°C) experiments, is shown in Figure 6.8. The decomposition of $FeCu(ox)_2$ is more complex than those of either the Co or Ni salts described below. From the low temperature rate - time traces, at 270 and 275°C, at least three processes could be distinguished, but at higher temperatures the second and third processes tended to merge. Values were selected for n_1, n_2, n_3, k_1, k_2, k_3, w_1, w_2 and w_3 for each isothermal experiment (270 - 285°C) as described above. Results are listed in Table 6.4. With so many adjustable parameters, values of the Avrami-Erofe'ev exponents, n_1, n_2 and n_3 were set initially = 3, and only adjusted if no other changes proved satisfactory. The weighting factors were adjusted independently, and $w_1 + w_2 + w_3$ is not necessarily = 1. A residual slow decay was not included in the analysis. The weighting factor for the first process, w_1, was approximately constant at 5-8%. Rate-time curves at 280 and 285°C were initially described by two distinguishable concurrent processes plus a residual slow decay. The rate coefficients estimated for apparent process 2 (labelled 2*) in this

way, however, showed little variation in temperature, and hence gave an apparent activation energy of effectively zero (Table 6.5). The large change in weighting factor, w_2, at the higher temperatures indicates the merging of processes 2 and 3 to give process 2*. In an attempt to improve the analysis, the first two values of k_2 and k_3 (i.e. at 270 and 275°C) were used to estimate the Arrhenius parameters of processes 2 and 3, and hence to estimate values expected for k_2 and k_3 at the higher temperatures (280 and 285°C). Rate-time curves at 280 and 285°C were then re-analyzed in terms of three processes. A resulting experimental and calculated rate-time curve at 270°C is shown in Figure 6.9. The estimated values of the Arrhenius parameters for the three processes are listed in Table 6.4.

Table 6.4.
RATE PARAMETERS FOR THE DECOMPOSITION OF $FeCu(ox)_2$
(Note: $t_0 = 0$ at all temperatures; $w_1 + w_2 + w_3 \leq 1$)
(* refers to merged processes 2 and 3;
refers to values predicted from low temperature results)

T/°C	n_1	n_2	n_3	w_1	w_2	w_3	k_1 /10^3	k_2 /10^3	k_3 /10^3
270	3	3	3	0.08	0.11	0.45	3.3	1.32	0.35
275	3	3	3	0.07	0.09	0.44	3.5	1.46	0.43
280*	4	2.5		0.06	0.38	0	4.0	1.3	
285*	4	3		0.05	0.53	0	4.0	1.4	
280#	4	3	3	0.06			4.0	1.61#	0.53#
285#	4	3	3	0.05			4.0	1.77#	0.64#
280	4	2.5	3	0.06	0.32	0.30	4.0	1.40	0.50
285	4	3	3	0.05	0.45	0.20	4.0	1.50	0.64

Values of k_1, k_2 and k_3 were then used in Arrhenius plots to estimate E_a and A. Values obtained are given in Table 6.5. From the α - time curves, it was only possible to distinguish between two processes . The final deceleratory stage (an overlap of process 2 and 3 above) of the α - time curve corresponded well with the contracting-area equation (R3) (α = 0.5 - 0.8). The α values for this stage, for $\alpha < 0.5$, were masked by the first

reaction and could not be calculated. An Arrhenius plot for the second, faster reaction, gave an activation energy of 155 ± 40 kJ mol^{-1} (see Table 6.5).

α - time curves, derived from isothermal DSC (290 - 320°C) experiments, included some irregularities as the sample reached the set isothermal temperature, and the curves were deceleratory (see Figure 6.10). It was not possible to isolate the individual decomposition steps and an overall activation energy of 61 ± 10 kJ mol^{-1} was obtained, using the R3 model, over a range of α = 0 - 0.9.

Kinetic data obtained for the decomposition of $FeCu(ox)_2$ are summarised in Table 6.5.

Table 6.5.

KINETIC DATA FOR THE DECOMPOSITION OF $FeCu(ox)_2$ IN N_2

T range/ °C	models	α-range	E_a/ kJ mol^{-1}	ln (A/s^{-1})
isothermal TG 270-300	R3	0.5-0.8	155 ±40	24.5±0.4
	An	process 1 2* 2 (based on 3 only two points)	 35.9 ± 8.7 3 ± 14 49 102	 2.23±0.04 -5.91±0.06 4.27 14.60
isothermal DSC 290-320	R3	0.0-0.9	61 ± 10	3.94±0.096
programmed T TG	R3	First stage Second stage	292 ± 2 202 ± 4	67.46±0.03 45.85±0.06
programmed T DSC	R3	0.2-0.9	253 ± 3	58.16±0.04

Activation energies obtained from the programmed temperature experiments, using either TG or DSC were similar, but were considerable higher than values derived from isothermal experiments.

Figure 6.8 The decomposition of $FeCu(ox)_2.3H_2O$ from isothermal TG at 270°C

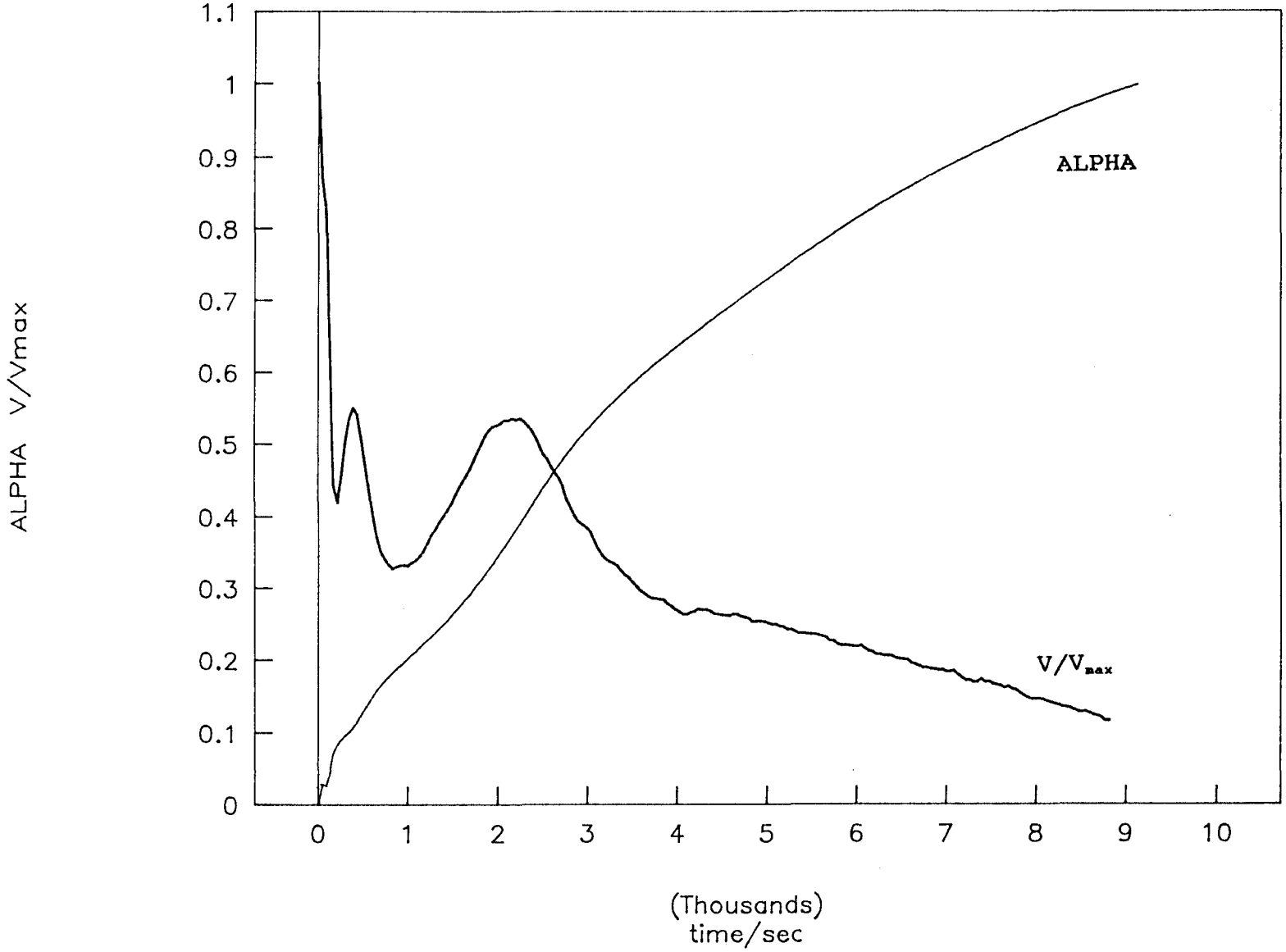

Figure 6.9 Experimental and calculated rate - time plots for the decomposition of $FeCu(ox)_2.3H_2O$ at 270°C

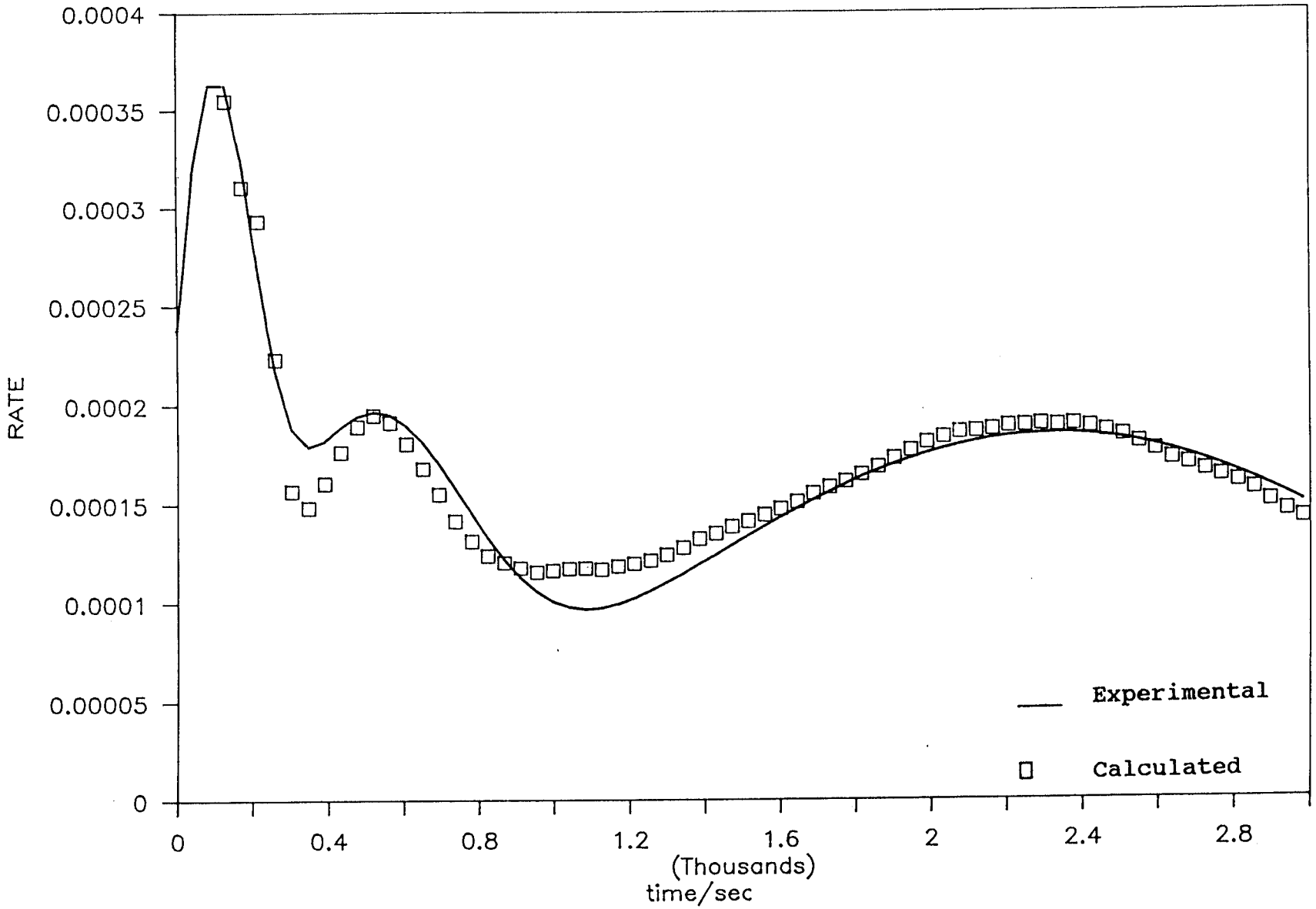

Figure 6.10 The decomposition of $FeCu(ox)_2.3H_2O$ from isothermal DSC at 300°C

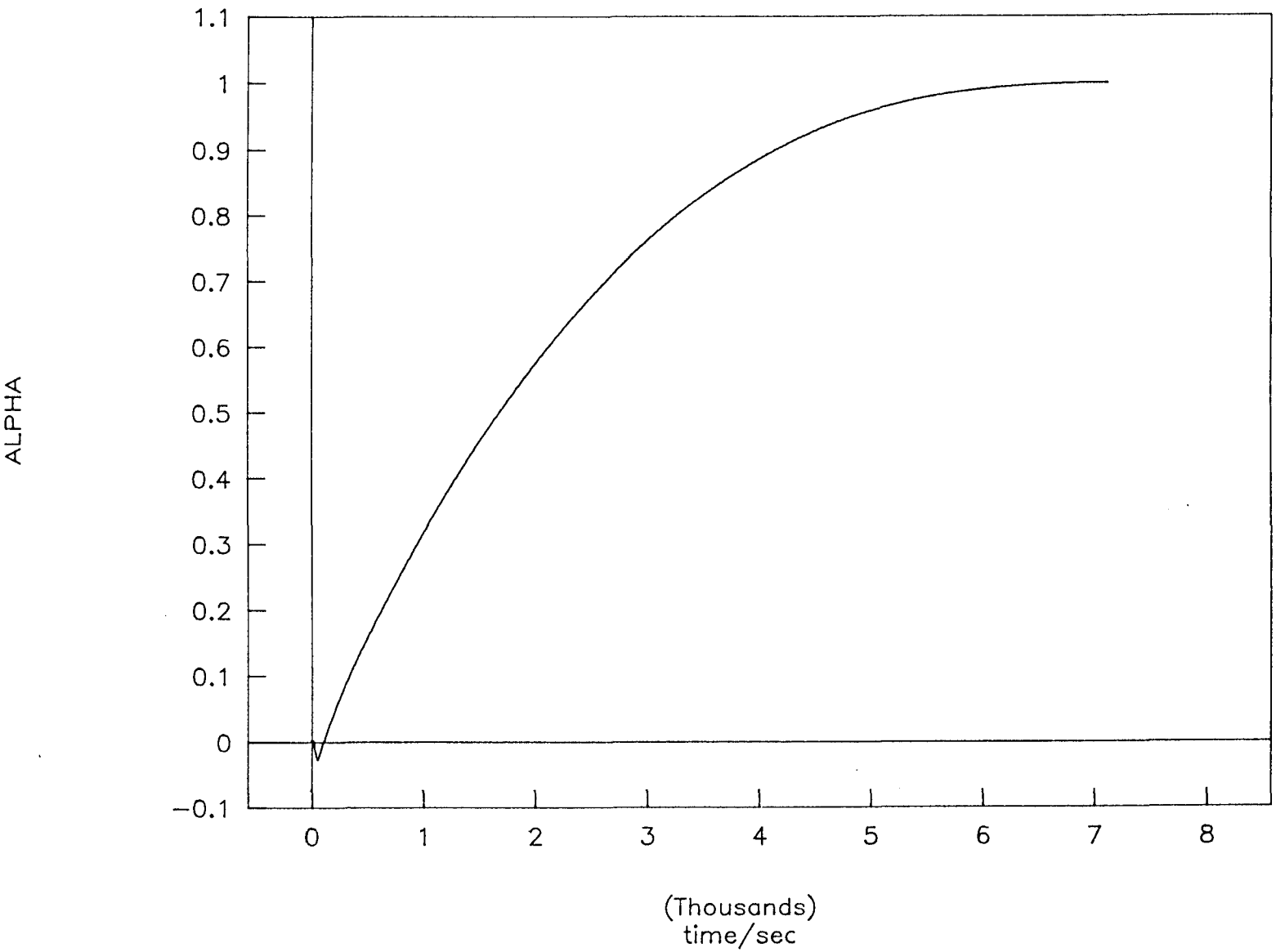

$CoCu(ox)_2$

An example of an α - time and rate - time curve, derived from isothermal TG (300 - 340°C) experiments, is shown in Figure 6.11. On the basis of the rate - time curves, the reaction was analyzed in terms of two concurrent processes. The values selected for n_1, n_2, k_1, k_2, w_1 and w_2 and t_o for each isothermal experiment (300 - 340°C) on the decomposition of $CoCu(ox)_2$ are listed in Table 6.6. Except at the lowest temperature studied, the values of the Avrami-Erofe'ev exponents, n_1 and n_2, were approximately constant at 5.0 and 2.0, respectively. The weighting factor varied in a narrow range from 0.28 to 0.40. The values of k_1 and k_2 were used in conventional Arrhenius plots to give the Arrhenius parameters for the two processes listed in Table 6.8. A resulting experimental and calculated rate-time curve at 330°C is shown in Figure 6.12.

Table 6.6.

RATE PARAMETERS FOR THE DECOMPOSITION OF $CoCu(ox)_2$

T/°C	t_o/s	n_1	n_2	$k_1/10^3$	$k_2/10^3$	w_1	$w_2=1-w_1$
300	0	4	2	1.7	0.369	0.23	0.77
310	0	4	2	2.4	0.317	0.34	0.66
320	60	5	1.8	3.2	0.484	0.34	0.66
330	300	5	2	6.5	0.650	0.29	0.71
340	24	5	2	9.0	1.285	0.37	0.63

The α - time curves also showed the overlap of two processes, an initial fast process and a slower process. The second, slow process could be described by the contracting-volume equation (R3) over the range α = 0.6 - 0.8. The α values for the second stage, for $\alpha < 0.5$, masked by the first reaction, were calculated from the R3 line. Values for the rate coefficient of the slow reaction were obtained from the slopes of the R3 lines, at various temperatures. These values were used in an Arrhenius plot, which resulted in an activation energy of 133 $\pm$ 7 kJ mol^{-1} for the slow reaction. This result was compared with the activation energy of 128 $\pm$ 3 kJ mol^{-1}, obtained from an Arrhenius plot, using the initial slopes of the slow reaction, for $\alpha < 0.5$. The use of initial slopes is based on

the assumption of a rate equation of the form $(d\alpha/dt) = k(1 - \alpha)^n$, so that when α is small $(d\alpha/dt) \approx k$ or $\alpha \approx kt$. The activation energy of the fast reaction was obtained using the difference between the initial slopes of the total and slow reaction steps. An Arrhenius plot using these rate coefficients gave an activation energy of 178 ± 39 kJ mol^{-1}.

The rate - time curves derived from isothermal DSC experiments (325°C and 330°C) for the decomposition of $CoCu(ox)_2$, were analyzed in terms of two concurrent processes, as described above, to obtain values for n_1, n_2, k_1, k_2, w_1 and w_2. The values obtained are shown in Table 6.7 and are compared with values predicted from TG results at 330°C.

Table 6.7.
RATE PARAMETERS FOR THE DECOMPOSITION OF $CoCu(ox)_2$
**values calculated at 330°C from TG results
t_o = 0 at all temperatures

T/°C	n_1	n_2	$k_1/10^3$	$k_2/10^3$	w_1	$w_2=1-w_1$
325	2.2	2	2.5	0.9	0.115	0.58
330	2.5	2.2	3.1	1.37	0.145	0.58
**	5	2	4.65	0.714	0.3	0.7

The α - time curves (see Figure 6.13 for an example) derived from isothermal (320 - 345°C) DSC experiments were initially approximately linear ($\alpha < 0.5$), followed by a deceleratory curve. The first stage of decomposition was therefore treated as a zero-order process and an activation energy of 92 ± 32 kJ mol^{-1} was obtained. The final stage of decomposition fitted the contracting-volume (R3) equation well and resulted in an activation energy of 101 ± 16 kJ mol^{-1}.

α - time curves for the evolution of gas, derived from the output of a thermal conductivity detector (TCD), during the isothermal decomposition of $CoCu(ox)_2$ at 345°C can be seen in Figure 6.14. Only CO_2 was evolved during decomposition. The curve generated from the TCD results has approximately the same shape as the α - time curve, generated from DSC results, over the later stages of reaction allowing for a 50 second time lag. Differences in the early stages of decomposition, $\alpha < 0.25$, indicate that the thermal effects do not match the gas evolution pattern during this part of the

decomposition.

The kinetic data, obtained for the decomposition of $CoCu(ox)_2$ in N_2 are summarised in Table 6.8.

Table 6.8

KINETIC DATA FOR THE DECOMPOSITION OF $CoCu(ox)_2$ IN NITROGEN

T range /°C	models	α-range	E_a/ kJ mol^{-1}	ln (A /s^{-1})
isothermal TG 300-340	R3 initial rate	0.6-0.8 <0.5 <0.5	133 ± 7 128 ± 3 178 ± 39	19.38±0.04 18.17±0.02 29.23±0.29
	An	process 1 2	123 ± 12 92 ± 22	19.37±0.13 11.26±0.24
isothermal DSC	zero order R3	<0.5 >0.5	92 ±39 101 ± 16	11.01±0.201 10.76±0.06
programmed T TG	R3	first stage second stage	221 ± 2 325 ± 5	52.11±0.05 69.4±0.023
programmed T DSC	R3	0.3-0.9	276 ± 5	68.28±0.078

The activation energy obtained for the first stage of decomposition from the programmed temperature TG experiment and the activation energy obtained from the programmed temperature DSC experiment are comparable, but values are again higher than those obtained from isothermal experiments.

Figure 6.11 The decomposition of $CoCu(ox)_2.3H_2O$ from isothermal TG at 330°C

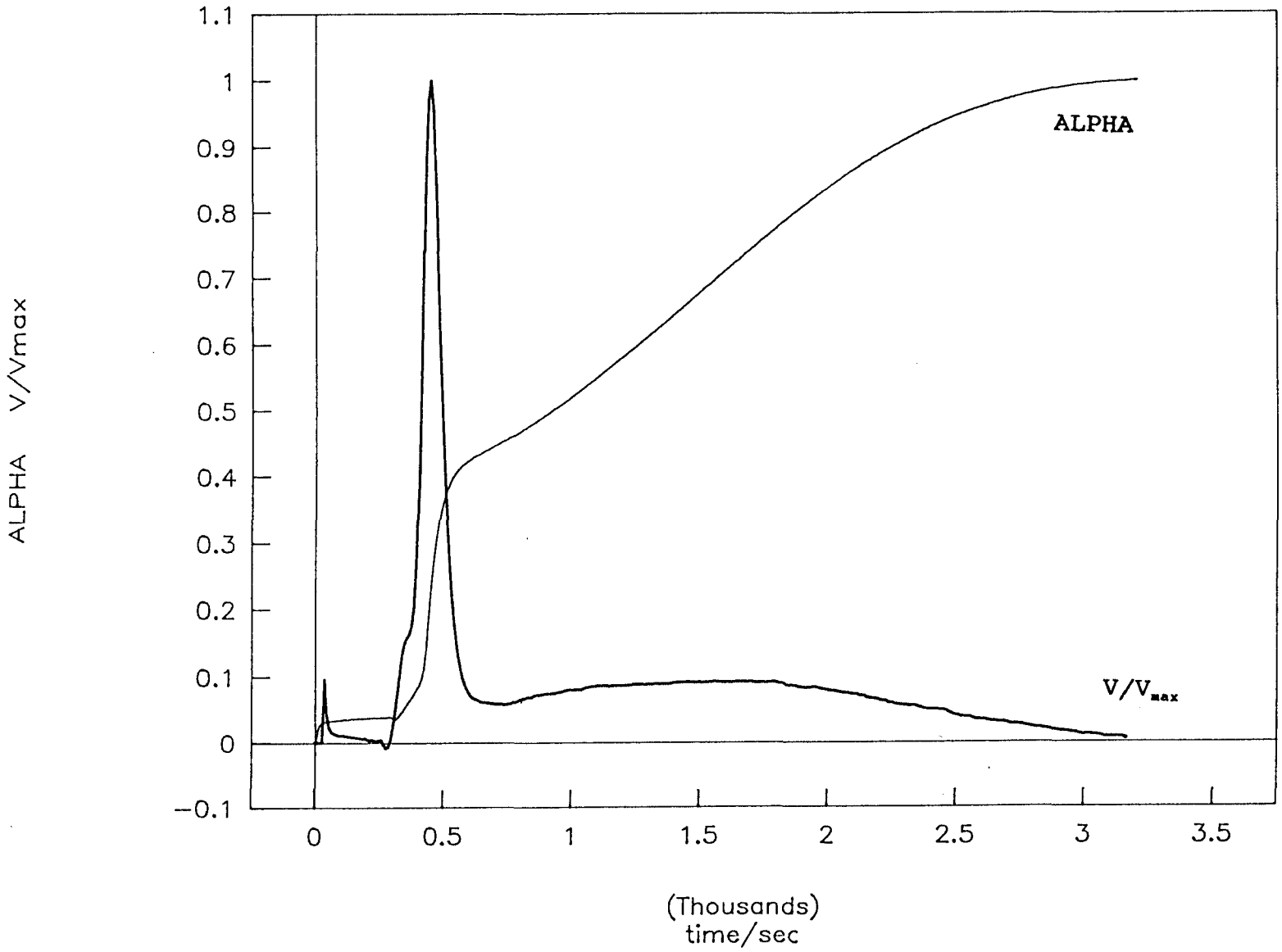

Figure 6.12 Experimental and calculated rate - time plots for the decomposition of $CoCu(ox)_2.3H_2O$ at 330°C

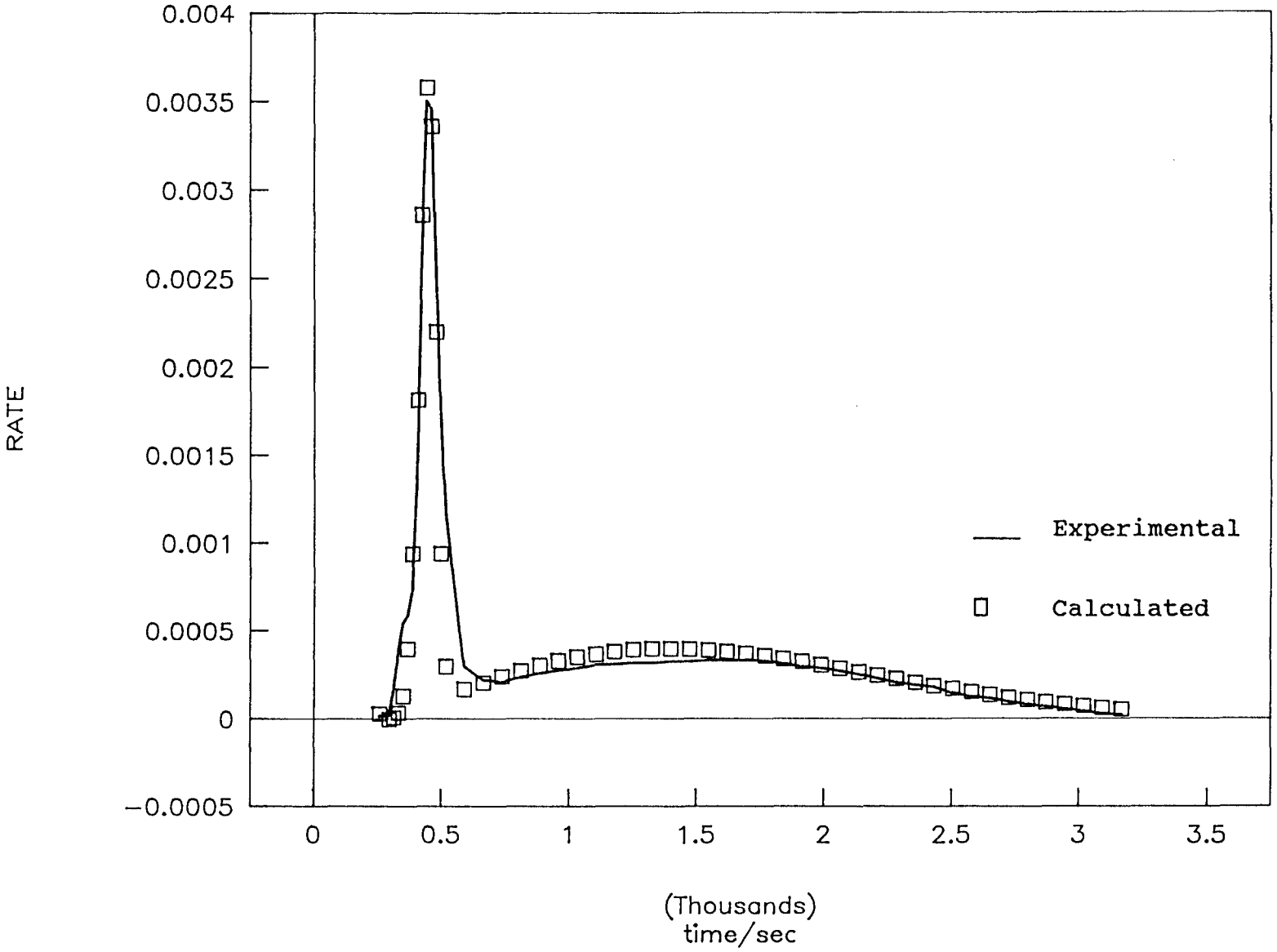

Figure 6.13 The decomposition of $CoCu(ox)_2.3H_2O$ fron isothermal DSC at 330°C

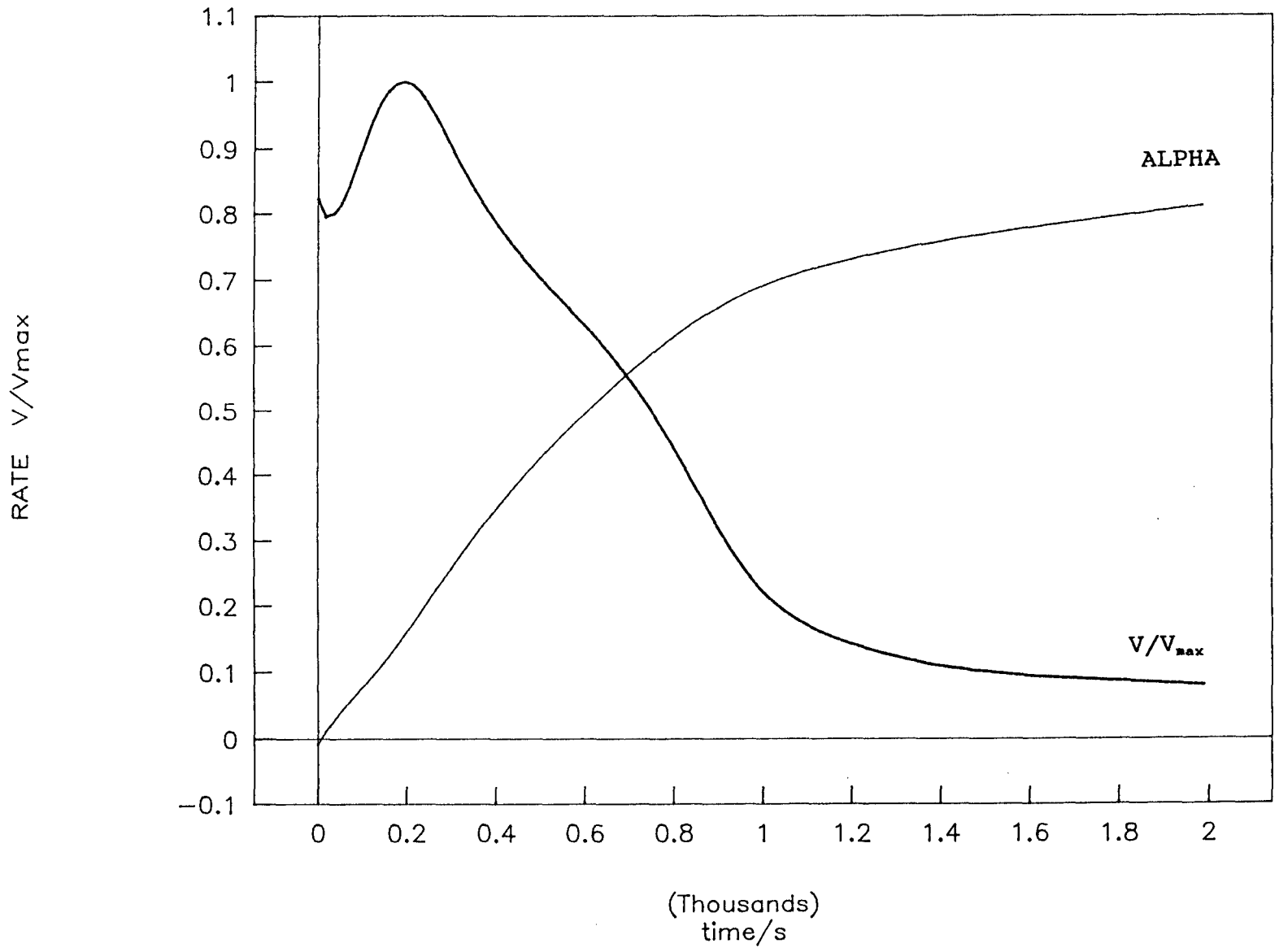

Figure 6.14 Gas evolved during the isothermal decomposition of $CoCu(ox)_2.3H_2O$ at 340°C

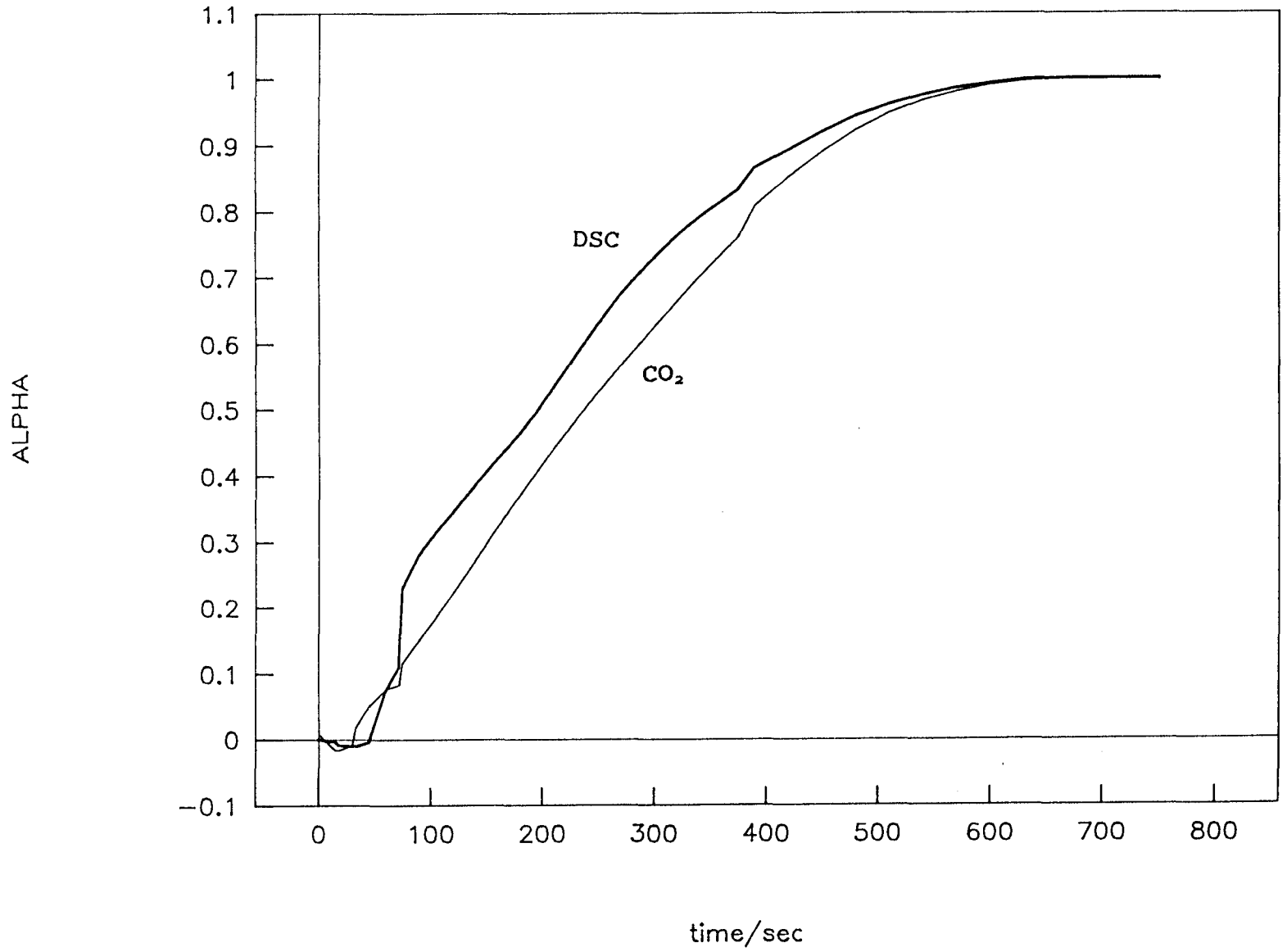

$NiCu(ox)_2$

The α - time and rate - time curves (see Figure 6.15 for an example) derived from isothermal TG (320 - 345°C) experiments for the decomposition of $NiCu(ox)_2$ were analyzed in terms of two processes. Table 6.9 lists the values of n_1, n_2, k_1, k_2, w_1 and w_2, selected for each isothermal experiment (320 - 345°C). Except for the higher temperature run at 345°C, the values of n_1 and n_2 were constant at 4.0 and 2.0, respectively. The weighting factors were approximately constant, with w_1 only varying between 0.30 and 0.33, and $w_2 = 1 - w_1$. The value of k_1 remained approximately constant at 0.0038. The values of k_2 were used in an Arrhenius plot to give the values of the activation energy and A, shown in Table 6.11. Since the values of k_1 were approximately constant with change in temperature, the apparent activation energy for the first process, was approximately zero. A resulting experimental and calculated rate-time curve at 330°C is shown in Figure 6.16.

Table 6.9.

RATE PARAMETERS FOR THE DECOMPOSITION OF $NiCu(ox)_2$
$t_o = 0$ at all temperatures

T/°C	n_1	n_2	$k_1/10^3$	$k_2/10^3$	w_1	$w_2=1-w_1$
320	4	2	3.8	0.308	0.31	0.69
325	4	2	3.7	0.381	0.33	0.67
335	4	2	3.8	0.400	0.33	0.67
345	5	2	3.8	0.791	0.30	0.70

The α - time curves were analyzed by fitting the second, slow reaction with the contracting-volume equation (R3) (α = 0.5 - 0.8). The values for the second stage, for α < 0.5, were calculated from the R3 line. The slopes of the R3 lines, at various temperatures, were used in an Arrhenius plot, which gave an activation energy of 94 $\pm$ 8 kJ mol^{-1} for the slow reaction. An activation energy of 91 $\pm$ 2 kJ mol^{-1} was obtained using the initial slopes of the slow reaction (α < 0.5), as discussed under $CoCu(ox)_2$. The rate coefficients for the fast reaction were obtained using the difference between the initial slopes of the total and slow reaction steps. An Arrhenius plot gave an activation

energy of 145 ± 24 kJ mol^{-1}.

The isothermal (320°C) DSC curve consisted of three processes (Figure 6.17) and the rate parameters, n_1, n_2, k_1, k_2, w_1 and w_2 estimated for these processes are listed in Table 6.10. They are compared with values estimated from an isothermal TG experiment at 320°C.

Table 6.10
RATE PARAMETERS FOR THE DECOMPOSITION OF $NiCu(ox)_2$
**values expected from TG at 320°C

T/°C	n_1	n_2	n_3	w_1	w_2	w_3	k_1 /10^3	k_2 /10^3	k_3 /10^3
**	4	2	3	0.31	0.69	0	3.8	0.31	0.5
320	2	2	2	0.08	0.13	0.59	6	2	0.5

Isothermal (320 - 340°C) DSC runs on $NiCu(ox)_2$ were converted to α - time curves. The first stage of the curve ($\alpha < 0.7$) was linear. This was treated as a zero-order reaction and an activation energy of 75 ± 42 kJ mol^{-1} was obtained. The second stage of decomposition was fitted by the R3 equation and an activation energy of 12 ± 1.5 kJ mol^{-1} was obtained for the range α = 0.7 - 0.9.

The evolution of gas from isothermal DSC runs on $NiCu(ox)_2$ at 345°C, in N_2, was followed by a thermal conductivity detector (TCD). In some runs a cold trap was introduced to trap CO_2 evolved, so that CO only could be detected. These runs were compared with runs in N_2 without a cold trap, i.e. CO plus CO_2. The gases evolved during the isothermal (345°C) decomposition of $NiCu(ox)_2$ were found to be both CO and CO_2. α - time curves for the evolution of CO plus CO_2 were generated and the trace for CO was subtracted from that for CO and CO_2 to obtain a profile for CO_2 evolution. α - time curves obtained from the isothermal DSC peak and evolved gas detection (CO plus CO_2) can be seen in Figure 6.18. From the α - time curve representing the evolution of CO plus CO_2 it is clear that the evolution of gas takes place in two overlapping stages. The α - time curves for the evolution of the two gases do not coincide (see Figure 6.19), hence the composition of the gaseous mixture is changing with time and the heat effects measured by DSC will also be affected. The α - time curve, representing CO_2 evolution is deceleratory and roughly corresponds to the later part of the α - time curve generated

from the DSC results, i.e. for α = 0.5 - 1. The α - time curve for the evolution of CO reaches a plateau region at α = 0.8 and the gradually increases again up to α = 1. In an attempt to quantify the amounts of CO and CO_2 evolved, the area under the CO_2 curve was multiplied by the area for one mole of CO_2, obtained from the $CoCu(ox)_2$ experiment. It was found that 3.37 moles of CO_2 were evolved for each mole of $NiCu(ox)_2$. This means that 0.63 moles of CO is evolved and the approximate reaction stoichiometry is thus:

$NiCu(ox)_2 \rightarrow 0.37Ni + 0.37Cu + 0.63(NiO + CuO) + 0.63CO + 3.37CO_2$

Results of the decomposition studies done on $NiCu(ox)_2$ are summarised in Table 6.11.

Table 6.11.

KINETIC DATA FOR THE DECOMPOSITION OF $NiCu(ox)_2$ IN NITROGEN

T range/ °C	models	α-range	E_a/ kJ mol^{-1}	ln (A /s^{-1})
isothermal TG 330-345	R3 initial rate	0.6-0.8 <0.5 <0.5	94 ± 8 91 ± 2 145 ± 24	10.11±0.05 10.49±0.01 22.09±0.15
	An	process 1 2	 1.4 ± 2.4 104 ± 30	 -5.31±0.02 12.92±0.19
isothermal DSC 320-340	zero order R3	<0.7 0.7-0.95	75 ± 42 12 ± 2	7.25±0.22 -6.75±0.005
programmed T TG	R3	first stage second stage	41 ± 1 285 ± 5	14.78±0.048 59.91±0.11
programmed T DSC	R3	first stage second stage	175 ± 3 227 ± 4	43.6±0.18 52.85±0.08

Again, there is agreement was between the activation energy values obtained for the second stage of decomposition, from the programmed temperature TG and DSC experiments, but these values are considerable higher than values obtained from isothermal experiments.

Figure 6.15 The decomposition of $NiCu(ox)_2.3.5H_2O$ from isothermal TG at 320°C

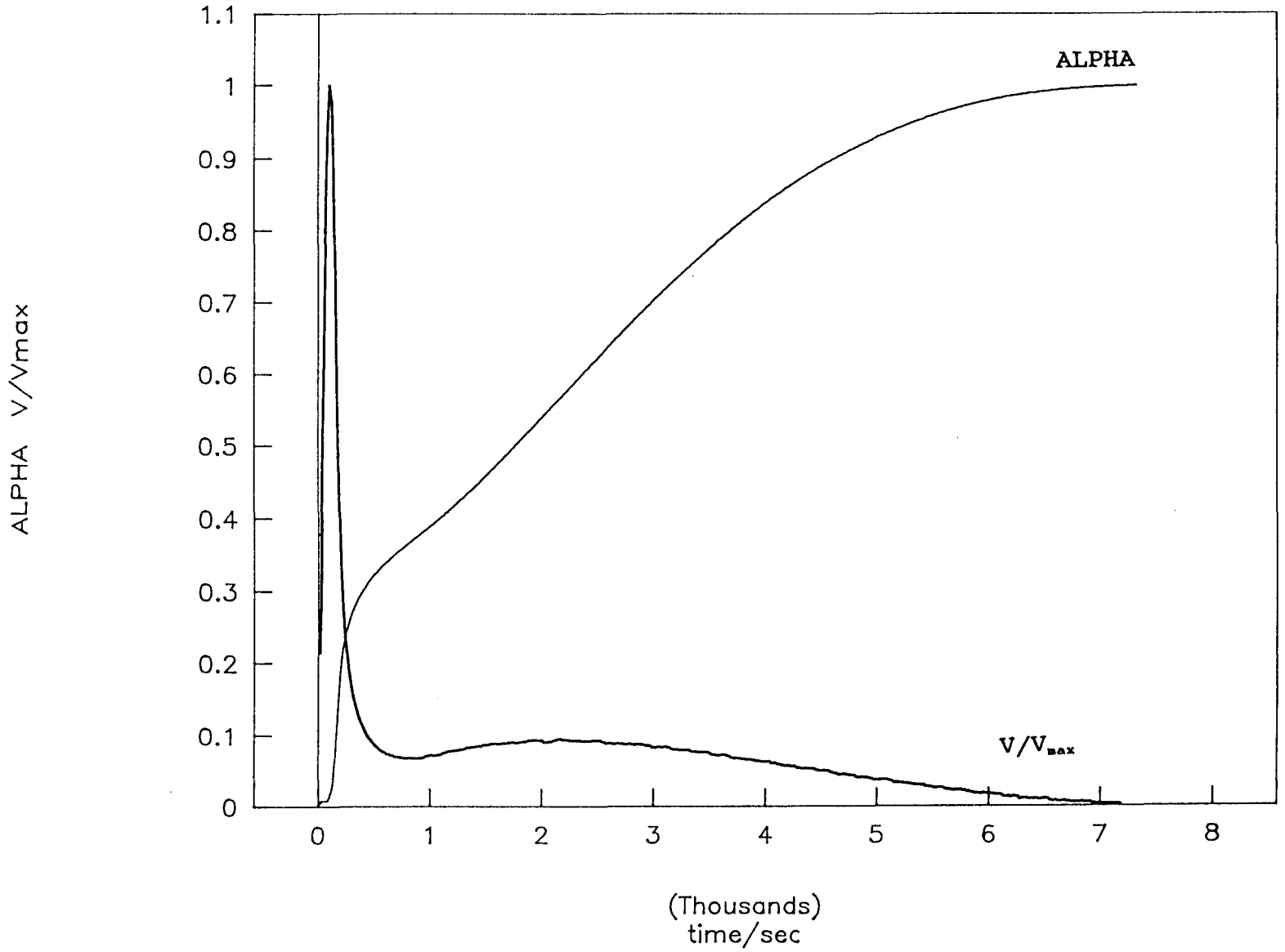

Figure 6.16 Experimental and calculated rate - time plots for the decomposition of $NiCu(ox)_2.3.5H_2O$ at 325°C

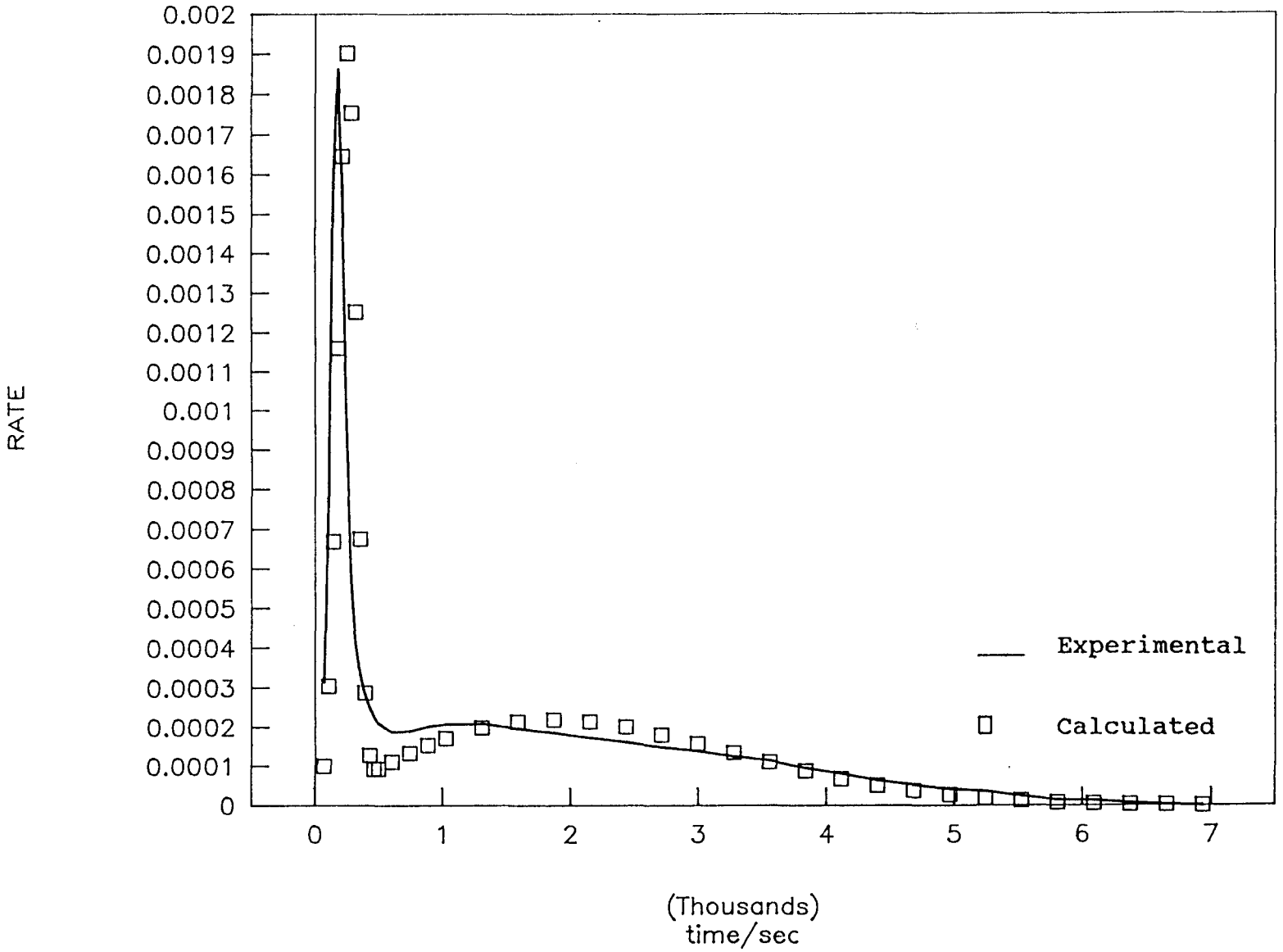

Figure 6.17 The decomposition of $NiCu(ox)_2.3.5H_2O$ from isothermal DSC at 320°C

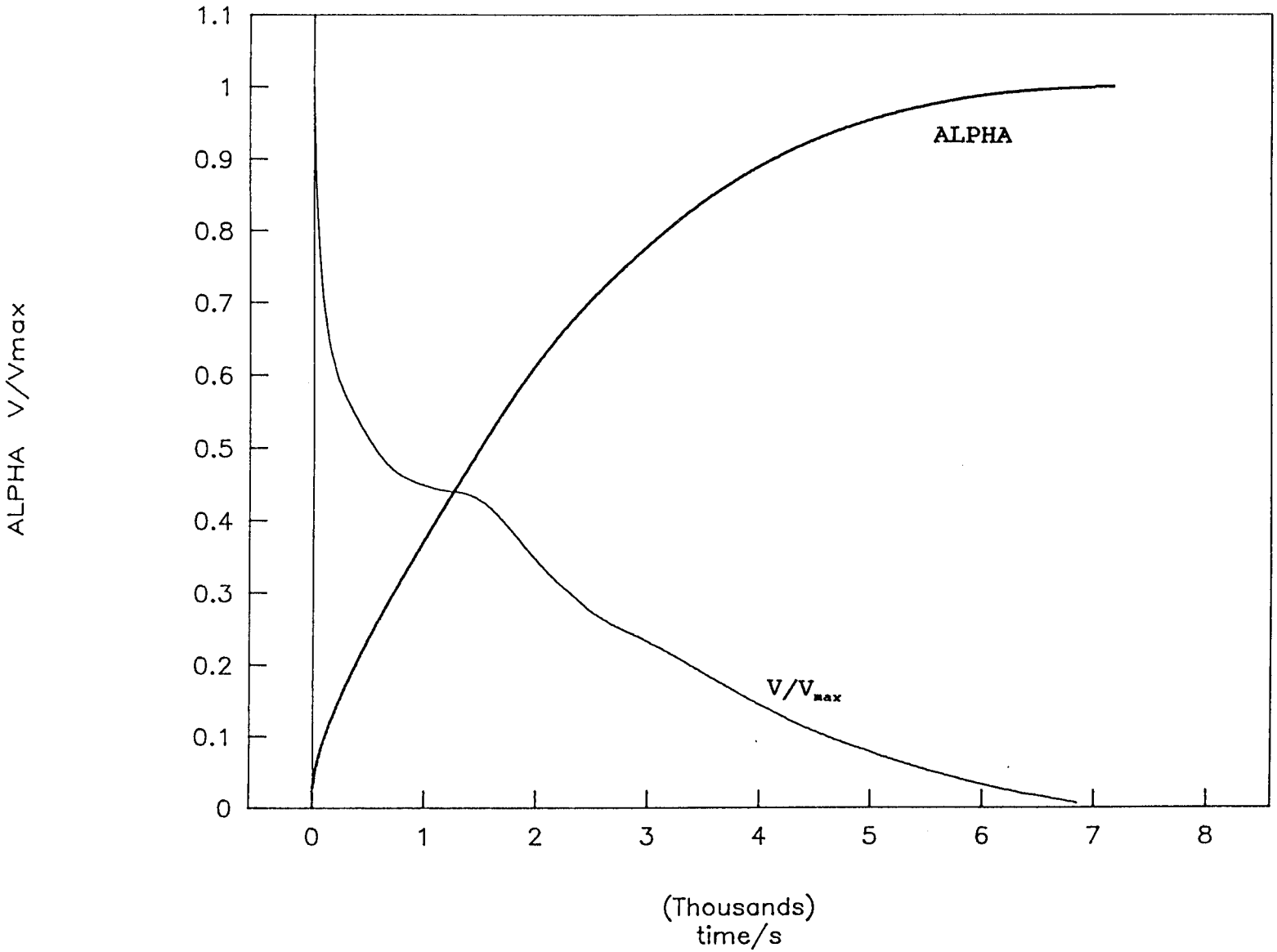

Figure 6.18 Total gas evolved during the isothermal decomposition of $NiCu(ox)_2.3.5H_2O$ at 345°C

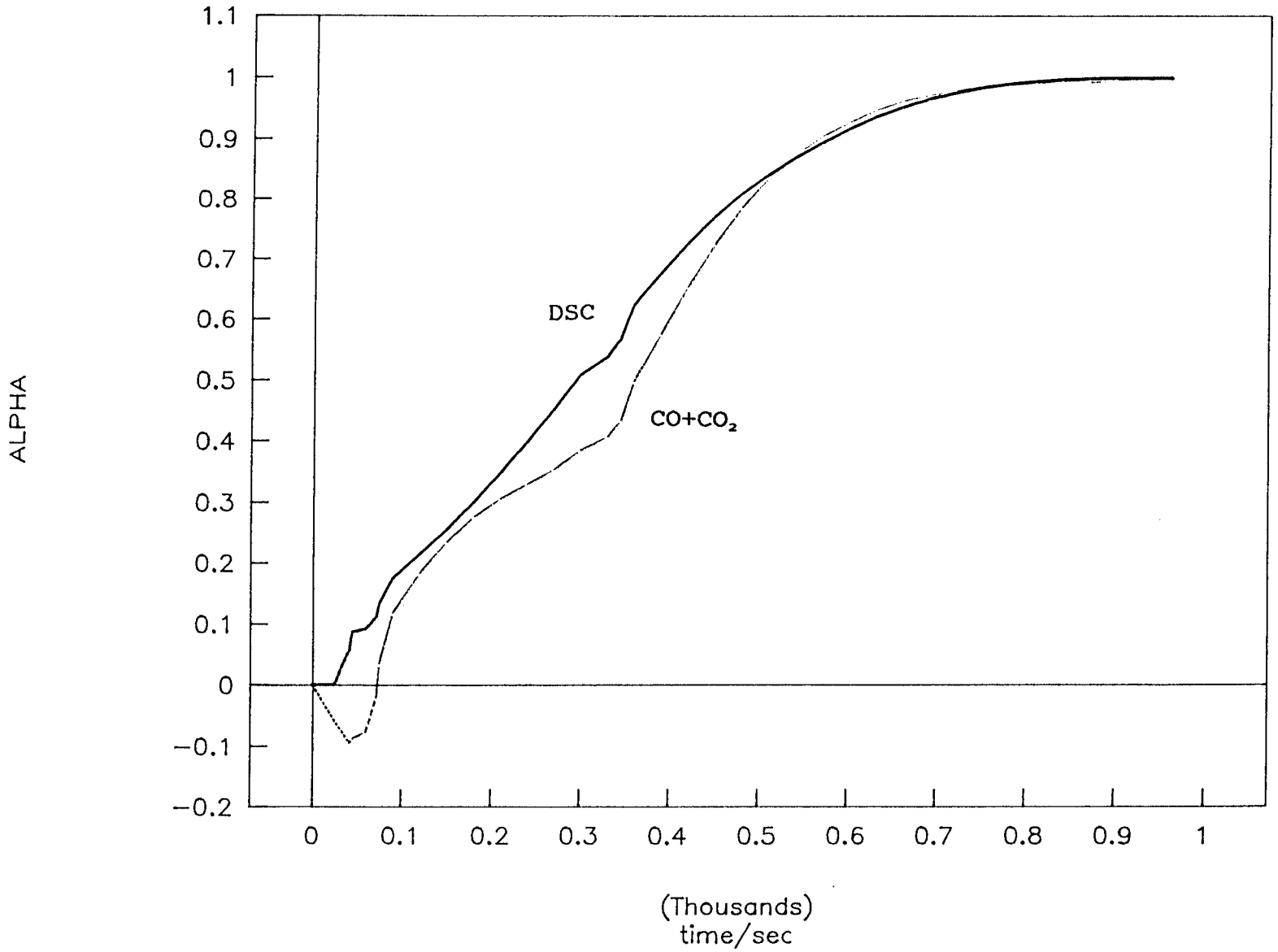

Figure 6.19 Different gases evolved during the isothermal decomposition of $NiCu(ox)_2$ at 345°C

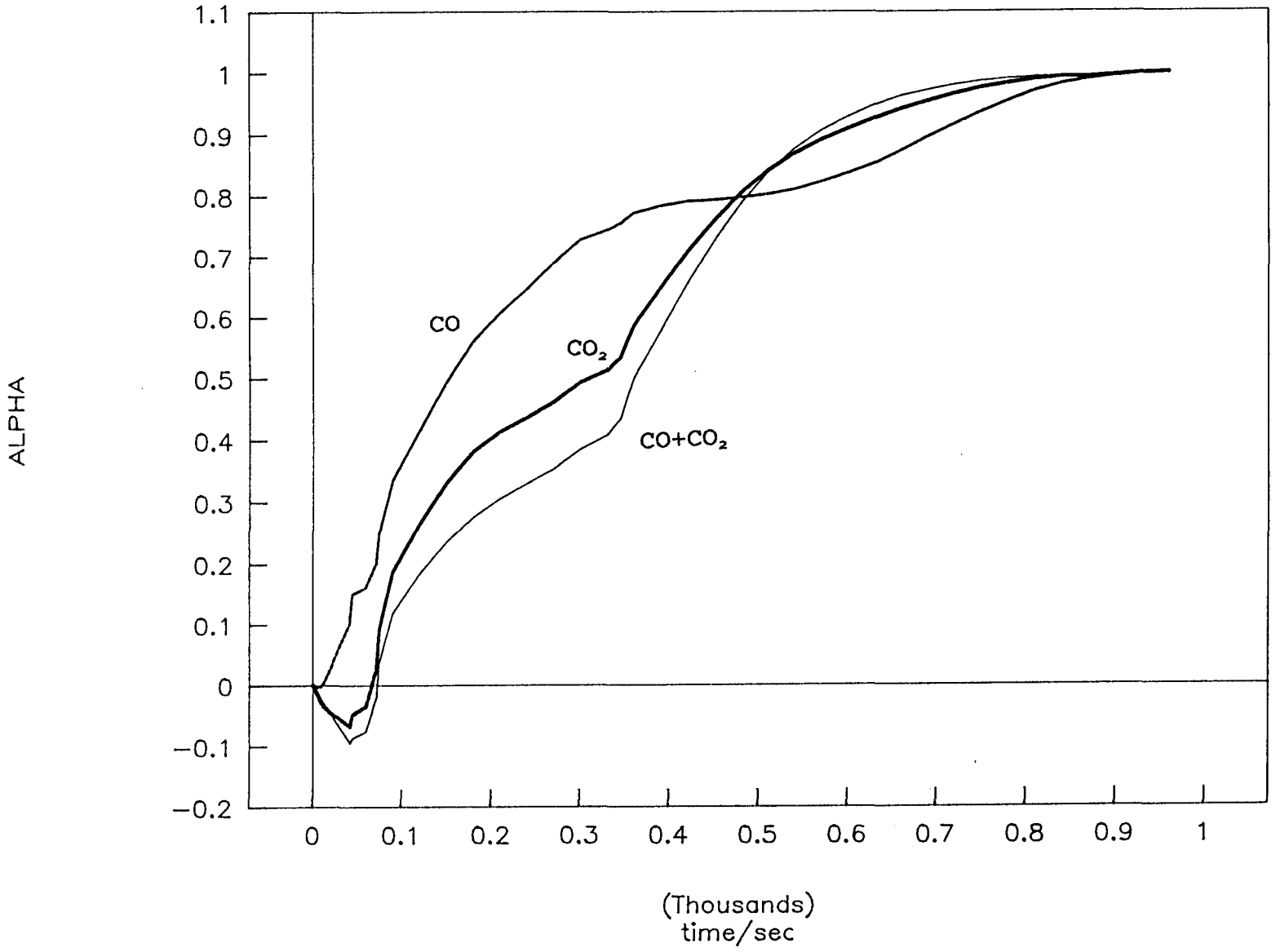

$FeCu(ox)_2.3H_2O$ was shown to contain coprecipitated Cuox (see XPD, section 3 and Thermal analysis, section 4). Since the other mixed oxalates give two initial processes and $FeCu(ox)_2$ three, it is possible that the first process might be the decomposition of the Cuox impurity.

For the thermal decomposition of $CoCu(ox)_2$, time corrections were required to match the processes. The first process comprised 23-30% of the total rate, but its activation energy, 123 kJ mol^{-1}, was higher than that of the second process, 93 kJ mol^{-1}. These values were not very different from values obtained from the linear and deceleratory parts of the α - time curves.

The decomposition of $NiCu(ox)_2$ was similar to that of $CoCu(ox)_2$, above, except that the first process, comprising of 30-33% of the total rate, had an apparent activation energy of approximately zero, while the activation energy for the second process was 104 kJ mol^{-1}.

THE COMPENSATION EFFECT AND THE MIXED METAL OXALATE DECOMPOSITIONS

A plot of ln A against E_a for decomposition, using values obtained for the first process for $FeCu(ox)_2$ and $CoCu(ox)_2$, and the second process for $NiCu(ox)_2$ can be seen in Figure 6.20. The limited data indicate a compensation effect.

Figure 6.20 Compensation effect for the decomposition of the mixed oxalates

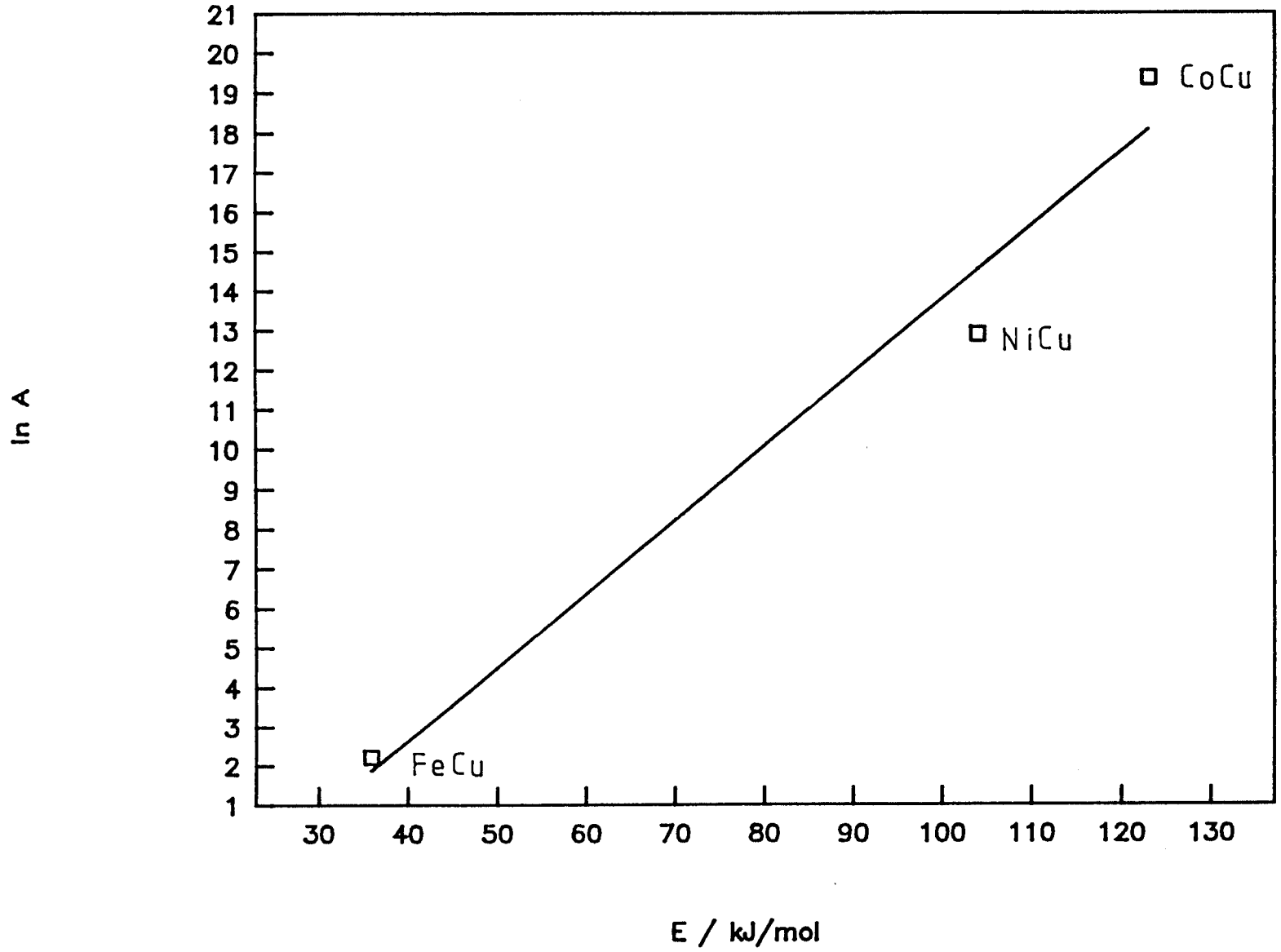

6.3 DISCUSSION

Dehydration of the individual oxalates

The dehydrations of the individual oxalates were generally found to be deceleratory processes, fitted by either the R2 or R3 models. It is difficult to distinguish between these two models [81]. Dehydration of powders is often described in terms of removal of water from surfaces followed by movement of the reaction interface into the particles. The activation energy values are not very dependent upon the model used in the estimation. A compensation effect was apparent from the limited data available (Fe, Co, Ni). The E_a values varied between 68 (for Niox) and 158 kJ mol^{-1} (for Coox). The temperature range for the isothermal experiments was 165 - 205°C.

Decomposition of the individual oxalates

Information on the decomposition of Feox was obtained in this study, and was compared with literature reports on the decomposition of the other individual oxalates. The isothermal decomposition of Feox in N_2 is mainly deceleratory (R3). The activation energy of 141 $\pm$ 22 kJ mol^{-1} is comparable with other values reported for the decomposition of Feox [60] and values for other oxalates, except the very high values for the decomposition of Niox and Cuox, reported by Mu and Perlmutter [60]. An apparent compensation effect was observed from the limited data.

Muraishi and Yokobayashi [78] have recently reported compensation effects for the thermal dehydration and thermal decomposition of a series of lanthanide oxalates, lanthanide malonates and lanthanide succinates. Except for the decomposition of the succinates, the compensation plots showed two different linear regions for the light and heavy lanthanides.

Attempts have been made to give physical meaning to the parameters B and C in the compensation equation, $\ln A = B E_a + C$. Zsako *et al* [82] suggest that B characterizes the strength of the bond being broken when gaseous products are formed. The stronger

the bond to be ruptured, the smaller the value of B. Parameter C is proposed [82, 83] to be related to the structure of, and defects in, the starting material, or to the mobility of constituents of the crystal lattice. According to this theory the B value for the decomposition of the individual oxalates would be expected to be smaller than the B value for the dehydration of the individual oxalates. The compensation parameters for the dehydration and decomposition of the individual oxalates are summarised in Table 6.12.

Table 6.12

THE COMPENSATION PARAMETERS FOR THE DEHYDRATION AND DECOMPOSITION OF THE INDIVIDUAL OXALATES

Reaction	B	C
individual oxalates		
dehydration	0.291 ± 0.010	-9.4 ± 0.7
decomposition	0.285 ± 0.004	-21.7 ± 0.2

B has similar values for the decomposition and dehydration reactions. There is no generally acceptable explanation of the compensation effect, and the variations observed in kinetic parameters reported for similar treatments of different preparations of the same compound, and from the use of different experimental techniques or kinetic analyses on a single preparation, often do not allow any confident conclusions to be made.

Dehydration of the mixed oxalates, $MCu(ox)_2.nH_2O$

The dehydrations of the mixed oxalates were found to be mainly deceleratory and were generally fitted by the R2 model. Programmed temperature measurements for TG and DSC gave good agreement and results were comparable (only slightly higher) to isothermal results. The activation energy values were not very dependent on the nature of M (Fe, Co, Ni) and were similar to the values obtained for the dehydration of the individual oxalates.

Decomposition of the mixed oxalates, $MCu(ox)_2$

These decompositions were all complex, and that of M = Fe was the most complex. Isothermal rate - time curves provided the most information about the early stages of reaction, which appear to involve overlapping sigmoid processes. These curves could be described by the Avrami-Erofe'ev model with different parameters for each contributing process. At the higher end of the range of isothermal temperatures used, the resolution of the contributing processes decreased and this could lead to anomalous results. For M = Fe these early processes generally had low activation energies (0 - 50 kJ mol^{-1}) and contributed from 20-50% of the overall rate. The deceleratory regions of the α - time curves could be fitted by the R3 model with higher activation energy: 61 kJ mol^{-1} (DSC) to 155 kJ mol^{-1} (TG).

The compensation parameters obtained from plots of ln A against E_a for the dehydration and decomposition of the mixed oxalates are listed in Table 6.13.

Table 6.13.

THE COMPENSATION PARAMETERS FOR THE DEHYDRATION AND DECOMPOSITION OF THE MIXED OXALATES

Reaction	B	C
mixed oxalates		
dehydration	0.26 ± 0.16	9.9 ± 2.1
decomposition	0.19 ± 0.03	-4.8 ± 2.1

B is smaller for the decomposition than for the dehydration of the mixed oxalates. Zsako *et al* [82] suggest that the stronger the bond to be broken, the lower the value of B, and this is supported by the results for the mixed metal oxalates.

Programmed temperature experiments, using either TG or DSC, generally gave considerably higher values for E_a than those obtained from programmed temperature and isothermal experiments. This is an indication of the complexity of the reactions being examined. Isothermal studies at higher temperatures showed the decreased resolution of the concurrent processes, and such overlap will be even more marked under programmed temperature conditions. The agreement between the kinetic parameters from programmed temperature and isothermal experiments is better for the simpler processes involved in the reactions of the individual oxalates and for the dehydration of the mixed oxalates. For complex processes, agreement between kinetic parameters derived from TG and DSC results (and DSC and TCD results) cannot be expected to be good since thermal effects will not parallel mass changes.

The complexity of the kinetics is too great for any mechanistic conclusions to be drawn and the Arrhenius parameters can only be regarded as empirical guides to the temperature dependence of the competing processes identified.

CHAPTER 7 X-RAY PHOTOELECTRON SPECTROSCOPY

X-ray photoelectron spectroscopy (XPS) studies were carried out on Niox.$2H_2O$, Coox.$2H_2O$, Cuox, Feox.$2H_2O$, NiCu(ox)$_2$.$3.5H_2O$, CoCu(ox)$_2$.$3H_2O$ and FeCu(ox)$_2$.$3H_2O$ by Dr C. Strydom, University of Pretoria.

7.1 SAMPLE PREPARATION

All of the above oxalates, individual and mixed, except for Cuox, contain water of crystallisation (Table 3.1) and thus samples had to be dehydrated under controlled conditions, prior to investigation. The X-ray photoelectron spectra were recorded, using a VG Scientific ESCALAB Mk. II instrument. Non-monochromatic Mg K_α (1253.6 eV) radiation was used. The base pressure was lower than 10^{-10} mbar in the analyzer. All samples were cooled to liquid nitrogen temperature and coated with a 1 nm thick gold layer. The Au 4f XPS peaks were recorded for each sample. Static charge-corrected binding energies were obtained by means of the calibrated energy of 84.0 eV for the Au $4f_{7/2}$ peak maximum value [85-87]. Charge corrections varied between 6.40 and 8.00 eV. The peak positions were determined by linear background subtraction and a least-squares fitting procedure.

7.2 RESULTS

The charge-corrected binding energies for the various peaks for the different oxalate compounds are listed in Table 7.1. The results correlate reasonably well with related literature values [88]. Some of the changes are very small and within the limits of accuracy of the instrument for the wider peaks (0.1 eV).

The Cu-containing compounds

The generalization by Siegbahn *et al.* [89] that the higher the binding energy, the greater the effective positive charge is on a metal ion, is used to compare results. If the oxidation numbers are equal, positive shifts of binding energy values in the atom or ion

under analysis, increase with increases in electronegativity of neighbouring atoms [90]. From the Cu 2p peak data it seems that the decreasing order of positive charge on the Cu ion in the different compounds is

$NiCu(ox)_2 > Cuox \approx CoCu(ox)_2 \approx FeCu(ox)_2$

Multiplet splitting (the energy difference between the two 2p peaks) is the result of spin interactions between unpaired electrons resulting from the photoionisation process and other unpaired electrons present in the system [85]. This separation between the two peaks also varies depending upon the environment of the atom or ion concerned. Any neighbour that tends to decrease the electron density at the metal ion (increase positive charge), will decrease the splitting. According to this the decreasing order of positive charge on the Cu ion is

$NiCu(ox)_2 > Cuox > CoCu(ox)_2 > FeCu(ox)_2$,

although the multiplet splittings of the two middle compounds only differ by 0.05 eV.

The modified Auger parameter (α') is defined as the sum of the binding energy of the major photoelectron peak (e.g. Cu $2p_{3/2}$) and the kinetic energy of the major Auger peak (e.g. Cu $L_3M_{45}M_{45}$) [88]. The greater the Auger parameter the more polarisable the ion in the compound. The change in Auger parameter is greater than the shift in binding energy and the Auger parameter is not dependent upon the charging effect. The decreasing polarisability of Cu in the different compounds is

$NiCu(ox)_2 > Cuox > CoCu(ox)_2 > FeCu(ox)_2$.

(This can also be seen as the decreasing order of possible positive charge on the Cu ions in the compounds).

The Fe-containing compounds

Adding copper ions to the Feox compound results in a decreased positive charge on the iron ion, as can be observed from both the decreasing values of the Fe $2p_{3/2}$ peak values and the Auger parameter. A more covalent type of bond thus occurs in the mixed oxalate than in Feox.

The Co-containing compounds

The higher value of 782.60 eV for the Co $2p_{3/2}$ peak in Coox, in comparison with the value of 781.25 eV for the $CuCo(ox)_2$ compound, indicates that the cobalt ion in the mixed oxalate has a smaller effective positive charge than the cobalt ion in Coox. The copper ion thus increases the electron density around the cobalt ion, resulting (possibly) in a more covalent bond between the cobalt ions and the oxalate ions. This result is confirmed by the multiplet splitting and Auger parameters as summarized in Table 7.1.

The Ni-containing compounds

Adding copper to Niox results in a more positive charge on the Ni ion, as indicated by the Ni $2p_{3/2}$ peaks and the Auger parameter. A more ionic bond (or a less covalent bond) between the Ni ion and the oxalate ions thus results.

Table 7.1.

XPS PEAK BINDING ENERGIES (eV) OF THE INDIVIDUAL AND MIXED OXALATES

(All values corrected for charging effects)

Peak	Cuox	Coox	$CoCu(ox)_2$	Feox	$FeCu(ox)_2$	Niox	$NiCu(ox)_2$
$Cu2p_{3/2}$	932.35	-	932.05	-	932.35	-	932.85
$Cu2p_{1/2}$	952.15	-	951.90	-	952.65	-	952.35
Cu2p multiplet splitting	19.80	-	19.85	-	20.30	-	19.50
Cu LMM	336.45	-	336.25	-	336.70	-	334.85
α'(Cu)	1849.50	-	1849.40	-	1849.25	-	1851.6
$Co2p_{3/2}$	-	782.60	781.25	-	-	-	-
$Co2p_{1/2}$	-	798.25	798.05	-	-	-	-
Co2p multiplet splitting	-	15.65	16.80	-	-	-	-
Co LVV	-	483.85	483.85	-	-	-	-
α'(Co)	-	1552.35	1551.00	-	-	-	-
$Fe2p_{3/2}$	-	-	-	710.70	709.75	-	-
$Fe2p_{1/2}$	-	-	-	724.65	too	-	-
Fe2p multiplet splitting	-	-	-	13.95	small	-	-
Fe LVV	-	-	-	551.15	550.55	-	-
α'(Fe)	-	-	-	1413.15	1412.80	-	-
$Ni2p_{3/2}$	-	-	-	-	-	857.85	857.95
$Ni2p_{1/2}$	-	-	-	-	-	875.65	too
Ni2p multiplet splitting	-	-	-	-	-	17.80	small
Ni LVV	-	-	-	-	-	411.75	411.75
α'(Ni)	-	-	-	-	-	1699.70	1699.80

7.3 CONCLUSIONS

The decreasing order of electronegativity of the atoms concerned [77] is :

Ni (1.91 Paulings) > Cu (1.90) > Co (1.88) > Fe (1.83)

This is in agreement with the Cu XPS results where the decreasing order of positive charge on the Cu ion is :

$NiCu(ox)_2$ > Cuox > $CoCu(ox)_2$ > $FeCu(ox)_2$.

Adding copper to Coox and Feox results in a more covalent type of compound, whilst adding copper to Niox results in a less covalent type of compound. This follows a trend opposite to that discussed above. The structures of the individual oxalates of Ni, Co and Fe are the same (see X-ray powder diffraction, section 3.3), whilst the structures of the mixed metal oxalates change more on addition of each new ion. This would explain the seemingly conflicting results, if compared to the electronegativity of the atoms. The terms covalent and ionic bonds are used in a relative manner. The more covalent in character an ionic bond, the stronger the bond, or the more ionic in character a covalent bond, the weaker the bond.

CHAPTER 8 CONCLUSIONS

Decompositions of transition metal oxalates in inert atmospheres have been grouped [1] into (a) those that form the metal and CO_2, and (b) those that form a metal oxide and a gaseous mixture of CO and CO_2. Group (a) has been further sub-divided into decompositions that are endothermic (the majority) and those that are exothermic. Copper(II) oxalate is a well-known example of an oxalate that decomposes exothermally [1, 19], other examples are the silver [20-26] and mercury(II) [27] salts.

The X-ray powder diffraction pattern of Cuox is different from those of the other oxalates, and Cuox does not form a hydrate. The latter not only supports a different structure, but also means that decomposition of Cuox is not preceded by the disruption of the crystal lattice experienced by the other oxalates during dehydration. The mixed oxalates ($MCu(ox)_2.xH_2O$) adopt the structure of the other metal oxalate (Mox) and not that of Cuox. Traces of a Cuox impurity were observed in $FeCu(ox)_2.3H_2O$ and $CoCu(ox)_2.3H_2O$.

A process common to all the oxalates studied, except Cuox, was the removal of water from the hydrates on heating. The enthalpies of dehydration of the individual oxalates varied from 100 to 134 kJ mol^{-1} in N_2, and were generally higher in O_2, from 122 - 144 kJ mol^{-1}. The dehydration temperatures, in N_2, increased in the order:
Zn (142°C) < Fe (162°C) < Co (175°C) < Ni (214°C).
The onset temperatures for dehydration were slightly higher in O_2, but followed the same trend.

Under isothermal conditions the fractional dehydration (α) - time curves were mainly deceleratory and could be described by the contracting-area (R2) or contracting-volume (R3) models. Activation energies measured ranged from 68 (Ni) to 158 (Co) kJ mol^{-1}. The comparable E_a and ΔH values for dehydration could indicate a low activation energy for the reverse reaction, i.e. hydration of the oxalates, if the "mole" referred to in Transition State Theory refers to the formula units used in the thermochemical calculations ($Mox.2H_2O$).

The hydrated mixed oxalates contain 3 to 3.5 moles of H_2O and the onset temperatures for dehydration increased in the order :

FeCu < CoCu < NiCu,

which is the same order as for the hydrated individual oxalates (139 (Fe) to 202 (Ni) °C). The temperatures are generally lower than for the related hydrated individual oxalates. The enthalpies of dehydration, calculated per mole of H_2O removed, are similar, lying in the range 50 - 75 kJ (mol H_2O)$^{-1}$.

The isothermal dehydration curves of the mixed oxalates were also mainly deceleratory and were generally fitted by the R2 model. Activation energies, obtained from programmed temperature TG and DSC experiments varied from 90 ($FeCu(ox)_2$) to 118 ($CoCu(ox)_2$) kJ mol^{-1}. The activation energies obtained from isothermal experiments were generally lower, but spanned a much wider range, i.e. from 47 ($FeCu(ox)_2$) to 130 ($CoCu(ox)_2$) kJ mol^{-1}.

The onset temperatures for the decomposition of the individual oxalates in N_2 increased in the order:

Cu (291°C) < Ni (331°C) < Co (355°C) < Fe (367°C).

These follow the opposite trend to the electronegativity values for the metals:

Fe (1.8) < Co (1.89) < Ni (1.91).

Which means that as the electronegativity decreases, the difference in electronegativity between the metal and oxygen increases, and the M-O bonds become stronger. This explains why Feox forms the oxide as decomposition product in N_2.

Semi-quantitative analyses of the gases evolved during decomposition of the individual oxalates under reduced pressure, showed that CO is formed in significant amounts in all the decompositions, with the proportions varying from one oxalate to another, and with extent of reaction of a given compound. Niox and Coox give mainly CO_2, but up to 20% CO overall. The proportion of CO for Feox was up to 30% and, for Cuox, was highest at up to 40%.

The estimates of the enthalpies of formation of the anhydrous individual oxalates given in Table 5.3, show that the order of magnitude (all negative values in kJ mol^{-1}) is

Cuox (734) < Coox (820) < Niox (835) < Feox (949)

A value of -857 kJ mol^{-1} is reported for Coox [77]. Dollimore and Evans [20] reported a value of -668 kJ mol^{-1} for Ag_2ox, which also undergoes exothermic decomposition in inert atmospheres, while Znox has an enthalpy of formation of -1000 $\pm$ 35 kJ mol^{-1} [49]. Decomposition in inert atmospheres of any metal oxalate with an enthalpy of formation of magnitude less than 787 kJ (mol of oxalate ion)$^{-1}$ (= - twice the enthalpy of formation of $CO_2(g)$) will be exothermic.

Factors which may determine the value of the enthalpy of formation of Mox, include those which have been examined [1, 31, 33] for their possible influence on the decomposition temperature, e.g. atomic or ionic radii, electronegativity, etc. Some of these factors have been collected in Table 8.1. There appears to be some correlation between the enthalpies of formation and the covalent radii, or very broadly with Pauling electronegativity.

Table 8.1
PROPERTIES OF THE METALLIC ELEMENTS, M IN Mox [77]

M	$\Delta H_{formation}$ of Mox / kJ mol^{-1}	1st ionisation energy /kJ mol^{-1}	Metallic radius / nm	Covalent radius / nm	Pauling electro-negativity
Ag	-668	731	0.144	0.152	1.9
Cu	-734	746	0.128	0.135	1.9
Co	-820	758	0.125	0.126	1.8
Ni	-835	737	0.125	0.121	1.8
Fe	-949	759	0.126	0.125	1.8
Zn	-1000	906	0.137	0.120	1.6

A considerable amount of information on the kinetics of the decompositions of the individual oxalates has been published (see Table 1.5). The spread of reported values for kinetic parameters and the varieties of kinetic models used to describe the reactions, emphasises a fundamental difficulty of the field of solid-state chemistry - the dependence of reactivity on many factors which may be difficult or impossible to control. Activation

energies reported for the decomposition of the individual oxalates range from 59 (Co) to 766 (Ni) kJ mol^{-1} [60, 64].

Decompositions in inert atmospheres of all the mixed oxalates studied were endothermic, but complex. The decomposition temperatures in N_2 varied from 345°C to 362°C. The trend followed: CoCu (345°C) < FeCu (351°C) < NiCu (362°C)
differs from the trends observed in the decomposition temperatures for the individual oxalates, i.e. Cu < Ni < Co < Fe. It is significant that the onset temperatures for decomposition of the mixed oxalates are all well above the onset temperature (291°C) for Cuox, heated under the same conditions, but in the same range as the other individual oxalates.

The enthalpies of formation of the anhydrous mixed oxalates given in Table 5.4, show that the order of increasing negative values is $CoCu(ox)_2 \approx FeCu(ox)_2 < NiCu(ox)_2$ and that the first two values are close to the sum of the individual values (Table 5.5).

It is clear from the XPS results that the electron environment of the Cu ion is affected by the addition of the other metal, in the mixed oxalates. It can therefore be concluded that the mixed oxalates consist of an intimate mixture, with alternating Cu and M ions, opposed to clusters of Cuox and Mox in a physical mixture. The increasing positive charge on the Cu ion (and therefore the binding energy) in the different compounds is:
FeCu ≈ CoCu < NiCu
which would explain why $NiCu(ox)_2$ decomposes at a higher temperature than $FeCu(ox)_2$ and $CoCu(ox)_2$. The covalent radius if Ni (0.121 nm) is smaller than that of Co (0.126 nm) and Fe (0.125 nm). A similar trend was observed in the infrared spectroscopy. The M-O stretching band for $NiCu(ox)_2$ (490 cm^{-1}) was at a much lower frequency than that of $CoCu(ox)_2$ (515 cm^{-1}) and $FeCu(ox)_2$ (515 cm^{-1}).

Under reduced pressure the proportion of CO, for $FeCu(ox)_2$, increased from about 35% in the early stages (low temperature, 260°C) to about 55% in the final stages (340°C). These proportions are higher than for Feox alone.

For $CoCu(ox)_2$, retained water was evolved during the early stages of decomposition (290-300°C), and the proportion of CO increased from very low values in the early stages (290°C) to about 50% in the final stages (340°C). The later proportions are higher than for Coox alone.

For $NiCu(ox)_2$, the proportion of CO increased from about 35% in the early stages (low temperature, 260°C) to about 55% in the final stages (340°C). These proportions are higher than for Feox alone.

When decomposition occurred in an inert atmosphere of N_2, the proportion of CO evolved generally decreased and CO was not detectable in the decompositions of Niox, Coox and $CoCu(ox)_2$. For decompositions in an atmosphere of CO_2, the proportion of CO, relative to that evolved in N_2, was unchanged for $FeCu(ox)_2$, increased from 28% to 70% for Feox, and decreased from about 50% to about 2% for Cuox and $NiCu(ox)_2$. Results are summarised in Tables 4.2 and 4.4.

The evolved gas analyses show that secondary reactions occur readily between the initial gaseous and solid products and that the final products are dependent upon the conditions governing removal of the gases. In addition to being possible secondary reactants, the solid products may catalyse reactions between gaseous products and their activity as catalysts may be strongly dependent upon the conditions existing during their formation.

The kinetics of decomposition of the mixed metal oxalates were complex and isothermal rate - time curves could be described in terms of several concurrent sigmoid and deceleratory processes. Isothermal α - time curves derived from TG, DSC and TCD measurements did not give very good agreement, again indicating the complexity of the processes with the balance between mass and thermal effects changing with time. The complexity was too great to allow any detailed mechanistic conclusions to be drawn.

The Arrhenius parameters derived should be regarded as empirical factors describing the temperature dependencies of the competing processes involved. Apparent activation

energies obtained from programmed temperature TG and DSC experiments, were in the increasing order: NiCu < FeCu < CoCu
which is the reverse order of onset temperatures for decomposition (CoCu (345°C) < FeCu (351°C) < NiCu (367°C)).

Thus the mixed oxalates, $MCu(ox)_2$, behave more like Mox than Cuox, but the Cu still has an influence on the behaviour.

REFERENCES

1. D. Dollimore, *Thermochimica Acta*, **117** (1987) 331.

2. D.J. Eve, Paper prepared for the 21st SACI convention, (1971) Grahamstown

3. S. Caric, *Bull. Soc. franc. mineral. et crist.*, **82** (1959) 50-6.

4. J. Dubernat, H. Pezerat and J.P. Lagier, *C.R. Acad. Sc. Paris*, **266** (1968) 1357.

5. J. Dubernat and H. Pezerat, *J. Appl. Crys.*, **7** (1974) 387.

6. H. Schmittler, *Monatsber. Deut. Akad. Wiss. Berlin*, **10**(8) (1968) 581.

7. F. Mazzi and C. Garavelli, *Periodico mineral*, **26** (1957) 269.

8. O. Asai, M. Kishita and M. Kubo, *J. Phys. Chem.*, **63** (1959) 96.

9. J.J. Girerd, O. Kahn and M. Verdaguer, *Inorg. Chem*, **19** (1980) 274.

10. D.R. Bloomquist, J.J. Hansen, C.P. Landee, R.D. Willil and R. Buder, *Inorg. Chem*, **20** (1981) 3308.

11. L. Dubicki, C.M. Harris, E. Kokot and R.L. Martin, *Inorg. Chem.*, **5** (1966) 1.

12. R.L. Martin and H. Waterman, *J. Chem. Soc.*, (1959) 1359.

13. A. Glaizes, F. Maury and J. Galey, *Inorg. Chem.*, **19** (1980) 2074.

14. H.G.M. Edwards, D.W. Farwell, S.J. Rose and D.N. Smith, *J. of Molecular Structure*, **249** (1991) 233.

15. B.N Figgis and D.J. Martin, *Inorg. Chem.*, **5** (1966) 100.

16. K.T. McGregor and Z.T. Soos, *Inorg. Chem.*,**15(9)** (1976) 2159.

17. Y. Kuroda and M. Kubo, *J. Am. Chem. Soc.*,**64** (1960) 759.

18. D. Dollimore, *Thermochimica Acta*, **11** (1977) 185.

19. L.P. Burleva, V.M. Andreev and V.V. Boldyrev, *J. Thermal. Anal.*, **33** (1988) 735.

20. D. Dollimore and T.A. Evans, *Thermochimica Acta*, **178** (1991) 263.

21. J.Y. MacDonald, *J. Chem. Soc.*, (1936) 832.

22. J.Y. MacDonald, *J. Chem. Soc.*, (1936) 839.

23. A.F. Benton and L. Cunningham, *J. Am. Chem. Soc.*, **57** (1935) 2227.

24. F.C. Prout, *Trans. Faraday Soc.*, **44** (1948) 206.

25. J.Y. MacDonald and C.N. Hinshelwood, *J. Chem. Soc.*, **127** (1925) 2764.

26. D. Dollimore and T.A. Evans, *Thermochimica Acta*, **179** (1991) 49.

27. E.G. Prout and F.C. Tompkins, *Faraday soc. Trans*, **43** (1947) 148.

28. V.V. Boldyrev, I.S. Nev'yantsev, Y.I. Mikhailov and E.F. Khairetdinov, *Kinet. Katal.*, **11** (1970) 367.

29. D. Dollimore and D. Nicholson, *J. Chem. Soc.*, **178** (1964) 908.

30. D. Dollimore, D.L. Griffiths and D. Nicholson, *J. Chem. Soc.*, (1963) 2617.

31. J. Fujita, K. Nakamoto and M. Kobayashi, *J. Phys. Chem.*, **61** (1957) 1014.

32. D. Broadbent, J. Dollimore, D. Dollimore and T.A. Evans, *J. Chem. Soc. Faraday Trans.*, **87**(1) (1991) 161.

33. K. Nagase, K. Sato and N. Tanaka, *Bull. of the Chem. Soc. of Japan*, **48**(2) (1975) 439.

34. J. Robin, *Bull. Soc. Chim. Fr.*, (1953) 1078.

35. D. Dollimore, *Thermochimica Acta*, **177** (1991) 59.

36. G. Fornasari, S. Gusi, F. Trifiro and A. Vaccari, *Ind. Eng. Chem. Res.*, **26** (1987) 1500.

37. P. Porta, G. Moretti, M. Musicanti and A. Nardella, *Catal. Today*, **9** (1991) 211.

38. X. Xiaoding, E.B.M. Doesburg and J.J.F. Scholten, *Catal. Today*, **2** (1987) 125.

39. K. Fujimoto and T. Oba, *Appl. Catal.*, **13** (1989) 289.

40. J.E. Baker, R. Burch and S. Golunski, *Appl. Catal.*, **53** (1989) 279.

41. D. Waller, D. Stirling and F.S. Stone, *Faraday Discuss. Chem. Soc.*, **87** (1989) 107.

42. P. Porta, R. Dragone, G. Fierro, M. Inversi, M. Lo Jacono and G. Moretti, *J. Chem. Soc. Faraday Trans.*, **88**(3) (1992) 311.

43. H. Langbein and S. Fischer, *Thermochimica Acta*, **182** (1991) 39.

44. B.D. Dalvi and A.M. Chavan, *J. Thermal. Anal.*,**14** (1978) 331.

45. E.A. Gusev, S.V. Dalidovich, V.A. Shandakov and A.A. Vecher, *Thermochimica Acta*, **89** (1985) 391.

46. D. Dollimore and D.L. Griffiths, *J. Therm. Anal.*, **2** (1970) 229.

47. E.D. Macklen, *J. Inorg. Nucl. Chem.*, **29** (1967) 1229.

48. H.L. Saha and S. Mitra, *Thermochimica Acta*, **116** (1987) 53.

49. E.D. Macklen, *J. Inorg. Nucl. Chem.*, **30** (1968) 2689.

50. K. Umemura, *J. Chem. Soc. Japan*, **6** (1975) 968.

51. D. Dollimore, D.L Griffiths and D. Nicholson, *J. Chem. Soc.*, (1963) 2617.

52. A. Gorski and A.D. Krasnicka, *J. Therm. Anal.*, **32** (1987) 1229.

53. A.K. Nikumbh, A.E. Athare and V.B. Raut, *Thermochimica Acta*, **186** (1991) 217.

54. D. Dollimore and D. Nicholson, *J. Chem. Soc.*, (1962) 960.

55. N. Deb, P.K. Gogoi and N.N. Dass, *J. Therm. Anal.*, **35** (1989) 27.

56. N. Deb, P.K. Gogoi and N.N. Dass, *J. Therm. Anal.*, **36** (1990) 465.

57. D. Broadbent, J. Dollimore, T.A. Evans and D. Dollimore, *JCS Faraday Trans.*, **87** (1991) 161.

58. N. Deb, N.N. Dass and P.K. Gogoi, *Thermochimica Acta*, **198** (1992) 395.

59. D. Dollimore, J. Dollimore and D. Nicholson, *J. Chem. Soc.*, **380** (1965) 2132.

60. J. Mu and D.D. Perlmutter, *Thermochimica Acta*, **49** (1981) 207.

61. A. Venkataraman, N.V. Sastry and A. Ray, *J. Phys. Chem. Solids*, **53** (1992) 681.

62. D. Dollimore, T.A. Evans and Y.F. Lee, *Thermochimica Acta*, **194** (1992) 215.

63. D. Broadbent, D. Dollimore and J. Dollimore, *J. Chem. Soc*, **A** (1966) 1491.

64. A. Taskinen, P. Taskinen and M.H. Tikkanen, "Reactivity of solids", Proc. 8th Int. Symp., Plenum, New York, 1977, 617.

65. P.W.M. Jacobs and A.R.Tariq Kureishy, *Trans. Far. Soc.*, **58** (1962) 551.

66. D.A. Dominey, H. Morley and D.A. Young, *Trans. Far. Soc.*, **61** (1965) 1246.

67. D. Broadbent, D. Dollimore and J. Dollimore, *J. Chem. Soc*, **A** (1966) 278.

68. J. Jach and M. Griffel, *J. Phys. Chem.*, **68** (1964) 731

69. E.G. Prout and M.E. Brown, Symposium on Chemical and Physical Effects of High Energy Radiation on Inorganic Substances, ASTM Spec. Tech. Pub. 359, (1964) 38.

70. W.K. Schaurte, Honours Project, Rhodes University, Grahamstown, 1989.

71. M.R. Spears, Honours Project, Rhodes University, Grahamstown, 1990.

72. A. Coetzee, Honours Project, Rhodes University, Grahamstown, 1991.

73. S. Fronæus and R. Larsson, *Acta Chem. Scand.*, **14** (1960) 6.

74. K. Nakamoto, "Infrared Spectra of Inorganic Coordination Compounds", Second Edition, John Wiley & Sons, New York, 1970, 244-247.

75. G.C. Nicholson, *J. Inorg. Nucl. Chem.*, **29** (1976) 1599.

76. P.W. Selwood, "Magnetochemistry", Interscience Publishers, New York, 1943, 212-218.

77. R.C. Weast (Ed), "Handbook of Chemistry and Physics", CRC Press, Florida, 67th Edn, 1986.

78. K. Muraishi and H. Yokobayashi, *Thermochimica Acta*, **209** (1992) 175.

79. H.J. Borchardt and F. Daniels, *J. Am. Chem. Soc.*, **79** (1957) 41.

80. A. Savitsky and M.J.E. Golay, *Anal. Chem.*, **8** (1964) 680.

81. M.E. Brown and A.K. Galwey, *Thermochimica Acta*, **29** (1979) 129.

82. J. Zsako, Cs. Varhelyi and K. Szilagyi, *J. Therm. Anal.*, **7** (1975) 41.

83. A.I. Lesnikovich and V.A. Levchik, *J. Therm. Anal.*, **30** (1985) 677.

84. S. Strivastava, *Polyhedron*, **4** (1985) 11, 1925.

85. C.R. Brundle and A.D. Baker, "Electron Spectroscopy : Theory, Techniques and Applications", Volume 1, Academic Press, London, 1977.

86. R.J. Bird and P. Swift. *J. Electron Spectrosc.*, 21 (1980) 227.

87. I.J. Matienzo, L.I. Yin, S.O. Grim and W.E. Swartz, *Inorg.Chem.*, 12 (1973) 12, 2762.

88. D. Briggs and M.P. Seah, "Practical Surface Analysis by Auger and X-ray Photoelectron Spectroscopy", Wiley, New York, 1983.

89. K. Siegbahn, C. Nordling, G. Johnson, J. Hedman, P. Hedan, K. Hamrin, U. Gelius, T. Bergmark, L. Werme, R. Manne and Y. Baer, "ESCA, Applied to free molecules", North-Holland, Amsterdam, 1969.

90. V.I. Nefedov, "X-ray Photoelectron Spectroscopy of Solid Surfaces", VSP, Utrecht, 1988.

91. D.D Wagman *et al.* "Selected Values of Chemical Properties", NBS Technical Notes 270-3 to 270-8.

APPENDIX

LIST OF FIGURES

Figure 1 d-spacings obtained for Cuox

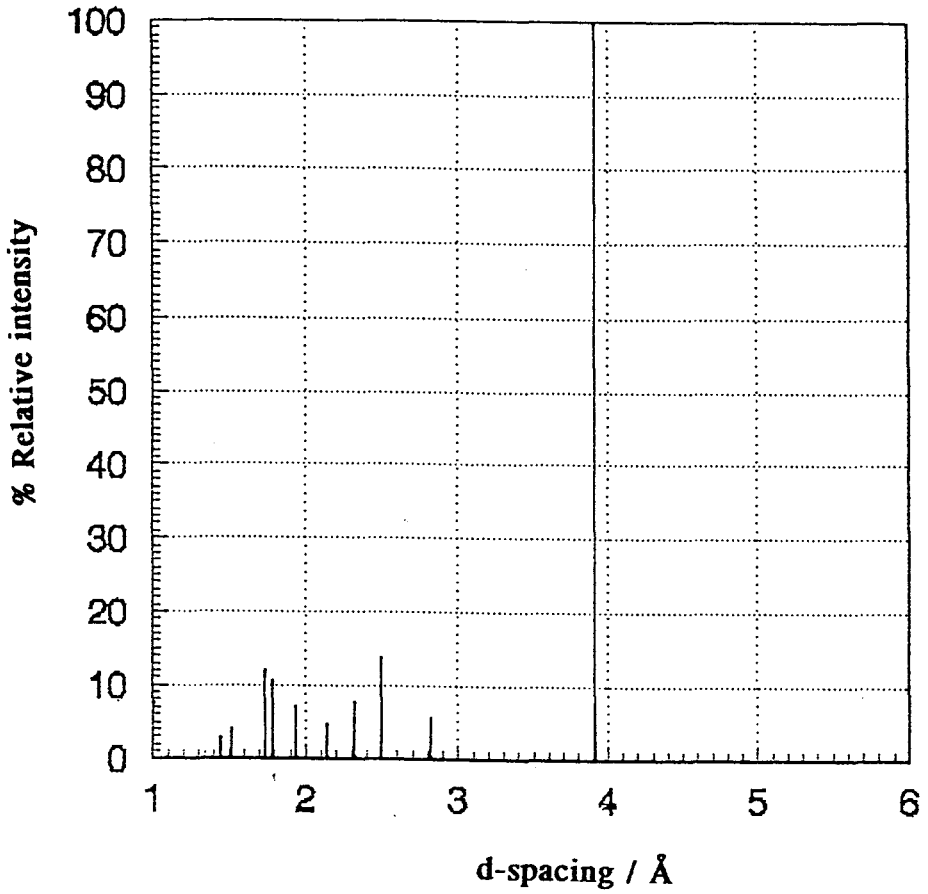

Figure 2 d-spacings obtained for Feox.2H_2O.

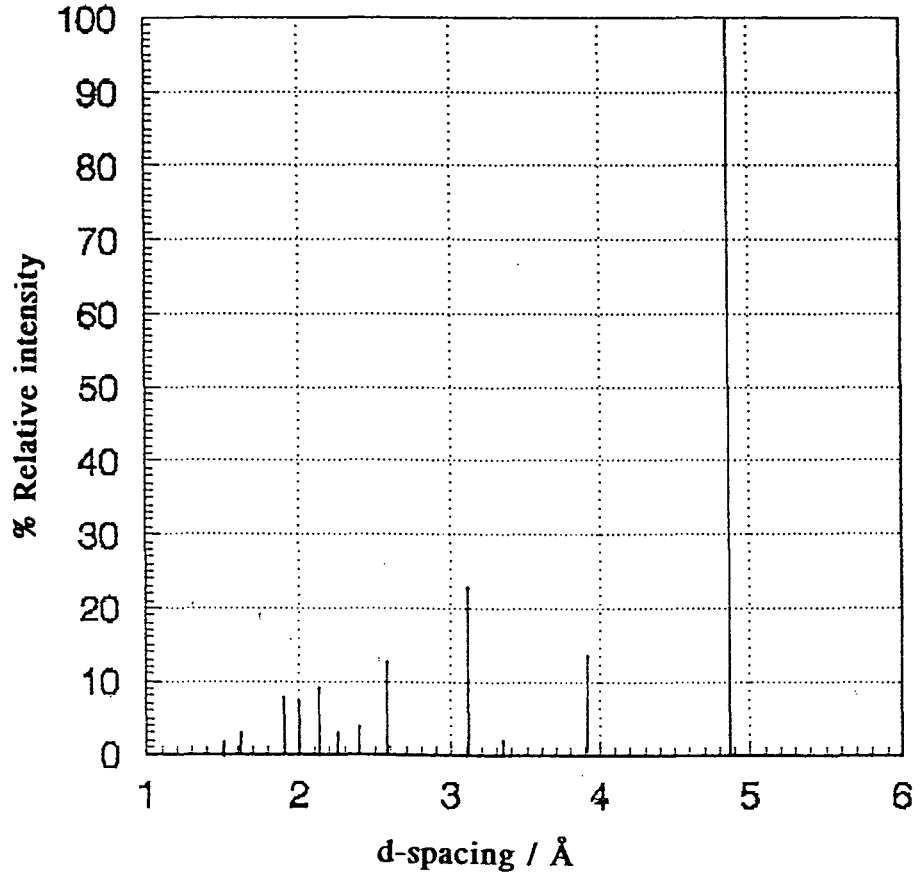

Figure 3 d-spacings obtained for Coox.$2H_2O$.

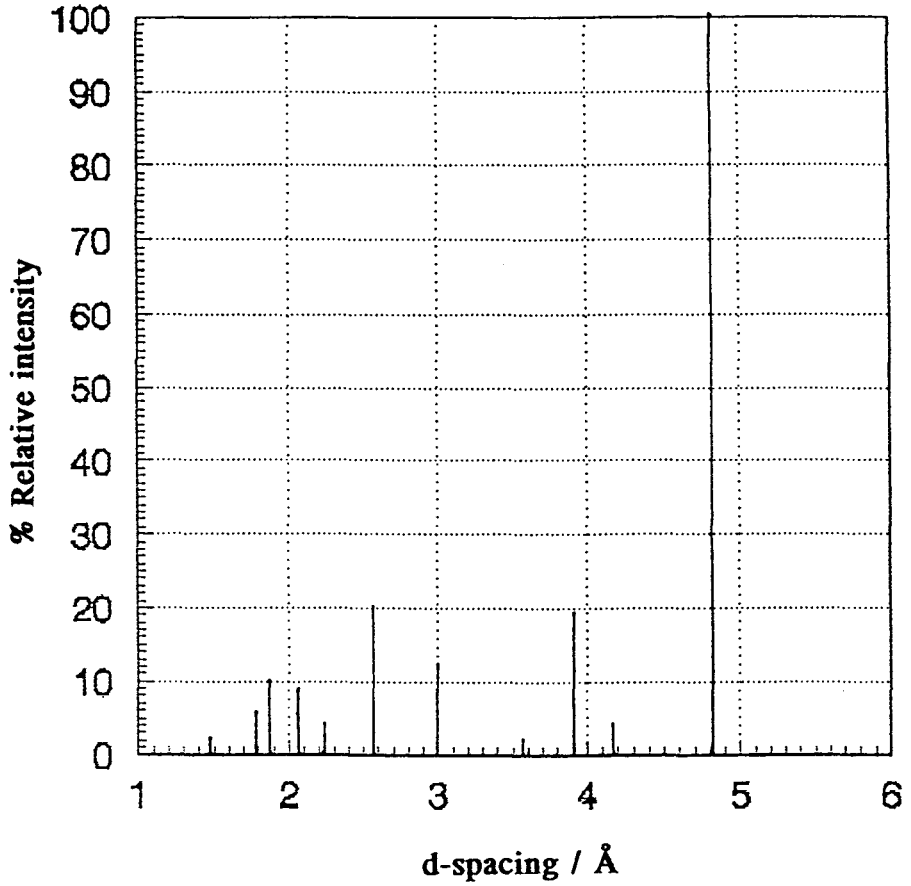

Figure 4 d-spacings obtained for Niox.$2H_2O$.

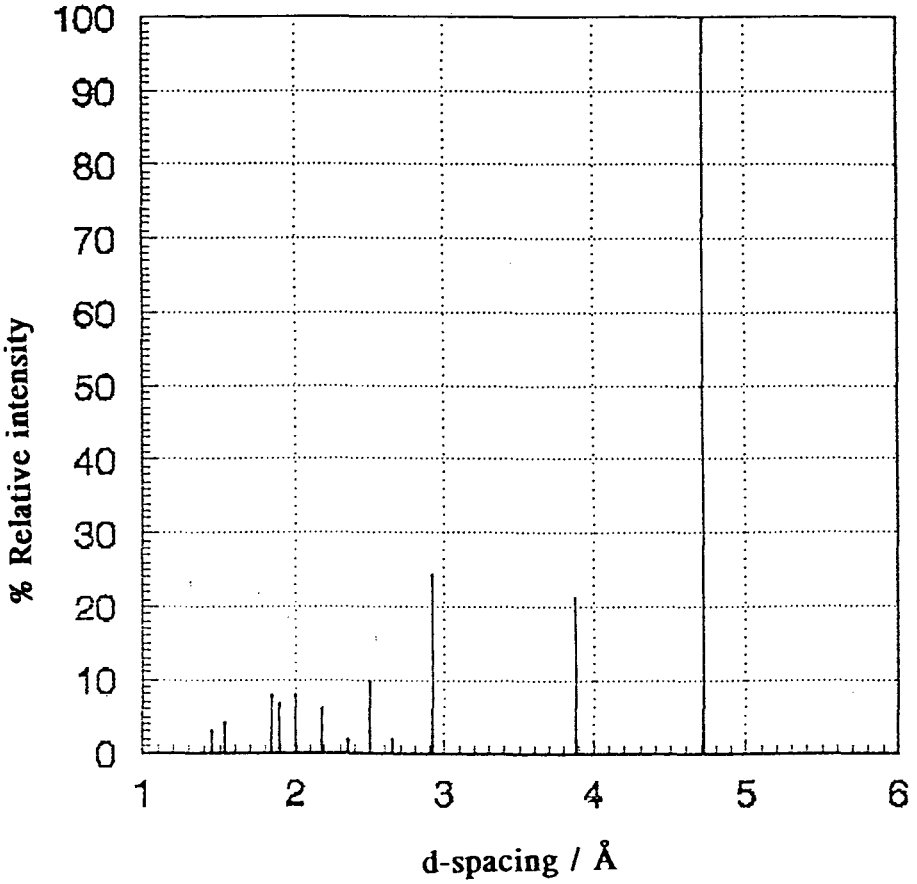

Figure 5 d-spacings obtained for Znox.$2H_2O$.

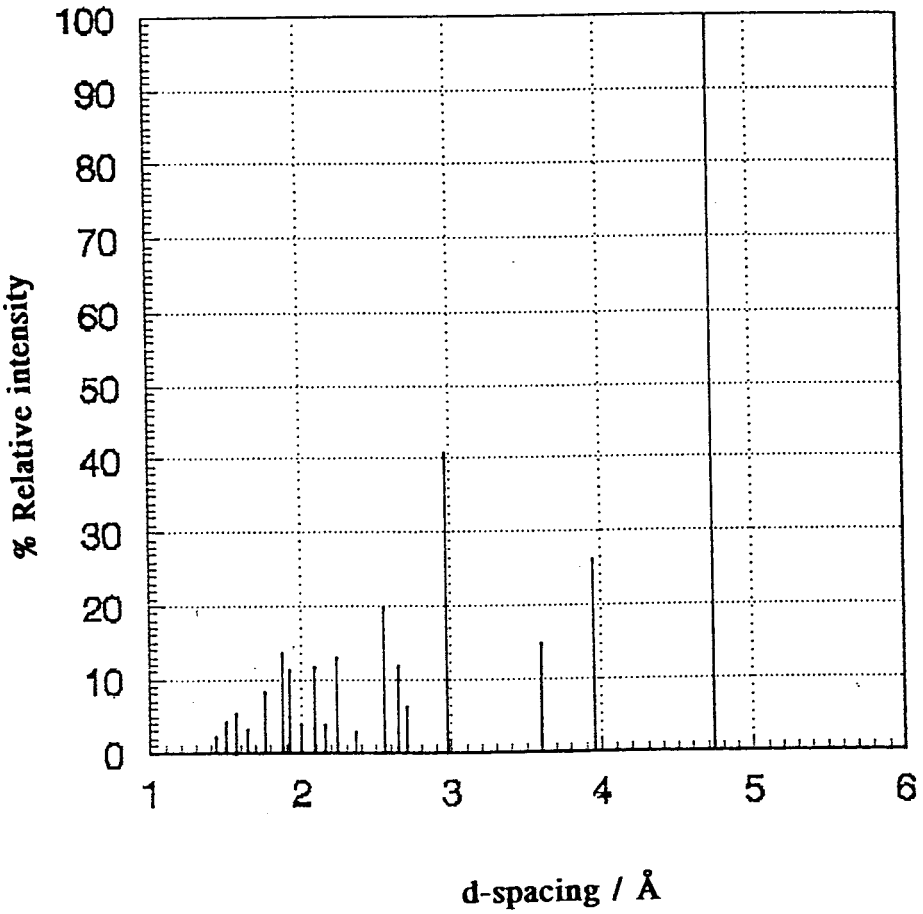

Figure 6 d-spacings obtained for $FeCu(ox)_2.3H_2O$.

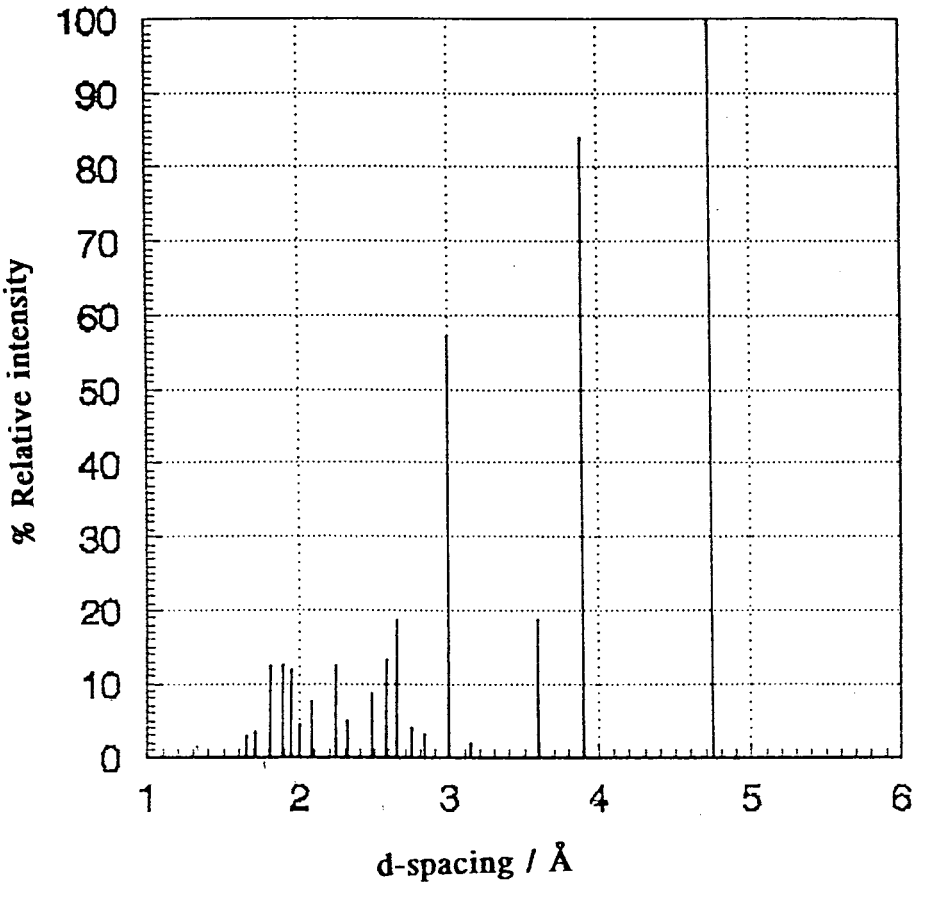

Figure 7 d-spacings obtained for $CoCu(ox)_2.3H_2O$.

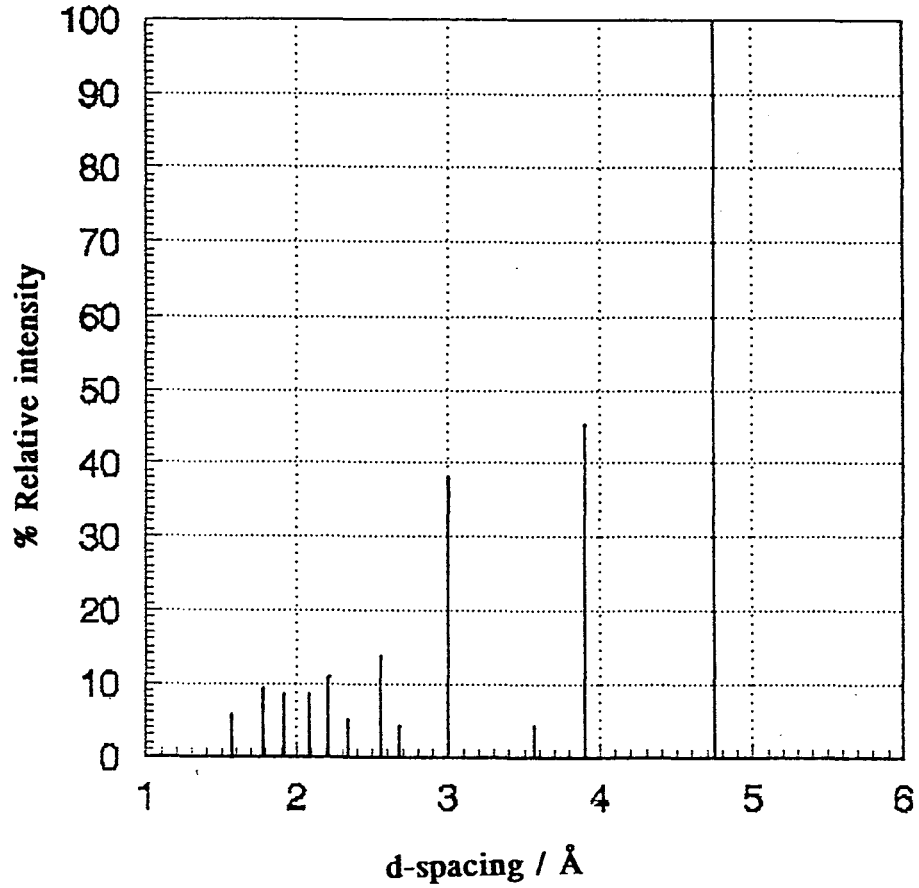

Figure 8 d-spacings obtained for $NiCu(ox)_2.3.5H_2O$.